University of Hradec Králové

Faculty of Informatics and Management

DOCTORAL THESIS

2021 **Jean Sebastien Mambou, M.C.A.**

University of Hradec Králové

Faculty of Informatics and Management

Center for Basic and Applied Research

Classification Framework for Anomaly Detection in Medical Images

DOCTORAL THESIS

Author: Jean Sebastien Mambou, M.C.A

Supervisor: Prof. Ing. Ondřej Krejcar, Ph.D.

Hradec Králové 2021

Acknowledgements

Firstly, thank you to my supervisor, prof. Ondřej Krejcar, for the support during this doctorate study and for allowing me to be part of it. It is an ambitious project, and this document only reveals part of the efforts we have invested. I also thank my GrandPa, Mr Mambou Jean Claude, who contributed financially and morally during my studies. My family and all the people who, willingly or not, have shaped my experience for the past four years. Prof. Josef Hynek, Prof. Petra Maresova, Prof. Ali Selamat, and Prof. Kamil Kuca, thank you for supporting my research papers. Thanks to Ebogo Manga Elizabeth and Manga Yannick Stevanin for contributing to building the man I am today. Special thanks to Fortune Kabasele for all the support you have given me. Magne Elise, Melissa Fanny, and Kapeo Annick, well, you know. I am grateful to Prof. Albert Kabasele for supporting me with numerous pieces of advice.

Ultimately, I would like to acknowledge every one of the utmost importance to me, although they are miles away. I thank my family for their blind confidence in me and their unconditional support. Conceivably having you all in my life is the best of luck.

Declaration:

I declare that I worked on this dissertation independently, using cited literature and other sources.

In Hradec Králové 2021

Jean Sebastien Mambou, M.C.A

Annotation

Title: Classification Framework for Anomaly Detection in Medical Images

This thesis focuses on detecting abnormalities in the context of medical images (breast cancer (BC) or brain tumor (BT)). By "Detection" is meant better localization of the area with a higher likelihood of cancer, primarily reflected by higher thermal radiation in a specific region. The successful implementation of any framework requires rigorous design and more up-to-date technology, such as a cloud-based platform. The considerable amount of new BC diagnoses also motivates me to bring up a much earlier diagnosis system. That is why I developed a systematic model capable of detecting abnormalities such as breast cancer in adult women over 26 years old. This dissertation presents a new framework to detect anomalies in medical images such as thermal images of a breast and magnetic resonance imaging of a brain.

Anotace

Název: Klasifikační framework pro detekci anomálií v lékařských snímcích

Tato práce se zaměřuje na detekci abnormalit v kontextu lékařských snímků (rakovina prsu (BC) nebo nádor na mozku (BT)). „Detekcí“ se rozumí lepší lokalizace oblasti s vyšší pravděpodobností rakoviny, což se projevuje především vyšším tepelným zářením v konkrétní oblasti. Úspěšná implementace jakéhokoli rámce vyžaduje přísný design a nejnovější technologie, jako je cloudová platforma. Značný počet nových diagnóz BC nás také motivuje k zavedení mnohem dřívějšího diagnostického systému. Proto vyvíjíme systematický model schopný detekovat abnormality, jako je rakovina prsu, u dospělých žen starších 26 let. Tato disertační práce představuje nový rámec pro detekci anomálií v lékařských obrazech, jako jsou termální obrazy prsu a magnetická rezonance v mozku.

The list of abbreviations

Performance	Formula	Description
Accuracy (A)	$\frac{TP+TN}{TP+FP+FN+TN}$	Correct prediction upon the total number of images
Precision (Pr)	$\frac{TP}{TP+FP}$	Correctly predicted images upon the total number of predictions as positive
Recall/Sensitivity (Rec)	$\frac{TP}{TP+FN}$	Correctly predicted images upon the total number of actual positive predictions
F1 score (F1)	$2 \times \frac{Pr \times Rec}{Pr+Rec}$	A combined measure of accuracy
Specificity (Sp)	$\frac{TN}{TN+FP}$	Correctly predicted as unfavorable upon the total number of actual negative predictions

Abbreviation	Explanation
PCA	Principal Component Analysis
RAD	Robust Anomaly Detection
CNCEC	Closest Neighbor Cluster Entity Center
SVM	Super Vector Machine
k-NN	K-Nearest Neighbor
FCM-ANN	Fuzzy C-Means and Artificial Neural Network
CANN	Conventional Artificial Neural Network
IoT	Internet of Things
WSI	Whole Slide Imagery
CAD	Computer-Aided Diagnosis
LR	Low Resolution
PLS	Partial Least Squares
BM3D	Block Matching 3D

ROI	Region Of Interest
ROC	Receiver Operating Characteristic curve
GA	Global Analysis

Contents

1. Introduction

A classification framework can help understand the models of software components by explaining their fundamental principles. As defined in (Crnkovic et al., 2011), a framework comprises several elements called components; each component is linked to another component to form a life cycle (see **Figure 1**). A component model defines standards for the observations and analysis properties that individual components must meet and classification methods for the components' composition. It is essentials to follow the lifecycle to implement a given model. Additionally, a framework can help assess a component model's suitability for a particular set of requirements or a specific application area.

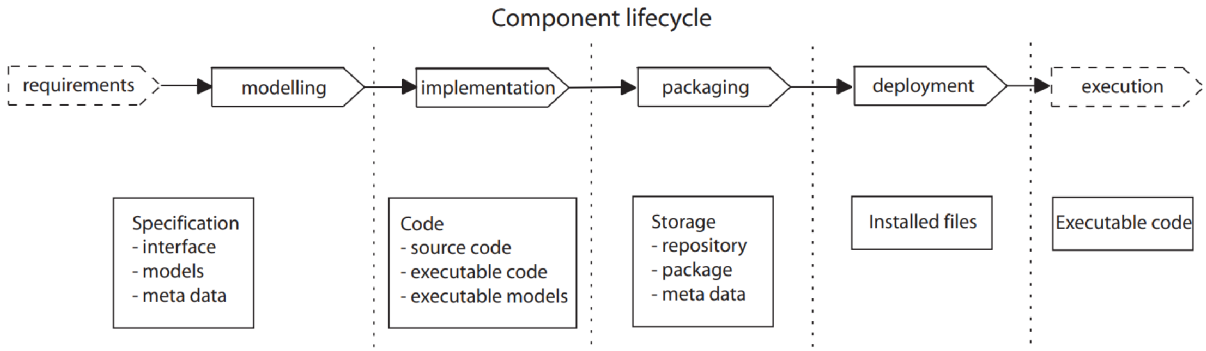

Figure 1. The list of components in a given framework describes a lifecycle that needs to be followed to implement and deploy the model (Crnkovic et al., 2011).

In multiple disciplines such as, but not restricted to signal processing, statistics, econometrics, finance, manufacturing, networking, and data mining, anomaly detection (also the detection of outliers) is the identification of rare items, events, or observations that raise suspicion by differing significantly from the majority of the data (Zimek & Schubert, 2017). As a rule, abnormal elements will result in bank fraud, a structural defect, medical issues, or errors in a text. Anomalies are also called outliers, novelties, noise, deviations, and exceptions. Through literature, anomaly detection techniques can be grouped into three categories (Chandola et al., 2009). Unsupervised anomaly detection techniques detect anomalies in an unlabeled test dataset, assuming that most elements in the dataset seem standard for those instances that appear to match least the rest of the dataset. Semi-supervised anomaly detection techniques build a model representing normal behaviour from a given set of normal training data, then test the learned model's probability to generate a test

instance. In contrast, supervised anomaly detection techniques require a dataset that has been labelled as "normal" and "abnormal" and involves the training of a classifier (the main difference with many other statistical classification problems is the inherent imbalanced nature of outlier detection).

Having clarity on “classifying framework” and “anomaly detection”, this study focuses on their application to medical images. It will support its founding through two case studies focusing on breast anomaly as a tumor in the breast and Brain anomaly as a tumor in the brain. With advances in Machine Learning (ML), in-depth analysis is now possible for medical Magnetic Resonance Imaging (MRI) images as well as Infrared Images (IR). Said that ML appears to be very powerful for tasks such as segmentation and classification, where Deep Neural Networks (DNN) play an essential role. Also, several delays can be observed in the hospitals' diagnosis workflow; the number of incoming patients and screen images can explain this. As in most developing countries, the population is getting older and sometimes faces several various Cancer such as brain cancer or Breast Cancer, which requires a considerable amount of a screening diagnosis to monitor the evolution or fight it by making screening images. All those generated images can be understood as a certain amount of data that doctors need to process.

Moreover, the volume of data created by various medical protocols, including diverse medical imaging methods, becomes overwhelming and confusing to analyze without automated solutions—the reason why the need for Computer-Aided Diagnosis (CAD) systems has increased. CAD, if coupled with powerful learning algorithms, will considerably boost the decision-making mechanism of doctors. Keeping this state of mind, the proposed Architecture will combine two sub-models which are respectively: a U-network (U-net), which will be responsible for extracting the area where the tumor is most likely to be present, and a "cancer stage" module which will work in some cases as the couple (mathematical morphology, DNN) where mathematical morphology and DNN will respectively take the output of the U-net as input, highlight the Region of Interest (RoI) and classify this RoI in one of the four stages (T1 to T4).

The other parts of this document are structured as follows: Section 2 will address the study's objective; Section 3 will discuss the content analysis chosen for this research; Section 4 will present the state-of-the-art model in infrared (IR) images and magnetic resonance (MRI); Section 5 will explain some fundamental concepts of our architecture; Section 6 will show the workflow

and contains two case studies; Section 7 will present results in the thesis's defined objectives; Section 8 will present the implementation of the given Architecture; Section 9 will discuss the fulfilment of the thesis dissertation. These key points are addressed one after another in the following chapters: At last, a conclusion will be given.

2. Goals of the Dissertation

Efficient Computer-Aided Diagnosis (CAD) systems are instruments intended to investigate medical data more efficiently in less time, to support doctors in their day-to-day tasks. In that state of mind, this thesis's main goal is to present *a novel framework for detecting anomalies in medical images, more specifically, brain tumor or breast cancer*. Still, it can be subdivided into two sub-goal to follow up the progress of the work efficiently.

- The first sub-goal is to design and implement a flexible model capable of detecting and classifying brain tumors or breast cancer.
- The second is to design and implement a working prototype.

The present image-based CAD systems will study various tasks and be subject to intense training on the problem inquiry features. The latter will be expressed and estimated using mathematical expressions. Through this research, the above main goal will be tackled using two case studies which will answer or delve into the research questions below:

- Considering thermal images of the breast taken under specific conditions, can a systematic model be developed to detect anomalies such as breast cancer in adult women over 26?
- Given MRI images of the brain taken under specific conditions, can a systematic model be developed to detect abnormalities like a brain tumor?

3. Methodology

The methodology concept refers to the primary way of "conducting" research or practice specialization in your daily activities. Therefore, the term research methodology refers to how research is carried out within a discipline, and this methodology is generally limited to the domain in question. Furthermore, research methodology refers to all methods explicitly used during the study. The goal is to describe and include all the parameters that led to acquiring a particular dataset (or findings) so that they can be replicated elsewhere and by other researchers wholly and accurately. To support my research, I apply qualitative content analysis on secondary data obtained from webofscience.com processed with the help of Atlas tools (*ATLAS.ti*, n.d.), and I further push the research using case studies.

3.1. Conceptual analysis

Conceptual analysis, also known as thematic analysis, is a qualitative analysis technique that selects a concept for consideration, and analysis involves identifying and counting its presence. At this stage, I will develop a coding scheme (see **Table 1**) that I will apply to the secondary data, thus extracting relevant information while being attentive to the research question specified in the previous section.

Table 1. The coding scheme of the content analysis

Category	Code	Example
Breast Cancer facts	age of breast cancer diagnosis	**"**We classified age into three groups: 20–40, 41–60, and 61–100 years." In (Guo et al., 2020). "Breast cancer is the primary cause of the increasing mortality rate among females aged 20 to 59 years old [4]. Thus, early detection of breast cancer can lower the female mortality rate." In (Siddiqui et al., 2021)
	breast cancer profile	"Using clustering methods on breast cancer profile, Perou et al. [10] recognised four distinct molecular classes of breast cancer based upon gene expression data: HER2, basal, luminal and normal. Extending the work, Sorlie et al. [11] subdivided the Luminal group into three: A, B, and C." in (Agrawal et al., 2019) "Female carriers of pathogenic variants in BRCA1/2 have a high lifetime risk of breast and ovarian cancer. For carriers of pathogenic variants in BRCA1, the average cumulative risks by age 80 years is 72% (95% confidence interval 65–79%) for breast cancer and 44% (36– 53%) for ovarian cancer, and the corresponding estimates for BRCA2 are 69% (61–77%) and 17% (11–25%) respectively [4]." in (Meiser et al., 2021)
	deadly cancer	"Breast cancer is the most prevalent and among the most deadly cancers in females" In (Tong et al., 2020).

		"Patients with breast cancer have highly variable survival lengths, indicating a need to identify prognostic biomarkers for personalized diagnosis and treatment" in (Tong et al., 2020) "Breast cancer is often a fatal disease that has a substantial impact on the female mortality rate" in (Siddiqui et al., 2021)
	each breast cancer is unique	"Every case of breast cancer is unique, and treatment must be personalized to incorporate a woman's values and preferences." In (Wyatt et al., 2019)
	invasive method	"The biopsy is another effective and precise breast cancer detection method. It involves taking a tissue sample from an affected part of the breast. This sample is then examined through a microscope by a pathologist, who detects and classifies the tumor. This method has recently played an important role in diagnosing breast and other types of cancers" in (Siddiqui et al., 2021)
	side effects of mammography	"The repetitive use of harmful radiation can also lead to cancer" in (G. Ma & Soleimani, 2020)
anomaly detection / Breast Cancer facts	a mammogram is not suitable for young women	"Mammogram, ultrasound, and biopsy are routinely applied to diagnose breast cancer and obtain those factors. In some cases, computerized tomography (CT) and magnetic resonance imaging (MRI) are also needed to conduct further tests. However, the mammogram, which is the standard method, is not suitable for young women as they have denser breasts." In (G. Ma & Soleimani, 2020) "reading mammographic images is quite challenging" in (Siddiqui et al., 2021) "10-30% of the breast glands depicted in mammographic images cannot be identified by radiologists" in (Siddiqui et al., 2021)
Why Breast cancer CAD?	Effectiveness of modern applications	"Tailored mobile applications may optimize care by facilitating shared decision making and knowledge transfer, and they may also enhance the experience of patients as they navigate through their breast cancer journey." In (Wyatt et al., 2019). "Computer-aided detection (CAD) systems have been used to improve different aspects of life, particularly in the health sector, for the last 20 years." In (Siddiqui et al., 2021) "Classification and segmentation are applied to the breast ultrasound dataset through CAD. Image classification is performed through the transfer learning technique with a pre-trained model, and then all images are categorized as either cancerous or noncancerous" in (Siddiqui et al., 2021) "This model, which was based on the support vector machine (SVM) and the extreme learning machine (ELM), obtained an accuracy of 94.11%. " in (Siddiqui et al., 2021)
	feasibility of a systematic model	"In this study, we demonstrated the feasibility of performing breast cancer distant recurrence prediction using machine learning as well as knowledge-guided convolutional neural network (K-CNN) with the aid of natural language processing (NLP) techniques. Comparing with previous approaches, we illustrated an implementation that required less clinical expertise and data curation." In (H. Wang et al., 2020) "Deep learning effectively assists existing methods, such as mammogram screening and biopsy, in examining and diagnosing breast cancer. This paper proposes an Internet of Medical Things (IoMT) cloud-based model for the intelligent prediction of breast cancer stages. The proposed model is employed to detect breast cancer and its stages. The experimental results demonstrate 98.86% and 97.81% accuracy for the training and validation phases, respectively. In addition, they demonstrate accuracies of 99.69%, 99.32%, 98.96%, and 99.32% for detecting ductal carcinoma, lobular carcinoma, mucinous carcinoma, and papillary carcinoma." In (Siddiqui et al., 2021).

** Due to space constraints, only the most relevant codes are listed here.*

3.2. Relational analysis

Having clarity of the essential themes and concepts extracted from the above sub-section,

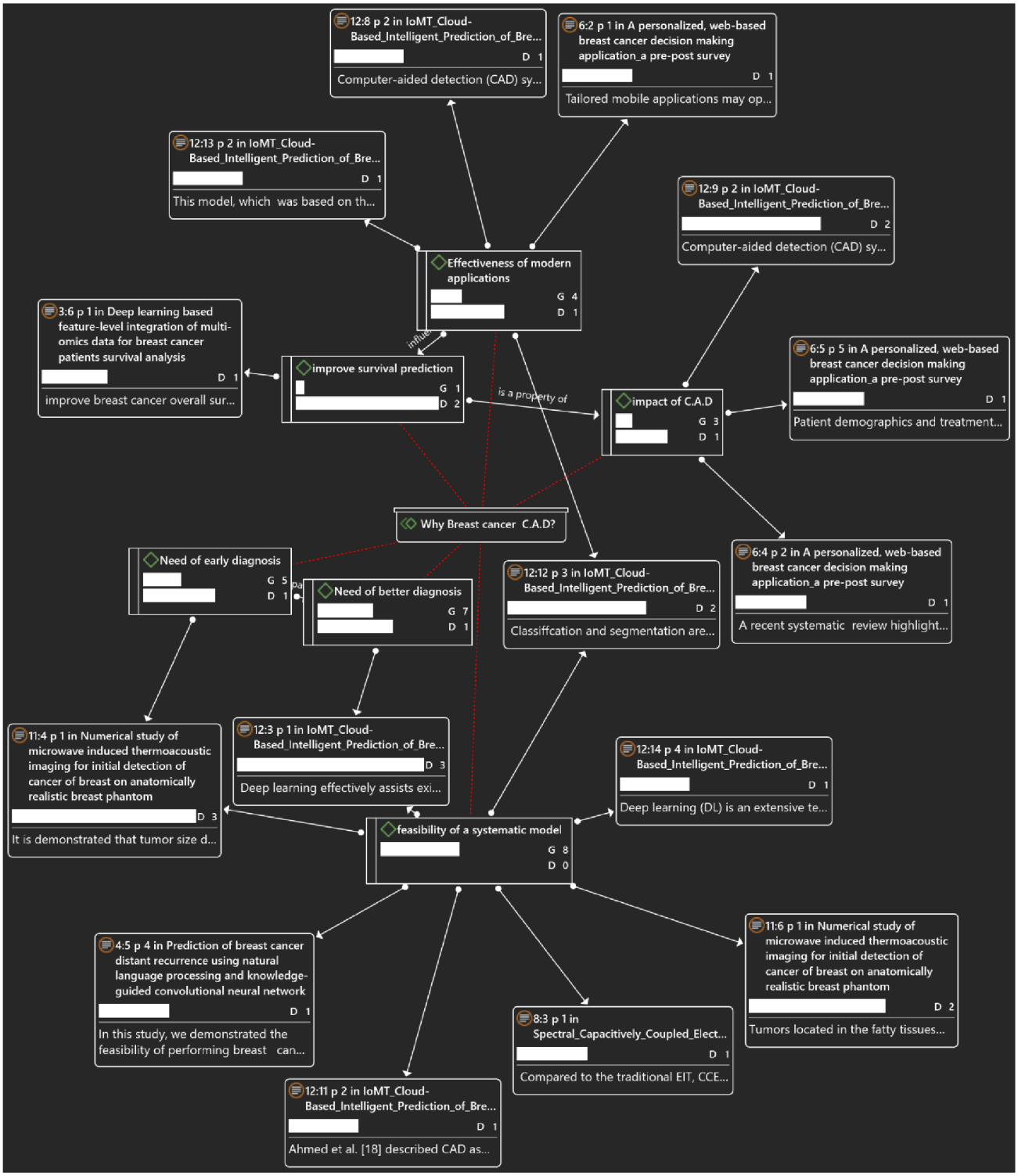

Figure 2. Relationships among entities: these entities answer the question " why breast cancer C.A.D?" and the figure shows the relationship between these entities for a better understanding. (the white arrows point to the quote, and the red arrows indicate the entities that belong to the category)

Now it's time to explore the relationships and ideas between the pieces to explain their meaning. As noted, (see

Figure 2) Computer-Aided Diagnosis (CAD) appears to be a relevant tool in current diagnosis systems, as physicians are faced with a considerable number of patients daily. Content analysis reveals the importance of better diagnosis and CAD tools to facilitate diagnosis further.

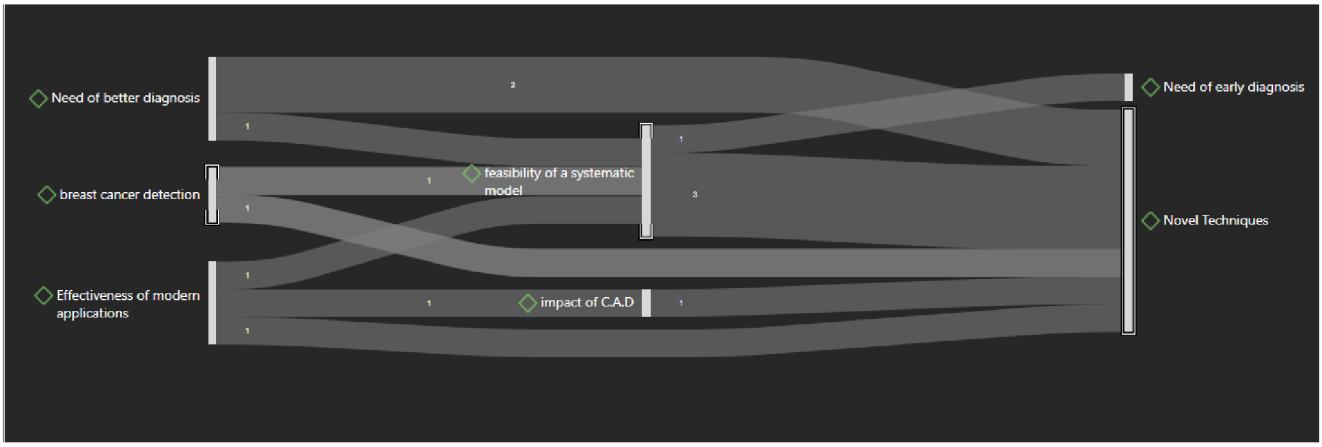

Figure 3. Relationship between the impact of CADs, their efficiency, their novelty in terms of techniques used and their feasibility.

Through the literature, several techniques have been explored, emphasizing the practical implementation of these methods. The analysis reveals a considerable number of articles in this direction and a strong relationship (see **Figure 3**) between the impact of CADs, their efficiency, their novelty in terms of techniques used and their feasibility.

Several CADs are already available, and modern CADs are based on machine learning techniques which are essential components of the proposed model of this thesis. Thus, this relational analysis (see **Figure 4**) and the case studies developed in section 6 have proven the feasibility of this model.

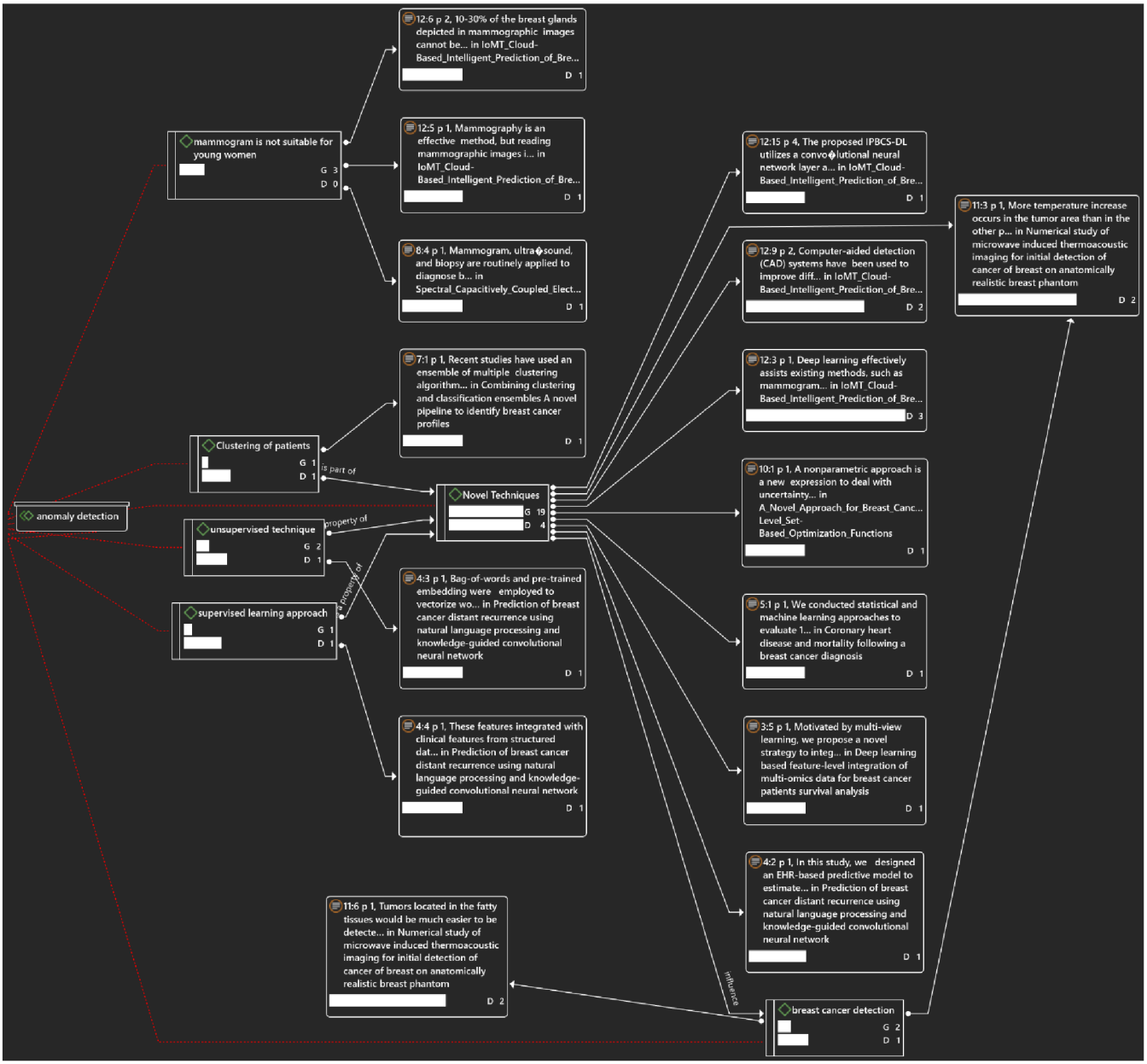

Figure 4. The analysis reveals a significant relationship between the quotes of several documents and the "novel technique" used here as a code. (the white arrows point to the quote, and the red arrows indicate the entities that belong to the category).

4. Related Works

For many, the term “anomaly detection” refers to the process of detecting a specific item that does not follow the rules or characteristics shown by the other components of the group. It is sometimes assimilated to an outlier; Over the past year, there has been a profound interest in the scientific community, with the direct consequence of a considerable number of articles talking about the so-called “anomaly detection” (see Table 1).

4.1.Anomaly detection and recent techniques

In the medical field, the term anomaly can designate a disease that is difficult to detect but can be estimated based on a collection of information from behavioural habits or blood samples. The presence of anomalies or outliers in time series data can negatively affect automated decision-making applications' effectiveness. For example, various services depending on traffic data can be negatively affected by anomalies in car traffic. The authors (Jia et al., 2019) presented in their article an automated method for detecting anomalies based on a supervised Long Short-Term Memory (LSTM) and a statistical analysis (Introduction to Statistical Learning, n.d.). They formed an LSTM neural network to predict non-robust statistical properties and combine them with robust properties to determine anomalies in time series data. They were considering the segmentation and adaptability of the parameters of their model for the anomaly test. Likewise, the supervised learning models trained on a market anomaly have often been used in research, as shown in (Malhotra et al., 2015). The latter (Malhotra et al., 2015) proposed an anomaly detection model using the LSTM neural network for time series data. The given method predicts the time series’ value based on the error, and the anomaly test is performed. However, the technique presented uses the LSTM network as a predictor of time series. Although, the method has been used to detect anomalies where this type of model is sufficiently adequate to predict a time series’ future values, as shown in (J. Zhou & Tung, n.d.), (X. Ma et al., 2015). Furthermore, no precise statistical analysis was carried out in the context of the work given.

The authors of (Salman et al., 2017) used linear regression and random forest to detect anomalies and their categorization in the multi-cloud environment. The method was precise (detection at 99%, categorization at 93.6%) for a particular data set. However, the technique used a labelled data set where the anomalies and their types are known before the training model.

Most of the time, the abnormalities are not known in advance, or new types of anomalies appear. Supervised learning on labelled anomalies cannot be used effectively in such cases, as there is not enough training data available. Principal Component Analysis (PCA) was also used for the detection of anomalies. Likewise, Netflix has proposed a method for detecting anomalies using Robust Anomaly Detection (RAD) (RAD — Outlier Detection on Big Data - Netflix TechBlog, n.d.). Here, the methodology detects any anomalies in the unusual login process or failed bank transaction to alert end users. However, the data that has been used here is in a different form and not historical data. *Grouping* is also another technique used in the literature to detect anomalies. The study (Lin et al., 2015) proposed a method to represent the nearest and Closest Neighbor Cluster Entity Center (CNCEC). The proposed method works better than the traditional approach based on k-NN or classic SVM. In their research, the authors (Pandeeswari & Kumar, 2016) proposed a method of detecting anomalies using a hybrid of clustering algorithms Fuzzy C-Means and Artificial Neural Network (FCM-ANN). The technique presented is more effective than the Nave Bayes classifier and the Conventional Artificial Neural Network (CANN), even for low-frequency attacks. However, new valid models appear frequently using the Internet of Things (IoT) sensors (Ahmed et al., 2016). Thus, incorrect classification in the clustering approach can disrupt the main objective of detecting anomalies.

Back to medicine, let's explore some research improvements. The authors of (Al-Olofi et al., 2018) introduced an increase in medical pathology practices in their study. They implemented Whole Slide Imagery (WSI), which is created using a computerized system that assembles, scans, and stores glass slides of pathology samples in digital images. WSI provides a pyramid construction multi-resolution of gigantic gigabytes due to the need to contain many tissue details. The authors noted significant difficulties faced in image analysis, data storage, and WSI phased transmission. They have developed a Computer-Aided Diagnosis (CAD) system to detect cancer abnormalities in WSI images of breast lymph nodes under Low Resolution (LR) and noise conditions.

Table 2. Anomaly detection reference through pieces of literature

Definition	Title	Year	Journal	Category (Web of Science (WoS))	Journal Rank (WoS)
"Anomaly detection is an important application field of evolutionary algorithm. Unlike traditionally anomaly detection, group anomaly detection aims to discover the anomalous aggregate behaviors in data points. "(Song et al., 2020)	Group anomaly detection based on Bayesian framework with genetic algorithm	2020	INFORMATION SCIENCES	COMPUTER SCIENCE, INFORMATION SYSTEMS	Q1
"Studies of anomaly detection often focus on pregnancies at risk for anomalies and on the yield of detailed sonography, topics less applicable to counseling low-risk pregnancies about the benefits and limitations of standard sonography." (Byrne et al., 2020)	Utility of follow-up standard sonography for fetal anomaly detection	2020	AMERICAN JOURNAL OF OBSTETRICS AND GYNECOLOGY	OBSTETRICS & GYNECOLOGY	Q1
"This paper is an effort to encapsulate the various developments in the domain of different unsupervised, supervised and half supervised brain anomaly detection approaches or techniques proposed by the researchers working in the domain of the Medical image segmentation and classification."(Bhatele & Bhadauria, 2020)	Brain structural disorders detection and classification approaches: a review	2019	ARTIFICIAL INTELLIGENCE REVIEW	COMPUTER SCIENCE, ARTIFICIAL INTELLIGENCE	Q1
"As this study is targeting anomaly detection (also known as outlier detection in a one-class scenario), the extent of deviation is also measured and verified against MRI results provided by a radiographer."(Rasheed & Tang, 2020)	Anomaly Detection of Moderate Traumatic Brain Injury Using Auto-Regularized Multi-Instance One-Class SVM	2020	IEEE TRANSACTIONS ON NEURAL SYSTEMS AND REHABILITATI	ENGINEERING, BIOMEDICA	Q2

			ON ENGINEERING		
"Reed–Xiaoli detector (RXD) is recognized as the benchmark algorithm for image anomaly detection; however, it presents known limitations, namely the dependence over the image following a multivariate Gaussian model, the estimation and inversion of a high-dimensional covariance matrix, and the inability to effectively include spatial awareness in its evaluation."(Verdoja & Grangetto, 2020)	Graph Laplacian for image anomaly detection	2020		COMPUTER SCIENCE, INTERDISCIPLINARY APPLICATIONS	Q1
"Anomaly detection is not limited to specific definitions of pathologies and allows for training on healthy samples without annotation. Anomalous regions can then serve as candidates for biomarker discovery. Knowledge about normal anatomical structure brings implicit information for detecting anomalies."(Seeböck et al., 2020)	Exploiting Epistemic Uncertainty of Anatomy Segmentation for Anomaly Detection in Retinal OCT	2020	IEEE TRANSACTIONS ON MEDICAL IMAGING	COMPUTER SCIENCE, INTERDISCIPLINARY APPLICATIONS	Q1
"Anomaly detection is a very vital area in medical signal and image processing due to its importance in automatic diagnosis"(Sedik et al., 2019)	Efficient anomaly detection from medical signals and images	2019	INTERNATIONAL JOURNAL OF SPEECH TECHNOLOGY	N/A	N/A
"To this end, this paper combines visibility attribute extraction network (VAE-Net) and bi-directional gated recurrent unit (BiGRU) into cascade networks to solve the tasks of attribute extraction and anomaly detection."(J. Zhang et al., 2019)	Visibility Attribute Extraction and Anomaly Detection for Chinese Diagnostic Report Based on Cascade Networks	2019	IEEE ACCESS	COMPUTER SCIENCE, INFORMATION SYSTEMS	Q1

“One major problem type of machine learning is anomaly detection. Its goal is to identify abnormal data points (outlier) between the normal data instances. Anomaly detection has a wide scope of applications in industrial and scientific areas.”(Schwenzfeier & Gruhn, 2018)	Towards a practical process model for Anomaly Detection Systems	2018	2018 IEEE/ACM 1ST INTERNATIONAL WORKSHOP ON SOFTWARE ENGINEERING FOR COGNITIVE SERVICES (SE4COG)	N/A	Q1
“MIL has never been used for anomaly detection in general, both at a global and local level. The advantage of MIL, over strongly supervised CAD systems, is that clinicians are not required to manually segment mammograms to collect the ground truth required for training: examination reports are enough for supervision”. (Quellec et al., 2016)	Multiple-Instance Learning for Anomaly Detection in Digital Mammography	2016	IEEE TRANSACTIONS ON MEDICAL IMAGING	COMPUTER SCIENCE, INTERDISCIPLINARY APPLICATIONS	Q1
“Algorithms for detecting anomalies in images can be divided into reference-based and reference-free ones. In reference-based methods, anomalies are detected by comparing the test image against a reference one that does not contain anomalies and can be used as a template. These methods are applied in many industrial scenarios, e.g., in semiconductor production where wafers correspond, up to some small misalignment, to a reference template”(Carrera et al., 2017)	Defect Detection in SEM Images of Nanofibrous Materials	2017	IEEE TRANSACTIONS ON INDUSTRIAL INFORMATICS	COMPUTER SCIENCE, INTERDISCIPLINARY APPLICATIONS	Q1

In particular, (Al-Olofi et al., 2018) studied a transfer learning approach to find scale correspondences between WSI levels using Partial Least Squares Regression (PLS). The learned scale maps can be used to detect anomalies in LR images and thus reduce computation costs in anomalies detection. Besides, the author (Al-Olofi et al., 2018) explored the outcome of various noise levels on detection performance where different simulated scenarios are applied. WSI images can be corrupted by Gaussian noise. Several denoising algorithms, namely denoising with PLS, Block Matching 3D (BM3D), and the combination of PLS and BM3D could be applied to improve the quality of WSI, hence enhancing the detection of anomalies.

4.2.Extraction of the region of interest in the Breast

The authors (Cheng et al., 2016; Huang et al., 2015) used the grey-level thresholding method to detect the contour of growing lesions in their study. First, the Region of Interest (RoI) was determined by thresholding, then a utility function of maximization was applied to the RoI to obtain the contour of the lesion.

The utility function was the mean radial derivative, which calculated the results of the radial direction from the start point to the limit. The starting point for each image was chosen as the center of return on the investigation. The Area Under the Curve (AUC) and the Receiver Operating Characteristic curve (ROC) were used to assess the performance, 0.91.

Authors (Moon et al., 2014) have proposed a method of segmentation of breast cancer based on clustering. The technique consisted of three parts: The first part was the quantitative grouping of tissues. The second was to differentiate the tissues inside a tumor from other tissues. Finally, 3-D mean shift clustering was used to select tumor tissues based on echogenicity.

Morphology and echogenicity characteristics were extracted, and logistic regression was used to classify benign and malignant tumors. The process achieved 89.19% sensitivity of tumor detection on a database with 148 tumors.

Shan et al. proposed a fully automatic segmentation of breast cancer, a method based on neutrosophic L-means clustering (Shan et al., 2012). They used an intuitive starting point selection algorithm to generate the RoI and proposed a new contrast enhancement method based on the frequency and spatial domain. As a result, a clustering method combined with neutrosophic logic, neutrosophic L-means clustering, has been developed. The technique achieved a True Positive Rate (TPR) of 92.4%, a false positive rate (FPR) of 7.2%, and a similarity rate of 86.3%; Hausdorff

Mean Error (AHE) of 22.5 pixels and Mean Absolute Error (AME) of 4.8 pixels on a Breast Ultrasound Segmentation (BUS) database with 122 frames, respectively.

Xian et al. (Xian et al., 2015) have developed a fully automatic segmentation method based on the characteristics of BUS images in the frequency and spatial domain. The technique consisted of two parts: fully automated generation of breast tumor RoI and robust RoI-based tumor segmentation. In the RoI generation step, a fully automatic reference point selection method was designed using breast anatomy, where the tumor location was in the middle of the pre-mammary layer and the retro layer of the breast. Note that the average offset algorithm was used to extend the reference points as starting points. Finally, the return on the investigation of the tumor was calculated by the seed points. A minimization cost function was used in the tumor segmentation step, and the frequency and spatial boundary information were used as a constraint of the cost function. The approach achieved 91.23% TPR, 9.97% FPR, and a similarity rate of 83.73% using a data set of 184 images.

Deep neural networks have been used for image segmentation and ranking. In (Cireşan et al., 2013), deep arrays have been proposed for histologic breast imaging and mammographic mass segmentation. Deep learning approaches have also been used in magnetic resonance. Segmentation of the image (Dolz et al., 2020), the radiographic image and the tomodensitometric image. A deep learning approach has been applied for the detection of breast cancer (*Automated Breast Ultrasound Lesions Detection Using Convolutional Neural Networks | IEEE Journals & Magazine | IEEE Xplore*, n.d.). Three network structures were used: patch-based LeNet (Lecun et al., 1998), U-Net (Ronneberger et al., 2015), and transfer learning with a pre-trained fully convolutional network (FCN) with AlexNet (Krizhevsky et al., 2012).

Going through authors (Rampun et al., 2018) paper, An SVM (Support Vector Machine) classifier is used in their study. The latter reveals the use of local pattern models (LPM) in mammograms to categorize mammographic density. To maximize the texture information, a multi-resolution method was adopted, and the impacts of many neighbourhood topologies were studied.

Despite the general interest in mammography, many effective models have emerged to overcome the challenges of mammography. In the same vein, several articles have mentioned the importance of near-infrared fluorescence (NIRF) in the cancer diagnosis process. One important aspect to note is the necessity for the object being analyzed to produce a powerful NIRF light signal so that the

taken image includes a considerable amount of information with a slight difference from the actual state of the breast.

To raise the likelihood of success, it is required to localize the cancerous area at its early stage and follow the treatment as strictly as possible. Despite this common notion, it is sometimes difficult to get accurate information on the tumor (tumor depth, thermogram, and heat) (Amri et al., 2016). In the same direction, authors (Boogerd et al., 2017) mention magnetic resonance imaging (MRI), slightly sensitive to lesions smaller than 1 cm due to their limited spatial resolution. According to the study (Kandlikar et al., 2017), which elaborated considerable negative aspects of frequent mammography, they point out the rate of false-positive diagnoses after ten years of mammography was 49.1%. Another research showed that a decrease in tumor progression could be observed by having a sentinel lymph node biopsy (NLS) (Pleijhuis et al., 2011). However, authors (Kontos et al., 2011) are warning for the idea that decision-making cannot be done just with breast cancer thermography data. Still, computer aide equipment (CAE) can use these images to get a positive outcome, as shown in (Avila-Castro et al., 2017). A simulation, which can be assimilated to a thermal distribution of located cancer cell of size 2 cm and subject to a metabolic ration of approximately 28,999 W / m3 (see **Figure 5**) which illustrates a temperature repartition between 36.858 to 37.362 degree Celsius, a various temperature distribution between cancerous cell and healthy cells from the same patient.

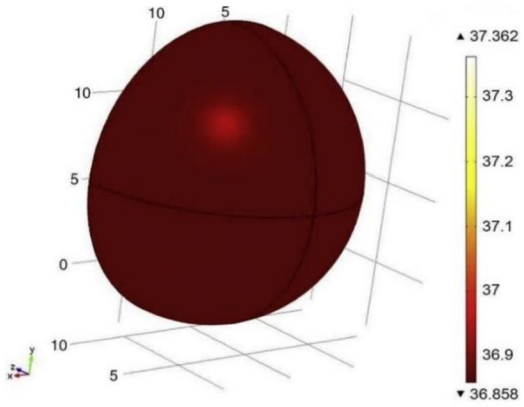

Figure 5. A thermal distribution of located cancer cells of size 2 cm and subject to a metabolic ratio of approximately 28,999 W / m3 (image derived from (Avila-Castro et al., 2017)).

After being cooled for 1 minute, the paper presented a max thermal contrast for a breast having a tumor of a 10 mm diameter and depth of 5 mm. The thermal graph processes are read, and its

associated time was obtained from the optimal transient thermal. Such analysis gives the parameters obtained from the breast's surface. While the warm-up phase, the area surrounding the cancerous cells will be more heat and gradually fall back to a stable temperature.

Authors (Isard et al., 1988) came out with a study on approximately five thousand patients subject to a diagnosis for 13 years in the US. Their research found that 88% and 89% survival rates can be observed for the patient at the early stage of breast cancer. Similarly, a survival rate is shown in the graph by red colour (see **Figure *6***) was estimated for ten years. As mentioned, the results of (Isard et al., 1988) allow dressing an indicator for breast cancer patients can be achieved by considering the outcome of the thermography of a breast. However, keys take away from the author's (Head & Elliott, 2002) approximately 5,000-patients for 13 years study, have survival rate between five and ten was considerably lower for patients having Cancer than patients with normal thermograms.

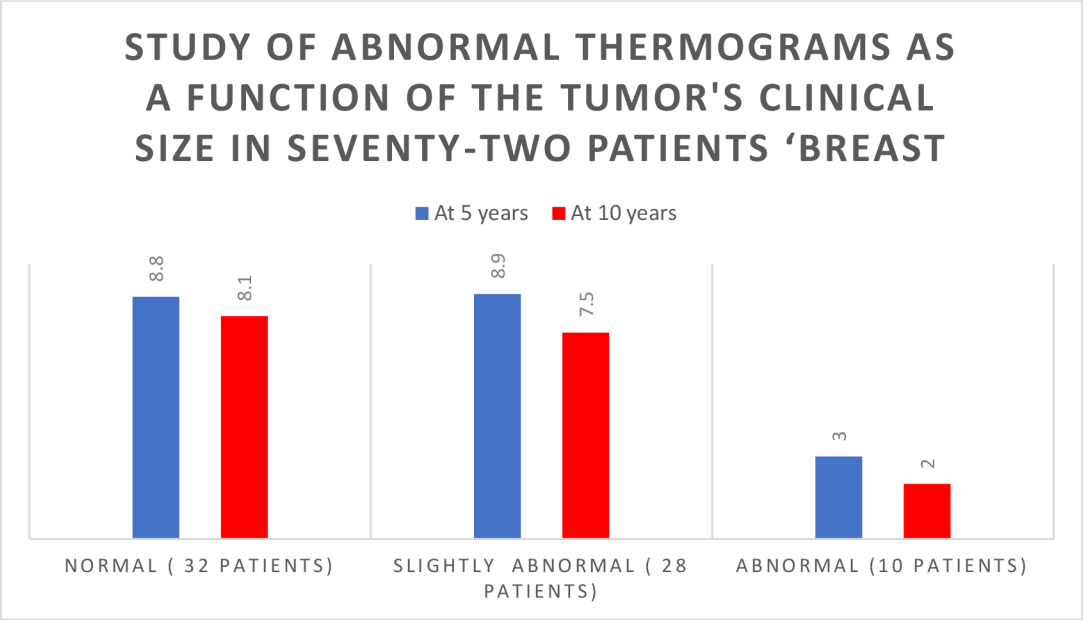

Figure 6. Study of abnormal thermograms as a function of the tumor's clinical size in seventy-four patients 'breast and a survival rate of seventy patients over thirteen years by a thermogram evaluation of five thousand patients (the range used in the Y-axis, is 0 to 10. In other words, 10 means 100 % survival rate).

The author (Isard et al., 1988) published research of around 5,000 patients subject to a diagnosis for 13 years in the US (Isard et al., 1988). Among them, seventy patients got a reasonable survival rate compared to the result of the thermogram. However, that was not the case described by authors in (Head & Elliott, 2002), where a lower survival rate was observed. Patients with healthy or abnormal thermograms could have a five-year survival rate of more than 80 % but less than 90%, compared to thirty per cent for people with strange thermograms. Also, taking twenty per cent of those people, a survival rate was greater than 70% but less than 82% (See **Figure 6**). Based on these results, (Head & Elliott, 2002) sum up by considering thermography as an important prognostic indicator, especially for patients with tumors in their breast. Main elements of the study performed on 5040 patients (Isard et al., 1988): Survival rates at 5 and 10 years (twenty per cent to thirty per cent) were considerably lower for a patient diagnosed with breast cancer and having abnormal thermograms than those with normal thermograms. The author's conclusions in [35] confirm the importance of thermography in a forecast of patients with breast tumors.

Another author (Head & Elliott, 2002) came out with research on 326 subjects in the United States(US) (Head & Elliott, 2002). Only 28 % of abnormal thermograms were observed among one hundred subjects without breast cancer. In the opposite of the one hundred patients, prior diagnoses with breast cancer were made. Also, authors (Lozano & Hassanipour, 2019) remarked that more than seventy patients with fifty-three per cent of patients with cancer size less than 2 cm had a non-conform thermogram. It was also shown that a high level of ferritin concentrations was present in patients with abnormal thermograms and three prognostic indicators related to tumor growth: Proliferation index and DNA synthesis. Author (Lozano & Hassanipour, 2019) results also support the impact of accurate thermography on diagnosing a breast tumor.

Looking at several other factors, two particular points can be elaborated:

A genetic aspect: considering the author (S. J. Mambou et al., 2018), a clinical research project of 12 medium-term cancerous breast cells suggested twelve domains of study intending to enhance the processes of breast cancer treatment and detection rates of that disease. Bearing in mind, the goal of the study (come out with efficient tools to identify possible genetic predisposition of a given patient) in the third part of the paper, two genes (BRCA1 and BRCA2) were determined after looking at patients with suggestive family history and after obtaining their genetic test. The latter confirmed that a high risk of getting Cancer could be observed in patients with a genetic

predisposition. Besides, considering the sensitivity and complexity of genetic tests, such as significant risk hereditary of breast cancer, should come with an appropriate interpretation. Also, looking at recent studies, BRCA1 / 2 mutations treatment can be achieved using poly (ADP-ribose) polymerase inhibitors (PARPs) on patients with breast cancer.

Stages aspect: Authors (S. Mambou et al., 2019a) can assign one of the four stages to a given breast tumor:

- T1: The breast's tumor is about 20 millimetres (mm) and can be subclassified into either (T1a or T1b or T1c): a tumor (T1a) has a size greater than 1 mm (or close to 5 mm); a tumor (T1b) has a size greater than 5 mm but less than or equal to 10 mm; (T1c) a tumor has a size greater than 10 mm (or close to 20 mm);
- The tumor (T2) is more significant than 20 mm (or close to 50 mm).
- The tumor (T3) is more critical (or close to 50 mm).
- T4: Cancer has grown into the chest wall. This category can be divided into four sub-categories based on the given size of the cancerous area: At T4a, the tumor has developed in the chest wall; At T4b, cancer has evolved in the skin; at T4c, Cancer has already set in the chest wall and skin; at T4d, an inflammatory area is visible on the breast.

In a recent study (Krishna & George, 2021), the authors mentioned the lack of sufficient expertise in rural parts of India, which contributes to a higher death rate from breast cancer. This finding can be related to most of the non-develop countries. Despite the high death rate from breast cancer, very little existing work has been explored to integrate screening techniques with machine learning approaches and real-time communication to remote areas, secondary or tertiary hospitals. This approach is needed to develop scalable and affordable breast cancer screening technologies for the clinical prediction of breast abnormalities in remote country regions. Their research aims to produce a portable infrared imaging solution for remote breast health monitoring at a lower price. They introduced an architecture that takes advantage of an infrared image acquisition module (IAM), a transmission module (TM), and a screening module (SM).

The IAM comes with a thermal camera and associated software for acquiring thermal images of the breast. SM is the combination of four sub-modules such as pre-processing module (PM), automatic segmentation module (ASM), feature extraction module (FEM) and Classification module (CM). The main challenge in implementing MS is that the penetration of diagnosis

approaches based on thermography is hampered by the misclassification common in breast cancer diagnosis. The main reasons for this misclassification are low signal-to-noise ratio (SNR) and inefficient segmentation of breast regions in thermograms. An edge preservation technique based on a co-occurrence filter is adopted to design the PM to address these challenges. They use morphological and Distance operations where FEM extracts both statistical features and wavelet-based features from segmented breast ROIs.

In the authors' study (Jevnisek & Avidan, 2017), the co-occurrence filter is an edge-preserving filter that provides information about the boundaries within a texture and the boundaries between textures. This filter uses a bilateral filter (BF) to produce the weighted average of the neighbouring pixels of a reference pixel. The co-occurrence filter replaces a range of Gaussian filters in the BF, using a co-occurrence matrix, which provides pixel values that periodically co-appear within textured regions of an image. The more frequent pixels will have a higher weight in the co-occurrence matrix, which, when averaged together, smooths the image's texture. Pixel values that unusually co-occur will have a lower range in the co-occurrence matrix and will not mix [36]. Mathematically, a linear filter takes the form expressed in Eq (1)

$$G_i = \sum_{j \in \mathbb{N}(i)} \frac{W(i,j).G_j}{W(i,j)} \qquad (1)$$

Where G_i and G_j are output and input pixel values, i and j are pixel indices and $W(i,j)$ is the weight of the contribution of pixel i to the output of pixel j. The co-occurrences of the pixels in the image are integrated into the co-occurrence matrix. Overall, all the co-occurrences, the distances loaded by their distance in the two-dimensional plane, are incorporated into the matrix. And the effect of co-occurrence filtering on the breast thermograms is shown in the figure below (see **Figure 7**).

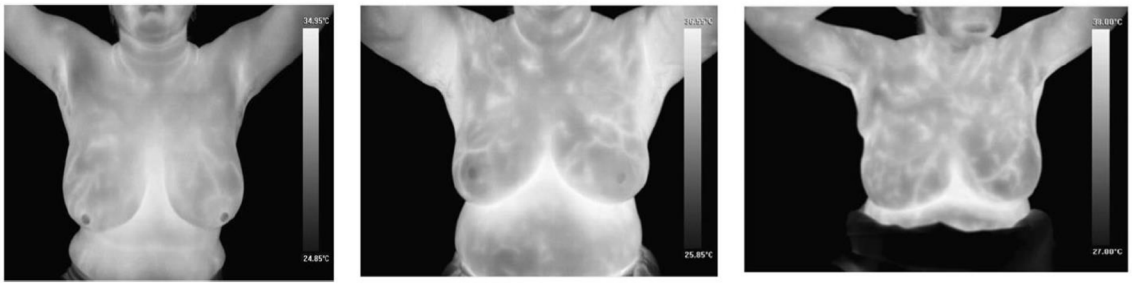

Figure 7. the effect of co-occurrence filtering on the breast thermograms (Krishna & George, 2021)

The subjective analysis showed that the pretreatment based on the co-occurrence filter refines the edges in the breast regions and preserves the boundaries that provide heat information patterns in thermograms.

To achieve automatic segmentation of the mammary region in a thermogram, authors (Krishna & George, 2021) proposed a technique combining morphological operations and Distance Regularized Level Set Evolution (DRLSE). The method consists of four steps:

- Removing the neck and shoulder parts from the body
- Removing fundus
- Removing lower limit
- DRLSE

Removal of body parts from the neck and shoulders Unwanted areas of the breast thermogram should be removed to extract ROIs from the breast. Upper body parts such as the neck and shoulder areas are removed from the thermograms by calculating local minima from the full thermogram projection.

Background elimination Numerous studies have reported Otsu thresholding for background elimination in the image (Boquete et al., 2012; J. Zhang & Hu, 2008). As this proved the effectiveness of background suppression, i also applied Otsu thresholding to remove background in thermograms.

Extraction of the Lower Limit To reach the regions of the inframammary folds, it is essential to define the precise coordinates of the pixels in the lower curvature of the breast image. The intensity of tissue shine is high in the region of the inframammary fold, helping to restrict the lower limit. The variation in brightness of the image is deduced by measuring the gradient of an image. The gradient is zero in regions of uniform intensity, and it is a rapid amendment or a non-zero slope. The value of the gradient in the horizontal direction (Gx), the vertical direction (Gy), the magnitude of the gradient vector, and the direction of the gradient vector are calculated from the intensity of the grey image.

4.3.Deep models applied to Magnetic Resonance Imaging (MRI)

Before the advance in Computer vision, radiologists used to perform a manual segmentation of the region of interest just by considering multimodal information presented by MRI images and the anatomical and physiological knowledge acquired through training and experience. The procedure involves the radiologist going through several slices of images slice by slice, diagnosing the tumor, and carefully drawing the tumor regions manually. Besides being a long task, manual segmentation also depends on the radiologist, and the segmentation results are subject to significant Intra and inter-rater variability. However, hand-operated segmentation is popularly used to evaluate the effects of semi-automatic and fully automatic methods.

As previously mentioned, computer vision techniques have evolved over the past decades due to several significant contributions, such as the paper (S. Mambou et al., 2018), which proposed a classification scheme for brain tumors based on the combination of texture features: wavelets and deep neural networks (DNN). Officially, the proposed system included four modules: feature extraction, feature selection, tumor classification, and segmentation. Mainly, image noise is suppressed. Next, the feature matrix is produced by combining wavelet texture features [greyscale co-occurrence matrix (GLCM) + wavelet GLCM], where GLCM is used to extract the texture from an image by performing the gray level transition over two pixels; in other words, it provides a joint distribution of gray level pairs of neighboring pixels in an image. Then, the selection of the relevant characteristics is carried out using the oppositional flower pollination algorithm (OFPA) because a large number of features are significant obstacles to classification. Next, the author categorized the brain image based on the characteristics selected using DNN.

BraTS 2017 challenge (Kamnitsas, Bai, et al., 2017) top-performing submissions proposed several robust segmentation models (EMMA), and authors (G. Wang et al., 2018) offered to segment tumor subregions in cascade using anisotropic convolutions. EMMA takes advantage of a set of several independently formed architectures. In particular, EMMA combined the FCN (Long et al., 2015), U-net(Ronneberger et al., 2015), and DeepMedic(Kamnitsas, Ledig, et al., 2017) models and merged their segmentation predictions. While training, they used a batch size of 8 and a 3D patch crop of 64x64x64. Note that all the different EMMA models exhibited good generalization performance by winning the 2017 BraTS challenge. Authors (G. Wang et al., 2018) took a different approach, forming three networks for each tumor subregion in cascade. Each subsequent network took the output of the previous network (cropped) as an entry. Each network

had a similar structure and consisted of a large encoder part (with expanded convolutions) and a base decoder. They also break down the 3x3x3 convolution kernel into intra-slice (3x3x1) and inter-slice (1x1x3) kernels to save compute time and GPU memory. Authors (Isensee et al., 2019) have shown that a generic U-net architecture is adequate to reach competitive performance with some minor adjustments.

Brain tumor segmentation methods include discriminative and generative approaches. Discriminant and generative methods, respectively, extract characteristics from image representations, integrate prior knowledge, and model probabilistic distributions. The first method has flourished in recent years with the advancement of CNNs, as previous BraTS winners have demonstrated. The authors (Casamitjana et al., 2017) compare the performances of three CNN 3D architectures showing the importance of multi-resolution connections to obtain fine details in the segmentation of tumor sub-regions. The BraTS 2018 winner (Myronenko, 2018) proposed an asymmetric encoder-decoder architecture with a variational auto-encoder to reconstruct the image during training, which serves as a regularizer. At the same time, authors (Isensee et al., 2019) use traditional 3D-U-Net optimized evaluation metrics and co-trained with external data. The BraTS 2019 winners (Jiang et al., 2020) use two stages of a U-Net cascade formed from end to end. Finally(Zhao et al., 2020), applies several tips in three categories: data processing, model design, and optimization process to improve model performance. Brain tumors, Gliomas are the most common malignant with varying levels of aggression. The automated and precise segmentation of these malignant tumors on magnetic resonance imaging (MRI) is vital for clinical diagnosis. Convolutional Neural Networks (CNNs) have succeeded in various vision tasks such as classification, segmentation, and object detection. Fully convolutional networks (FCNs) (Long et al., 2015) perform end-to-end semantic segmentation for the first time with impressive results. U-Net (Ronneberger et al., 2015) uses an asymmetric encoder-decoder structure with hop-on connections to improve detail retention, thus becoming the dominant architecture for medical image segmentation. Many U-Net variants such as U-Net ++ (Z. Zhou et al., 2018) and Res-UNet(Z. Zhang et al., 2018) further improve image segmentation performance. Although CNN-based methods have an excellent representative ability, it is difficult to build an explicit long-distance dependency due to the limited receptive fields of the convolution nuclei. This limitation of the convolution operation raises challenges for learning global semantic information essential for dense prediction tasks like segmentation.

Inspired by the attention mechanism (Bahdanau et al., 2016) in natural language processing, existing research overcomes this limitation by merging the attention mechanism with CNN models. Nonlocal neural networks(X. Wang et al., 2018) design a plug-and-play nonlocal operator based on the self-attention mechanism capturing long-distance dependency in the feature map but suffers from high memory cost and calculation. Authors(Schlemper et al., 2019) proposed an attention-gate model, which can be integrated into standard CNN models with minimal computational overhead while increasing the sensitivity of the model and the accuracy of the prediction. On the other hand, Transformer (Vaswani et al., 2017) is designed to model long-term dependencies in sequence-to-sequence tasks and capture the relationships between arbitrary positions in the sequence. This architecture is proposed based solely on self-attention, completely freeing itself from convolutions. Unlike previous CNN-based methods, Transformer is not only powerful in modelling the global context but can also achieve excellent results on downstream tasks in the case of large-scale pre-training. Recently, Transformer-based frameworks have also reached top performance on various computer vision tasks. The authors of [7] presented a Vision Transformer which divides the image into patches and models the correlation between these patches in the form of sequences with Transformer, obtaining satisfactory results on the classification of the images. Another author (Touvron et al., 2021) further introduced a knowledge distillation method to form a Transformer.

5. Problem Definition

"Breast Carcinoma" appears as an uncontrolled growth of epithelial cells in the breast with approx 27% new cases in 2020 among 355 000 women in the European Union diagnosed with Breast Cancer (ESMO, n.d.). It is still the second death cancer after lung cancer for women(*Breast Cancer - Causes, Symptoms, Diagnosis, Treatment, Pathology*, 2020); this can be explained, as most of the time, Breast Cancer (B.C.) does not cause pain at its early stage (so less sign visible) but becomes painful when it has already spread among breast's tissues.

5.1.An essential overview of breast cancer

As shown in the figure (see **Figure 8**), breasts contend Glandular tissues responsible for producing milk, including fifteen to twenty lobules composed of several *alveoli*. This last is made of alveolar cells that secreted milk into the Lumen, then evacuated the fluid through the Duct. **Figure 8** shows the difference between a normal lobule and the abnormal one that can cause tumors.
Cells of Glandular tissue have receptors for hormones like progesterone, released by *Ovaries*, and prolactin released by *the Pituitary Gland*, which is responsible for the enlargement of the Alveolar, the division of cells, as well as their increase in number with a direct consequence of the increase of the lobular. Without those hormones, *Apoptosis,* which is program cell death necessary for Glandular cells' life cycle, will not happen.

B.C. can cause several complications, such as :

- The tumor causes local inflation, potentially damaging suspensory ligaments and lactiferous ducts, resulting in Fibrosis.
- Cancer can also invade pectoral muscle and skin.
- B.C. cells can find their ways into and block Lymphatic vessels, causing the skin to become dimpled and thickened.

They are several risks factors of B.C.; the most know can be enumerated as follow:

- Early age Menarche and Late age Menopause: Each time there is menstruation, there is an enlargement of the Alveolar and an increase of cells that go through *Apoptosis*.

Hence, genetic mutation is a risk for every cell division, leading to tumor formation (see **Figure 9**).

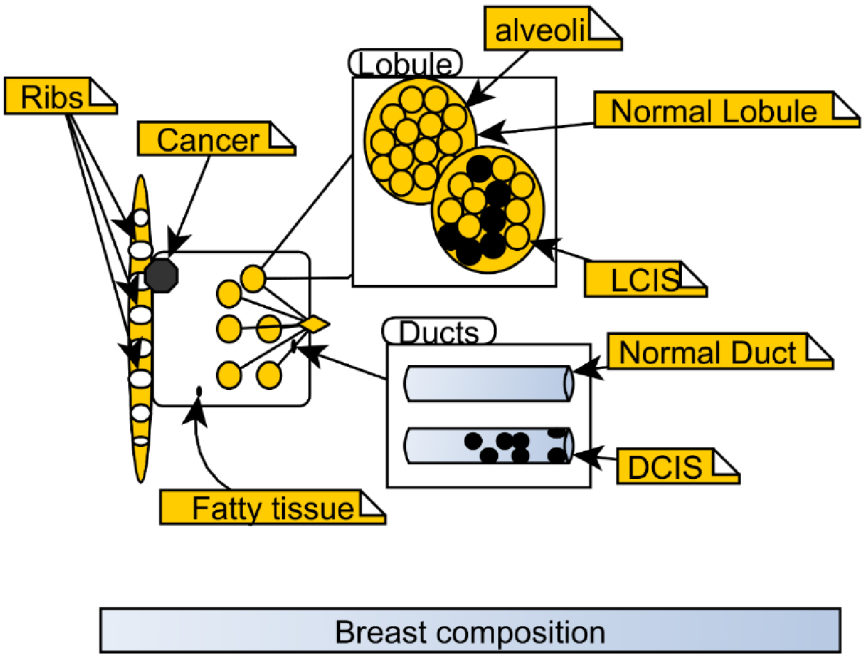

Figure 8. The breasts contend Glandular tissues responsible for producing milk, including fifteen to twenty lobules composed of several alveoli. This last is made of alveolar cells that secreted milk into the Lumen, then evacuated the fluid through the Duct. **(Own work).**

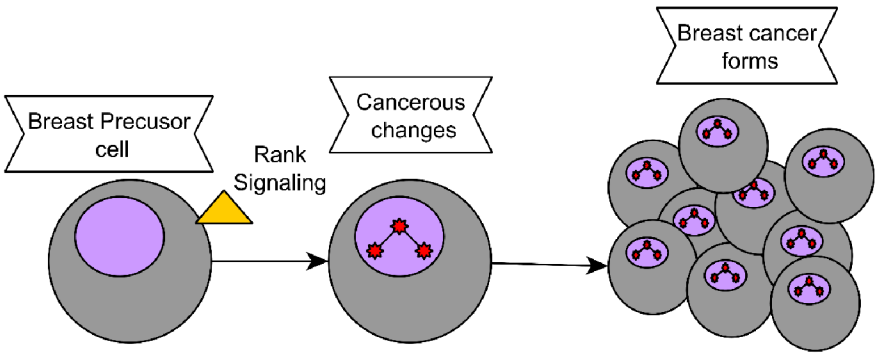

Figure 9. Breast precursor cells have receptors for hormones such as progesterone, which are responsible for the enlargement of the Alveolar, the division of cells. Therefore, for each division of cells, there is a potential risk of mutation. **(Own work).**

- The consumption of medicine containing Estrogen can also increase the risk of B.C.

- Another factor can be medical examination with ionizing radiation such as chest x-ray and computerized tomography (C.T.) scans.

- B.C. can also be caused by a mutation in Tumor suppressor genes such as the Breast Cancer Genes (BRCA-1 and BRCA-2) and TP53. These two are usually responsible for slowing down cell division or making cells Die if there is no cell division regulation**.**

As shown in Figure 4, the tumor, also known as in-situ Carcinoma, can be found in the Alveoli base membrane and can be of 2 types:

- Ductal Carcinoma in-situ (DCIS): here, the tumor cells grow inside the Alveolar, decreasing the space initially reserved for the Lumen (see **Figure 10**). It is good to pay attention here, as if it stays untreated, it can lead to Invasive Ductal Carcinoma. Also, cancer cells can traverse the lactiferous Duct and, through Pore, reach the skin. This last is known as Paget Disease of the Nipple and the fluid released is call Mobility Factor, both cause crust on the skin.

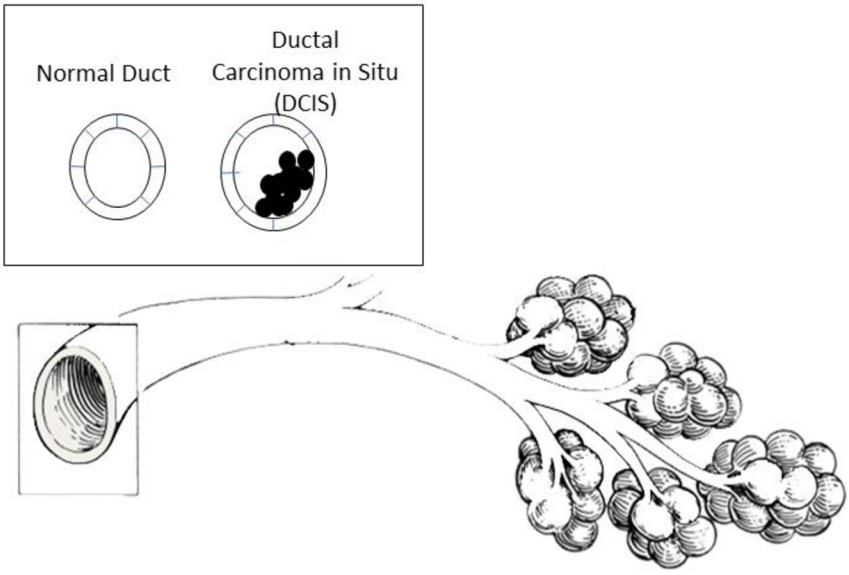

Figure 10. An illustration of Ductal Carcinoma in Situ (DCIS) present in the breast. A healthy duct is shown on the left side, whereas, on the right side, several mutations of the Duct's cells have occurred, leading to DCIS. (Own work).

- Lobular Carcinoma in –Situ (LCIS): here, several cells grow abnormally within the lobular. Contrary to DCIS, tumor cells do not cross the Alveolar membrane and do not spray (see **Figure *11***) through the breast. However, some cells have hormone receptors and grow when the previously mentioned hormones are present (*Breast Cancer - Causes, Symptoms, Diagnosis, Treatment, Pathology*, 2020).

Because early-stage B.C. is usually not painful, it increases the difficulty of having patients at the early stage of Cancer. Therefore, awareness campaigns need to be placed alongside less painful (de Groot et al., 2015; Whelehan et al., 2013) and more affordable diagnoses.

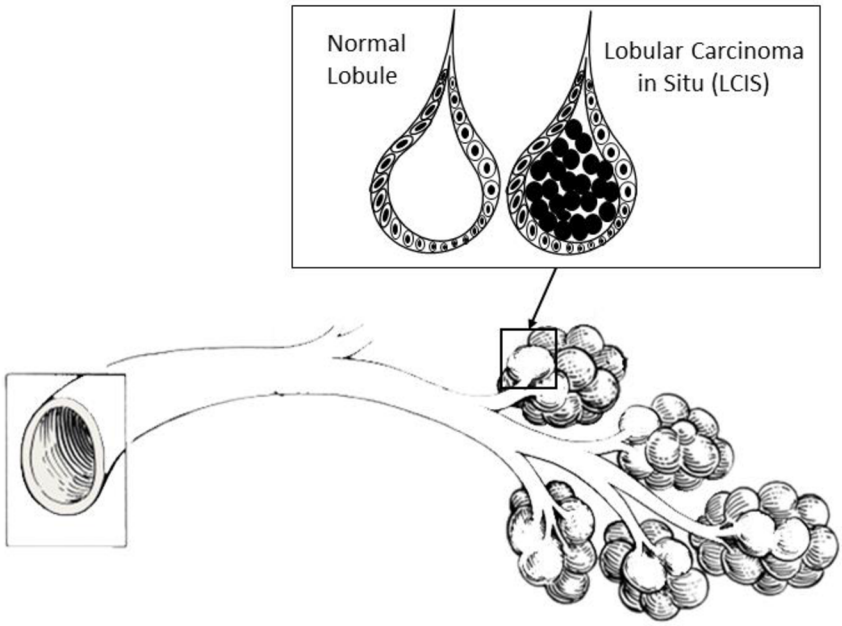

Figure 11. Lobular Carcinoma in Situ (LCIS) is present in the breast. A healthy Lobular is shown on the left side, whereas, on the right side, several mutations of Lobular cells have occurred, leading to LCIS. *(Own work).*

5.2.An essential overview of Brain tumor

The brain is the most complex organ(Foundation, n.d.) in the human body and the nervous system's control centre. It contains 100 billion notable neurons and controls mental processes such

as reasoning, imagination, memory, and language. It also interprets information from the senses. Besides, it controls basic physical functions such as breathing and heartbeat, essential to human beings.

A sliding membrane bounds the cerebral cortex (Cerebrum) and Cerebellum, called a tentorium (see **Figure *12***).

The membranes covering the brain (meninges), cranial nerves, pituitary or pineal gland are more susceptible to hose Primary brain tumors, which most of the time begins in tissues close to the brain or the brain itself (*Brain Tumor - Diagnosis*, 2012). Besides, Adult brain tumors are masses of abnormal cells that usually occur in adults resulting from uncontrolled cell growth in the brain.

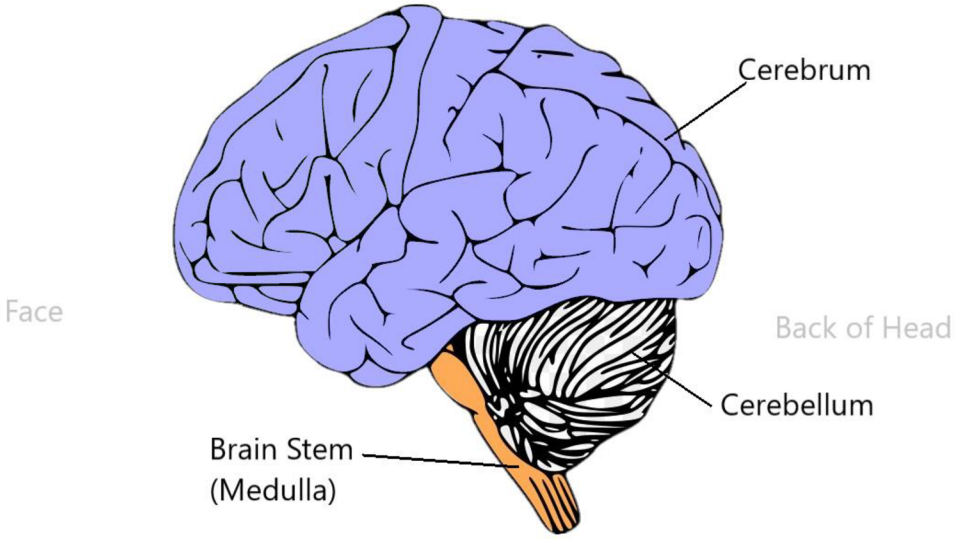

Figure 12. Simplify parts of the brain. This last controls basic physical processes such as breathing and heartbeat. A sliding membrane bounds the cerebral cortex (Cerebrum) and Cerebellum, called a tentorium. *(Own work).*

Primary brain tumors start when normal cells acquire mutations in their DNA. These mutations enable cells at increased rates to grow and divide themself continuously while healthy cells die, causing a tumor. There are several primary brain tumors; each gets its name from the kind of cells involved. Examples include:

- **Gliomas**: These tumors start in the spinal cord or the brain and include oligoastrocytomas, ependymomas, astrocytomas, glioblastomas, and oligodendrogliomas.

- **Meningiomas:** A meningioma is a collection of located muted cells that originates from the layers encircling your brain and spinal cord (meninges). Most meningiomas are not cancerous.
- **Acoustic neuromas (schwannomas):** These benign tumors develop on the nerves that control balance and hearing leading from your inner ear to your brain.
- **Pituitary adenomas:** Most of them are benign tumors that develop in the pituitary gland at the brain's base. These tumors can affect pituitary hormones with effects throughout the body.
- **Germ cell tumors:** a potential brain tumor can be due to germ cell tumors' propagation developed during childhood when the testes or ovaries form.
  Medulloblastoma starts in the lower back of the brain and spreads into the cerebrospinal fluid, and appears to be the most common cancerous brain tumor in children.
- **Craniopharyngiomas:** These rare, non-cancerous tumors start near the brain's pituitary gland, which secretes hormones that control many bodily functions. As the craniopharyngioma grows slowly, it can affect the pituitary gland and other structures close to the brain.

Examining a brain neoplasm can appear to be a life-threatening situation. But while the symptoms of most brain tumors are the same, not all tumors are malignant. Meningioma is the prevalent brain tumor, estimating about 30% of them and further meningioma details can be elaborated as follow (*The Most Common Brain Tumor*, n.d.):

- **Meningiomas can develop in different places**: These tumors originate from cells in the meninges, the brain's lining, and the spinal cord. So, technically, these are not brain tumors since they result from mutated brain cells. But they are still growing inside your skull, which means there's cause for concern. If a meningioma increases or causes swelling against the brain or other skull structures, it can cause brain tumor symptoms.
- **Meningioma symptoms depend on their size and location:** Meningiomas have symptoms typical of brain tumors such as headaches, vision problems, or seizures. A headache, even severe, is rarely a symptom of meningioma or any other brain tumor. Larger meningiomas can block the cerebrospinal fluid flow, causing hydrocephalus ("water on the

brain"), affecting walking and memory. Other tumor locations can affect your sense of smell, vision, hearing, or even the function of your pituitary gland.

- **A diagnosis of meningioma can occur when the doctor looks for something else:**
  The diagnosis of a brain tumor is often accidental. That is, the doctor finds a tumor on a CT scan or MRI while examining the individual for some other reason, such as a head injury or another neurological problem. When a doctor diagnoses a meningioma, you will have further tests to determine how the tumor is likely to behave. Based on this data, a neurosurgeon will recommend removing Cancer or merely looking at it to see if it is growing.
- **Most meningiomas do not spread:** It can be shocking for a person to be diagnosed with a meningioma - especially a large one - but these tumors are usually benign. This means that the tumor cells are not likely to spread to other parts of the body. That said, meningiomas can grow quietly for years without causing any problems - and they can get surprisingly large.
- **Treatment of meningioma: surgery - or not:** Sometimes, believe it or not, your doctor may recommend looking for a meningioma, especially if it is small and not causing problems. You will have regular MRI scans to check it.
  Otherwise, the primary treatment for meningiomas is surgery to remove them through a craniotomy or other procedure. Your doctor will explain what the operation will involve, the approach to accessing the tumor, and what to expect afterward.
  Tumors near the surface are generally easier to access than those along the base of the skull. Skull base tumors are those located deep in the skull, behind the nose, or eyes. These can be difficult and require surgeons with skills and expertise in this type of surgery.
  There are several new brain tumor surgery techniques, even for tumors deep in the skull, and some are less invasive.
  One system involves a camera-assisted tube that gently moves brain tissue aside so surgeons can reach the tumor with fewer cuts so that patients can recover faster. After your treatment, you will have regular MRI scans to ensure Cancer does not come back.
  In many cases, this will not be the case. After ten years, about 90% of patients who have had a meningioma have not seen a recurrence if the tumor was removed entirely, including the part of the brain lining from which it has grown.

Either way, the best thing to do if you are diagnosed with meningioma or any other tumor is to know the facts, stay informed, and work with the most experienced neurosurgeon and care team you have.

5.3. The need for better Computer-Aided Diagnosis.

Nearly seven thousand breast cancer cases are diagnosed in the Czech Republic each year, corresponding to more than 130 cancers per 100,000 women in the Czech population. Also, 1,900 breast cancer deaths among women in the Czech Republic were recently observed, with 34 breast cancer deaths per 100,000 women in the Czech community. As revealed (see Figure 13), breast tumors arrive as the principal cause of death in the Czech Republic (Pavlík et al., 2014; Population Changes in the Czech Republic, n.d.) and among the world's top 5 diseases. Various techniques have shown their apparition during the past few years, with one major disadvantage: the cost and the pain they can procure (Namikawa et al., 2015). One of the usual screening analyses is mammography, it is prevalent and usually recommended as the first screening diagnosis. However, the mammography screening diagnosis can be painful (Female Patients' Perception of Pain Caused by Mammography in the Western Region of Saudi Arabia, n.d.), and successive mammography for flighty years can lead to breast cancer. Therefore, it seems essential to propose a non-invasive method, less painful, less costly, and reliable enough to ease the diagnosis processing of doctors.

Brain tumor. Specialists do several analyses to detect or diagnose a brain neoplasm and determine the brain tumor's nature. They more often expand their investigation on the area around the primary zone of interest (area of Cancer) to see if cancer cells have expanded to other parts. The aforementioned is called metastasis and is rare for a brain tumor (*Brain Tumor - Diagnosis*, 2012). Imaging tests can help doctors determine how far Cancer has spread or is still a primary brain neoplasm. Due to the healthy impression of some patients, brain neoplasms are usually diagnosed when symptoms emerge. Ordinarily, a brain tumor is determined by an internist or a neurologist who analyses MRI images. Once an MRI scan reveals a tumor in the brain, the most usual way to select the type of brain neoplasm is to analyze a tissue sample's results after a biopsy or surgery. Among all cancers, brain tumors are estimated to be approximately 2% of all cancerous diseases. A recent survey showed that the amount of new brain tumor cases is around 800 people per year in the Czech population, with a slight predominance in men. In 2011, just in the Czech Republic, 8.5 per 100,000 men and 7.8 per 100,000 women were reported having a brain tumor. The number

of deaths was 7.5 per 100,000 men and 6.6 per 100,000 ladies per year. Therefore, it seems essential that the proposed method is less costly, reliable enough to ease and speed up the diagnosis process of doctors.

5.4. Understand Thermal Image

Planck's law describes the spectral density of electromagnetic radiation emitted by a black body in thermal equilibrium at a given temperature T when there is no net flow of matter or energy between the body and its environment. Every physical body spontaneously and continuously emits electromagnetic radiation. The spectral radiance of a body noted D describes the spectral emissive power per unit area per unit of solid angle for particular radiation frequencies. From Planck's radiation law, it was understood that the total radiated energy of a body increases with an increase in temperature and that the peak of the emitted spectrum shifts to shorter wavelengths. Taking this into account, the spectral radiance of a body for the frequency f at a specific temperature S, is computed as follow:

$$D(f,S) = \frac{2pf^3}{C^2}\frac{1}{\frac{pf}{e^{BS}-1}} \quad (1)$$

Where p is Planck's constant, B is Boltzmann's constant, and C is the speed of light in the medium, whether material or empty.

Thermal video, Infrared Thermography (IRT), and thermal imaging is a process in which a thermal camera takes an image of an object using infrared radiation emitted by the object, which are examples of the science of infrared imaging. Thermal imaging cameras typically detect radiation in the long infrared range of the electromagnetic spectrum (roughly 9μm to 14 μm) and produce images of this radiation, called thermograms. The infrared radiation is emitted by all objects whose temperature is above absolute zero according to the law of black body radiation (an idealized physical body that absorbs all incident electromagnetic radiation, regardless of frequency or angle incidence); thermography allows you to see your surroundings with or without visible lighting. It also makes it possible to see temperature variations. When viewed through a thermal imager, hot things stand out well against cooler backgrounds; humans and other warm-blooded

animals become easily visible in the environment, day or night. As a result, thermography is particularly useful for the military and other users of surveillance cameras.

5.5.Theoretical Modeling

Based on (Avila-Castro et al., 2017) study, suppose a breast is spherical an incident laser beam on the breast's skin surface. After reaching a constant state, irradiance can be observed due to the widespread incident light depending on the spot in the tissue $\delta = (x, y, z)$. Wm^{-2} is the units of δ representing the size of the amount of energy for a unit area in a unit time.

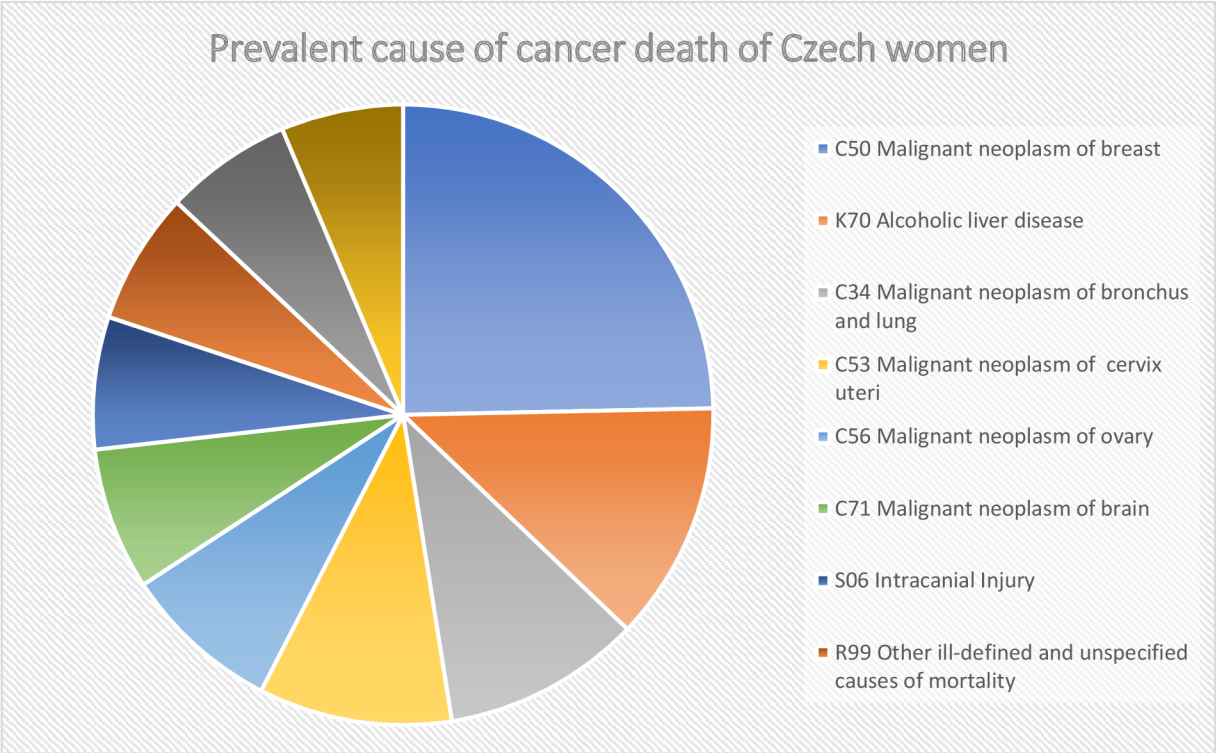

Figure 13. Prevalent cause of cancer death of women. This figure shows that breast cancer is the leading cause of death for Czech women. (Illustration built by the author, data derived from the study conducted by (Pavlík et al., 2014)) (Own work).

The transfer of irradiance to heat caused by the energy accumulated by the surface after a laser's incidence depends on retention and temperature (see **Figure 14**).

Thermal image screening diagnosis of breast cancer analyses the heat capacity HC_ρ of a particular region of the breast. This rise of temperature can be estimated by:

$$HC_\rho \approx \frac{1}{\rho} \times \left(\frac{dE}{dT}\right)_\rho \quad (1)$$

Where dE and dT are respectively the energy per unit volume and the temperature rise.

Looking at the heat generated by the tumor, the area's detection can be possible only if there is thermal conductivity from the tumor cells to the skin surface. Assuming that each layer of the breast is homogeny constituted, it is found empirically that a heat flux f, can be expressed with the gradient of the temperature to obtain the vector V_T .

$$V_T = \left(\frac{dT}{dx}, \frac{dT}{dy}, \frac{dT}{dz},\right) \quad (2)$$

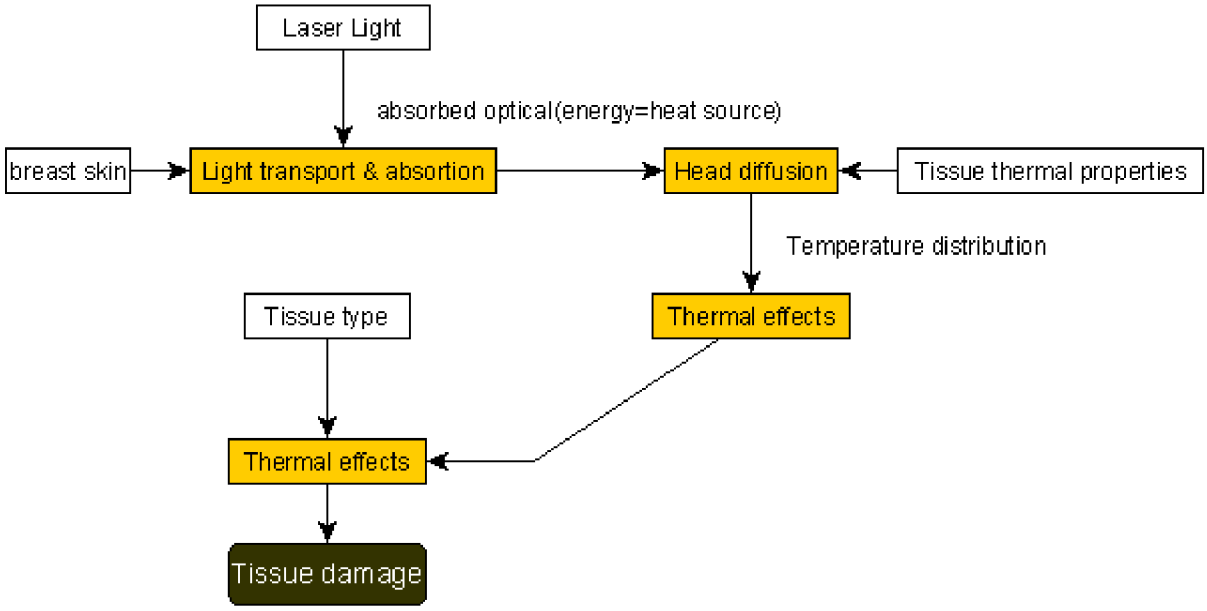

Figure 14. The different characteristics involved in the thermal interactions of light with a breast surface. (Own work)

Hence, a heat flux f can be expressed function to temperature gradient as below:

$$f = -kV_T \quad (3)$$

Given these notions, let look at few uses cases:

Assume an experimental setup where it is asked to take a picture of patients (Morales-Cervantes et al., 2018) study presented a similar process, where the Heat source (HC) marks as transmission can be assimilated to the breast tumor. A specimen can be seen as the set of breast tissue between the tumor and the surface of the skin and the device, which is a collection of IR cameras, the computer (processing device) and the HC (reflection).

Such architecture is commonly used in most of the known products, and base on (Boquete et al., 2012) (Head et al., 1993) studies, several issues can be encountered, which are for an IR screening diagnosis:

- The variation of room temperature where the experiment is happening, represented by HC (reflection).
- The accurate extraction of the region interest (ROI) at the preprocessing phase.
- The entire process is not combined into one device.

6. Design of proposed Framework.

The collection of images followed a specific standard; the patients were kept in a room at a temperature of x, during y minutes before capturing the breast's thermal image. Each image had a resolution of 640 × 480 pixels, and the camera used was a FLIR SC-620(Silva et al., 2014). A preprocessing of the image was made manually to ensure all images were clear and resized to 256 × 256 pixels.

Those images were then classified using the couple (InceptionV3, SVM), which was found powerful enough for this classification task in one of our research papers (S. J. Mambou et al., 2018). Looking a bit on the couple architecture, the last layer of InceptionV3 was removed to allow to get the featured layer l_{-1}.A dual form of SVM was used to separate each data point, where the computation of the soft margin of the SVM classifier (SVC) requires minimizing an expression of the form (equation: 4).

$$\left[\frac{1}{n}\sum_{i=1}^{n}\max\left(0,1-y_i(W^T x_i-b)\right)\right]+\prec\|w\|^2 \tag{4}$$

Where any hyperplane can be written as: $W^T x_i - b$ with W a normal vector to the hyperplane and $\prec$ a value small enough.

Minimization (4) can be described as a constrained optimization that can be solved using the dual Lagrangian. The latter gives the simplified problem (dual problem).

$$\begin{aligned}&\underset{\propto}{maximize}\ \sum_{i=1}^{n}\propto_i-\frac{1}{2}\sum_{i=1}^{n}\sum_{j=1}^{n}\propto_i\propto_j y_i y_j\left(X_i^T.X_j\right)\\&subject\ to\ \propto_i\geq 0, For\ all\ i=1,2,\dots,n\ and\ \sum_{i=1}^{n}\propto_i y_i=0\end{aligned} \tag{5}$$

Heading back to this section's primary objective, which is to describe the proposed architecture (see **Figure *15***), InceptionV3-SVM outputs the state of the breast (healthy or sick). For a healthy breast, no further processing is required, and the user is notified directly of the healthiness of the breast. Whereas, once a sick label is attached to the breast, the system triggers further analysis via the so-called "CancerStage" module, which is, in fact, the component that will categorize the tumor (cancerous area) in one of the four stages of breast cancer. A series of Mathematical morphology (threshold, blur, erosion, dilation) is described in one of our papers (S. Mambou et al., 2020), and a custom U-net with VGG19 is used as a down-sampling backbone. Given the recent progress

made in medical image analysis (Kim et al., 2011) and the steps resulted from these studies. The proposed framework comes with an agility that makes possible two approaches (manual selection and automatic selection).

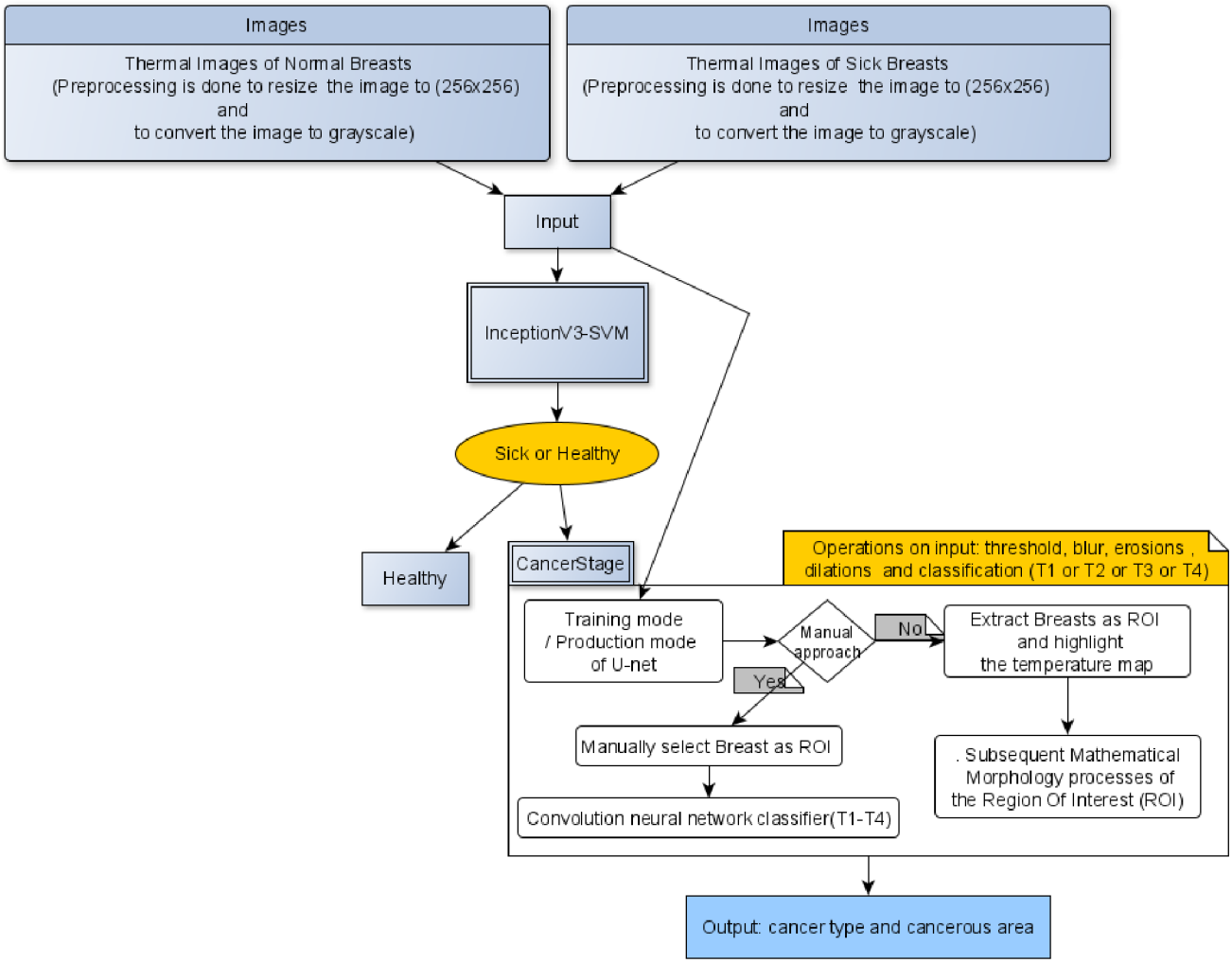

Figure 15. A workflow of the proposed architecture. Images are first classified as sick or healthy; those labeled as ill will be further analyzed, and through a custom U-net or a manual selection, will extract the ROI. The latter will be an additional process to get the type of cancer and the cancerous area. (Own work).

6.1. The Manual Selection of one breast for a localize Prediction (MSP)

Considering the processed dataset obtained from the preprocessing phase with resulting images of size 250 by 250. MSP component is fed with a batch of these images and subjected to analysis by

a custom model called MSP-Unet. The latter is composed of two main parts (see **Figure 15**):

- The first component (model): is presented as an intermediate element between the Input Layer and the classifier component. Once an image is fed to the model, it goes through a series of convolution layers, and a set of relevant features is passed to the next component to perform classification. A side note is: The model can be replaced by any u-net architecture taking as input a batch of shape images (batch, 256, 256, 1) and returning as output images of the same size as output (bach, 256, 256, 1).

- **The second component(model_1):** is presented as an output layer of the architecture. It takes as input the region of interest obtained from the precedent sub-model (model).

Each sub-model *model* and *model_1* can be further illustrated as a collection of the convolutional neural network, Maxpool, the flattened and dense layers that, when put together, can form a deep neural network (see **Figure 16**). On the left side of (see **Figure 17**), a u-net *model* is shown with an architecture derived from (*GitHub - Sevakon/Unet-Keras: U-Net: Convolutional Network for Biomedical Image Segmentation Using Keras*, n.d.). On the right side, a classifier is displayed with the output as one of the tumor categories.

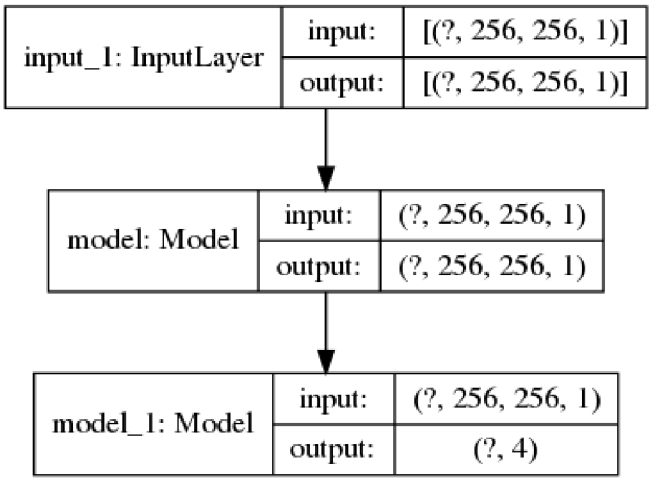

Figure 16. The final model is obtained by vertically combining two pre-trained models (u-net and sub-classifier) so that the output of the "model" in this case, the u-net becomes the input of "mode_1" in this case, the sub-classifier (Own work).

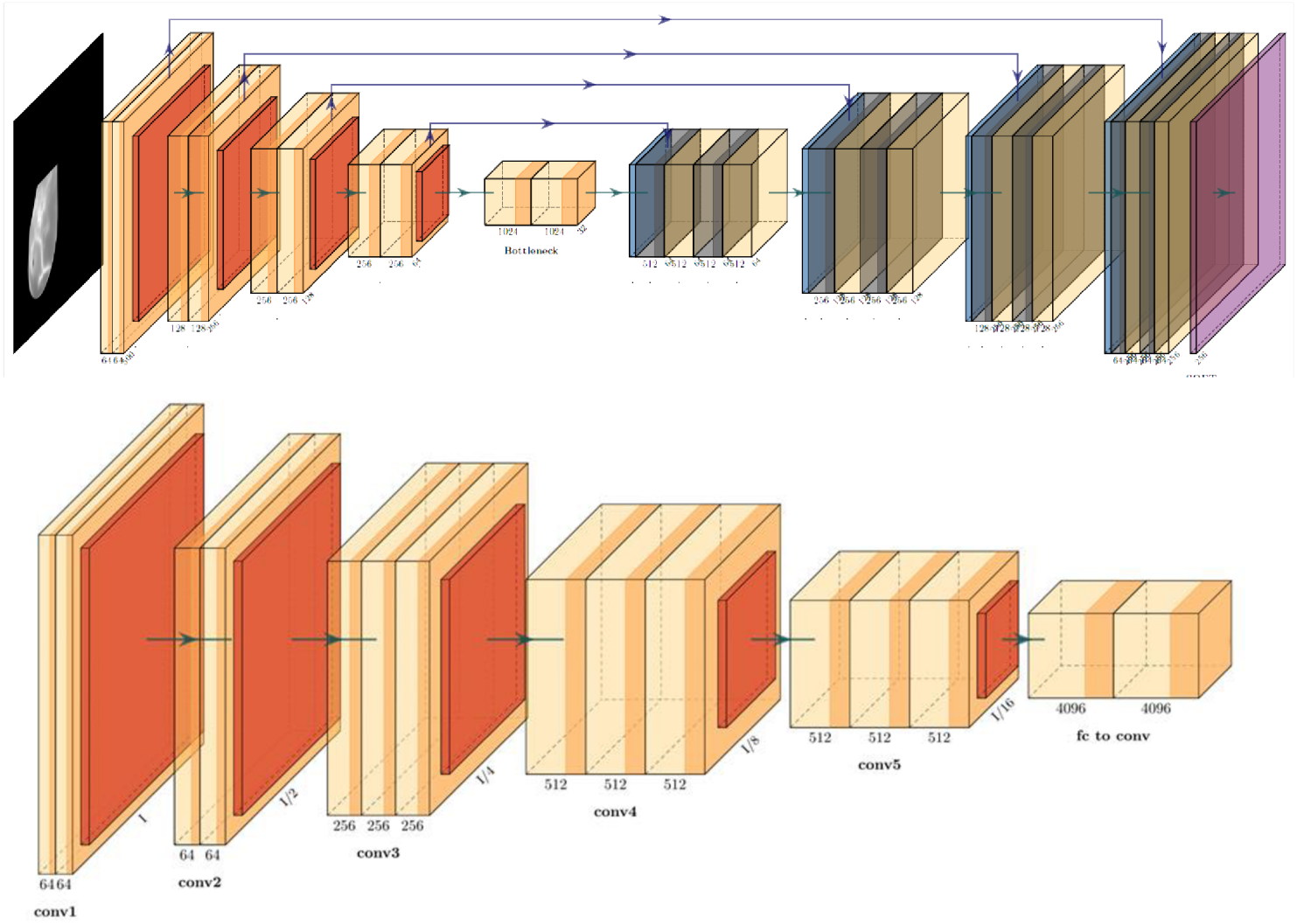

Figure 17. On the left, a modified u-net model is used here to extract the tumor area, and on the right, a classifier is taking as input the output of the u-model and returning the category of Cancer. (Own work)

6.2. The Automatic Extraction of the region of interest and the Global Analysis (GA)

Considering a batch of thermal images of the breast images converted or maintained in grayscale mode, it was questioned to propose an approach that will save time by removing the manual process from the previous subsection where the practitioner had to select the breast being analyzed. An alternative approach has been made possible by leveraging deep learning models' power on building custom Unet (see **Figure 19**). A down sampling backbone made from VGG19 net (pre-trained on an ImageNet dataset) gave an impressive result on extracting the breast regions.

As a side note, the custom model's downsampling component refers to a succession of convolutional neural network (CNN), max-pooling, batch normalization, and dropout operations where a CNN used a kernel convolution, a process in which a small matrix of numbers (called a kernel or filter) is passed over an image and transformed according to the values of the filter. The resulting feature map fm is calculated according to the following formulas (6) and (7), where the input image is denoted by In and our kernel by kn.

$$fm[r,c] = (In \times kn)[r,c] \tag{6}$$

$$(In \times kn)[r,c] = \sum_{t}\sum_{z} kn[t,z]In[r-t,c-z] \tag{7}$$

Where r and c are respectively rows and columns of the resultant matrix, with $r, c, t, z \in \mathbb{N}$

The latter can be subjected to subsequent Mathematical Morphology processes as described in our paper (S. Mambou et al., 2020). As a result, the areas with a high-temperature peak are highlighted (see **Figure 18**).

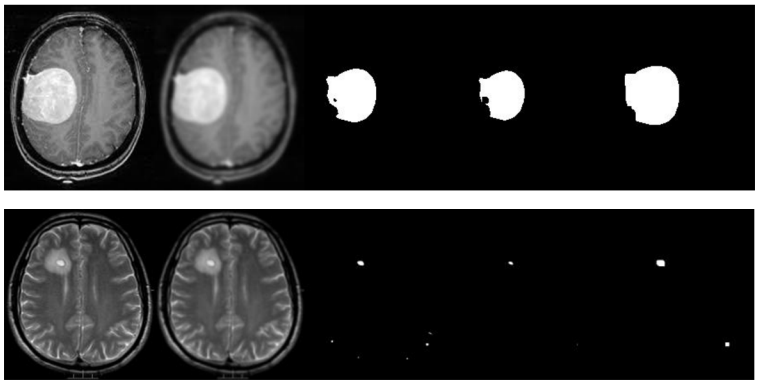

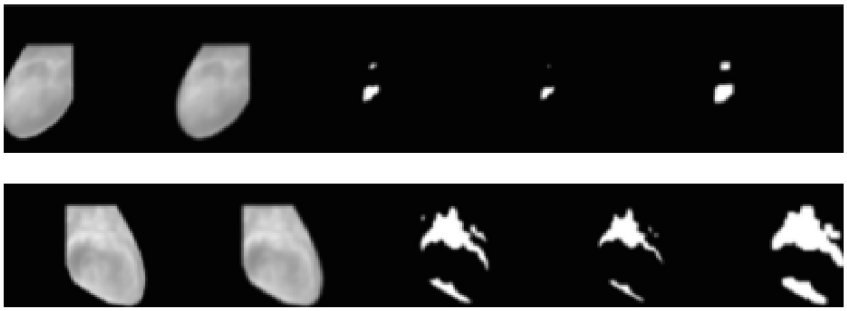

Figure 18. Extraction of the abnormal area. The first two images from the top are the MRI images of two different brains, and the remaining images are the thermal images of two different breasts. (Own work)

6.3. Case study 1: Deep models applied to IR breast Cancer

From the workflow (see **Figure 15**) described in the previous section, let's focus on the "StageCancer" component. It is subdivided into three sub-components, which can be listed as custom U-net (in training or test mode) or manual selection, responsible for extracting the area undergoing further analysis. The temperature map, which highlights the portions of the breast(s) with the highest metabolism (peak temperature in this case), and the subsequent mathematical morphology that detects the cancerous area (C.A.) and classifies C.A. in one of the four stages of cancer.

Let us draw our attention a little more to the U-net (see **Figure 19**), which is a concatenation of the Deep Neural Network (DNN). The first in our case is a pre-trained VGG19 (on the ImageNet dataset) used as a downsampling backbone; after several experiments with many DNNs such as InceptionV4, ResNet34, and ResNet10, VGG19 has been found to be more effective in our experiment. Designing the Up-sampling backbone was a bit difficult because it was a question of finding the suitable composition of Conv2DTranspose layers, which will respect the condition input shape equal to output shape.

U-net training inputs thousands of images and their associated mask subjected to a loss function (binary cross-entropy). The input size is set to (?,256, 256,1), and the resulting output size is (?,256, 256,1) due to unpadded convolution (Conv2D). This derived architecture (Ronneberger et al., 2015) minimizes overhead and maximizes GPU memory by favoring large input tiles over a large batch size. A pixel-by-pixel soft-max calculates the energy function (see Equation 7) on the final feature map combined with the cross-entropy loss function.

$$softMax = e^{\left(\frac{act_C(x)}{\left(\sum_{c'}^{C} e^{\left(act_{c'}(x)\right)}\right)}\right)} \quad (6)$$

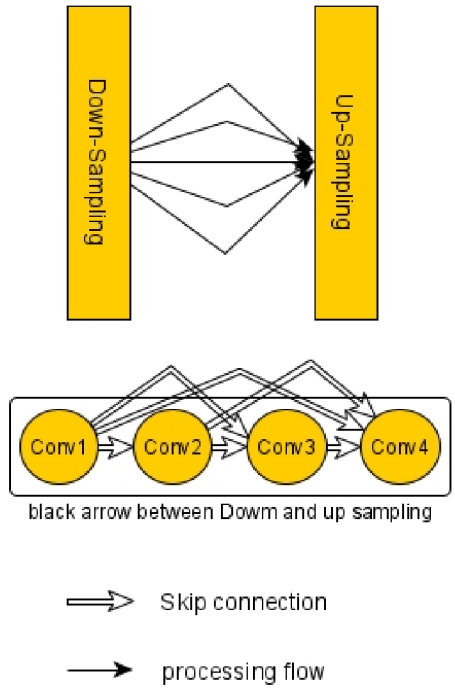

Figure 19. Customer U-net with skip connection. Keeping in mind the depth of our U-net, it was relevant to use Skip connections in the architecture to avoid fading gradients or alleviate the issue of saturation (degradation of the precision), where supplementing extra layers to significant deep model results in a higher training error. (Own work)

Where $act_c(x)$ represents the activation in feature channel "c "at the pixel position "x"

$x \in H \subset \mathbb{Z} \times \mathbb{Z}$, C represents the number of classes, and SoftMax is the approximated maximum function. During the training, the loss function ensures better accuracy by penalizing the deviation $softMax$ from 1.

$$Binary\ CrossEntropy = -\frac{1}{N}\sum_{i=1}^{N} y_i \,.\log\big(p(y_i)\big) + (1-y_i)\,.\ \log\big(1-p(y_i)\big) \quad (7)$$

Y is the label (1 for black points and 0 for white points), and p (y) is the predicted probability that the point will be white for all N points.

Once the model is adequately trained, it is time to test new images. These images must be entirely new for the system; in other words, they should not have been used during the training phase.

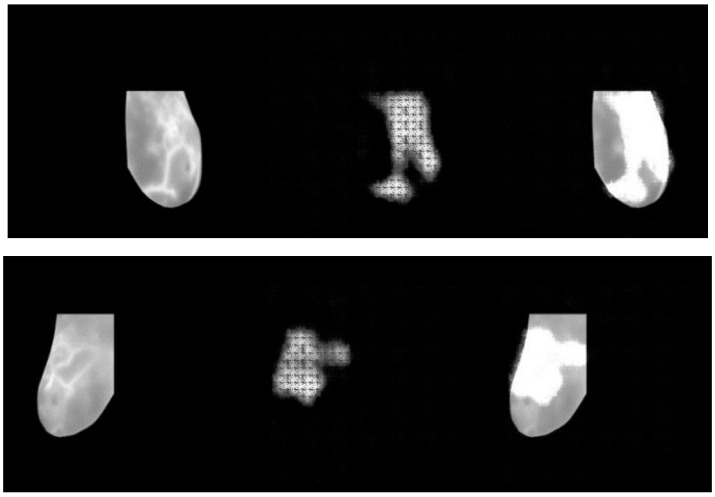

Figure 20. Given a completely new image, the system can determine the most relevant region of interest, as indicated by the white area of the image on the right. (Own work)

After applying another increase in data to the test set via data augmentation, the images were passed as input to the system. It appears that the system can quickly determine the most relevant region of interest (the area affected by the tumor) (see **Figure 20**) and classify Cancer (T2). However, tumor T0 and T1 are sometimes confused, and the image resulting is occasionally similar to the input (see **Figure 21**). Optimizing our architecture may imply the need for more data to handle such cases.

Figure 21. Given an entirely new healthy image, the system classifies it as a T1 tumor due to the slight anomaly detected as the most relevant region of interest, as indicated by the white area of the image on the right.

6.3.1. Manual extraction of the breasts

The preselected breast is input (see **Figure 22**) with a three-channel thermal image (R, G, B), an internal function is triggered to convert it to a grayscale image. The proposed model will take the grayscale image as input and detect the breast's cancerous area. In other words, looking at the figure (see **Figure 22**), the image on the right side, the resulting grayscale image on the left, will be processed so that the region of interest is highlighted in white. The frozen part of the model will extract the mask (feature) and give it as input to the newly added set of layers. At the end of the model, a softmax function will classify the image in the category associated with the output neurons with the highest probability.

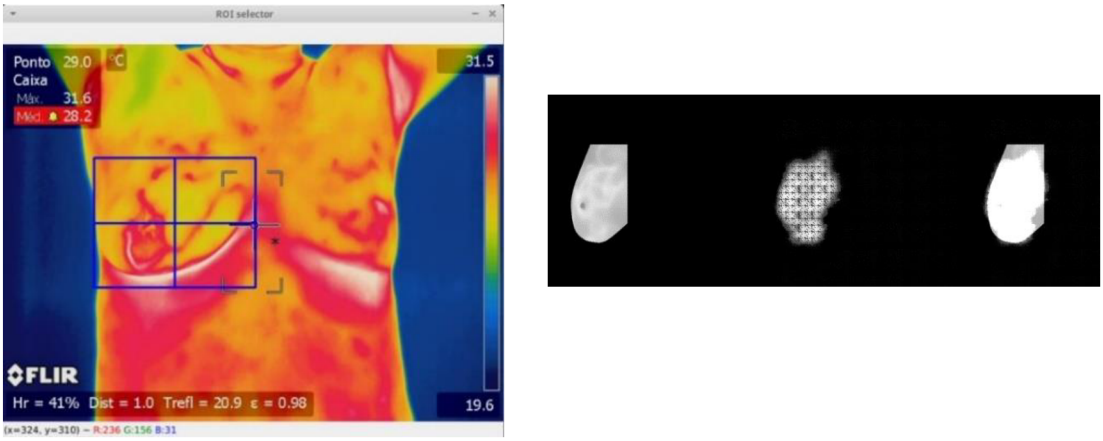

Figure 22. For each line, consider the left image, the model predicts the mask in the centre, and a combined view of a mask above the original image is obtained in the rightmost image(image derived from (*Visual Lab - Laboratorio de Computação Visual*, n.d.) and processed by the author). (Own work)

An extension of the system could take advantage of all the features specified above when input a thermal image with three channels (R, G, and Bs). However, the color image is converted to a grayscale image before further processing by the model (see **Figure 23** and **Figure 24**).

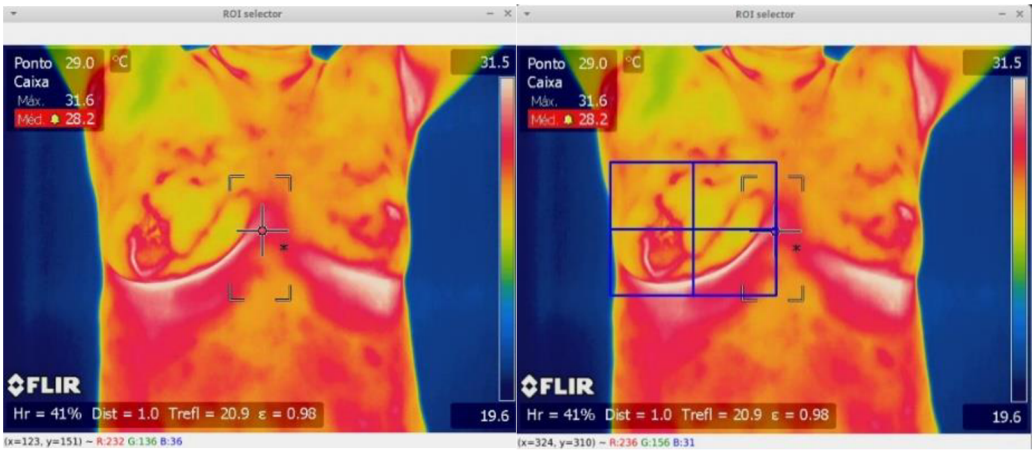

Figure 23. Breast selection from the thermal image and subject to further analysis. Here, the user carefully selects the region of interest and hits enter so that the system takes the selection into account. Images are derived from the dataset (image derived from (Visual Lab - Laboratorio de Computação Visual, n.d.) and processed by the author).

6.3.2. Automatic processing of the breast

Through experiments, threshold-based segmentation was found to be a necessary step after pattern recognition. Using a modified version of the U-Cancer module discussed in one of our papers (S. Mambou et al., 2019a) and the data augmentation process performed using the Keras package, classification was done by combining both components to the U-Net. One thousand steps and ten epochs were required to train the model and achieve a great validation mean intersection over Union (val_mean_io_u) (an accuracy of 0.9357 on the training data and 0.9093 on the validation data).

The goal was to accurately determine the area with the highest metabolic temperature, thus detecting the cancer cell area.

Epoch 5/10

1000/1000 [==============================] – ETA: 0s – loss: -0.9319 – dice_coef: 0.9319 – binary_accuracy: 0.9357 – true_positive_rate: 0.9448 – mean_io_u: 0.8719

Epoch 00005: val_mean_io_u improved from 0.76889 to 0.84513, saving model to vgg_unet_weights.20210506.hdf5

1000/1000 [==============================] – 292s 292ms/step – loss: -0.9319 – dice_coef: 0.9319 – binary_accuracy: 0.9357 – true_positive_rate: 0.9448 – mean_io_u: 0.8719 – val_loss: -0.8918 –

val_dice_coef: 0.8918 – val_binary_accuracy: 0.9093 – val_true_positive_rate: 0.9140 – val_mean_io_u: 0.8451

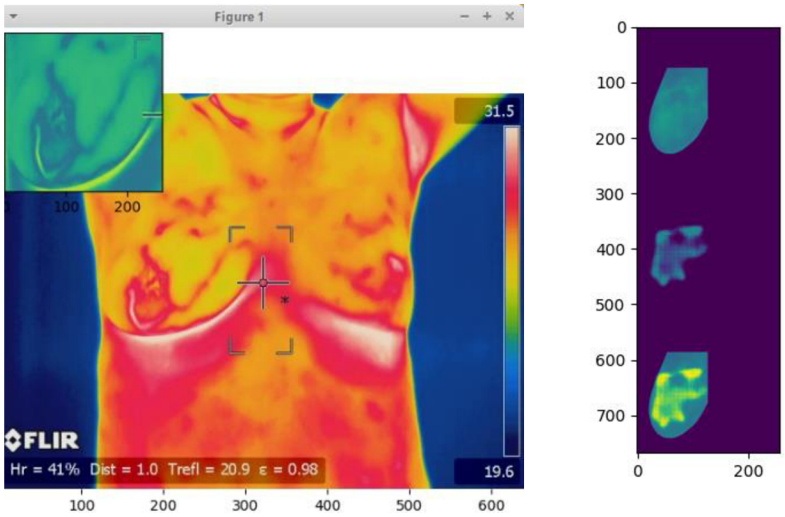

Figure 24. From left to right, breast selection and cancerous area detection occur. Here, the user's region of interest is given as input to the model; the resulting mask is obtained and applied to the breast to see the affected area (image derived from (Visual Lab - Laboratorio de Computação Visual, n.d.) and processed by the author). (Own work)

As the reader may have observed, few metrics were used to ensure the accuracy of our model:

- Dice Coefficient (F1 Score): Considering the predicted mask (m1) and the true mask (m2), the dice coefficient is two times the area of overlap divided by the total pixel of m1 and m2.
- Binary accuracy: as i deal with binary output (0 or 1) image, it refers to how much predicted output pixel (binary value) is equal to the true mask (also in binary value).
- True positive rate is the probability the predicted pixel (as 0 or 1) is effectively (0 or 1).
- Mean intersection over union: in this context, the predicted output is on a large scale from a binary class 0 or 1, where 1 represents the area that i want to emphasize and 0 the background (or vis-vers-a). meanIoU represents the average value of IoU for each class.

An accuracy, dice coefficient, and mean intersection over union graph were drawn during the training of the U-net model. After just five epochs, the model became stable (see **Figure 25**). In addition to this, other measures were used to adjust the parameters and evaluate the model (see List of Abbreviations).

Once the model was sufficiently trained, extracting (using the generated mask) the area subjected to further analysis was a question (see **Figure 26**). Using processes derived from subsequent morphology, the region of high metabolism was revealed and mapped to a specific color mapping where red represents the highest temperature.

6.3.3. Subsequent mathematical morphology

A threshold-based method: The Threshold Based Approach (TBA) is manageable and popularly used in the segmentation method (Cozzani et al., 2013). It considers the variation in gray value between the target objects and the background. It then determines one or more image thresholds using certain main parties to divide the image into one or more parts. Finally, the grey pixel value over the threshold is arranged in a zone class (Van Hulse et al., 2012).

TBA cannot only reduce a considerable volume of data but simplify the study and image-processing actions. Hence, in various circumstances, the Threshold Segmentation (T.S.) is quite significant before pattern recognition, feature extraction, and model analysis. It is particularly appropriate to the cases where the targets and the background have distinct grey levels. The benefits are high efficiency and simple operations (Wu & Yu, 2010).

Considering a situation where the objects and the background differ in grayscale intensities, it is practical to use a T.S. technique as it reaches high efficiency using simple operations.

Depending on the field in which T.S. is applied, two classes' methods can be enumerated, one is the method based on edge detection, and the other is the global threshold:

The global threshold technique: gains the benefit of information from the entire image (*A Dynamic Threshold Segmentation of Infrared Image--《Opto-Electronic Engineering》2002年06期*, 2019). It then determines the whole picture's optimal threshold, which can be a unique value or multiple thresholds. Besides, the "Ostu" method uses the grey value, which can cause variations within the classes to reach the most significant number as the optimal threshold.

Edge Detection Technique (EDT): determines the boundaries of objects in images. EDT is a processing method for finding the edges of an object in a given image. It operates by detecting discontinuities in brightness.

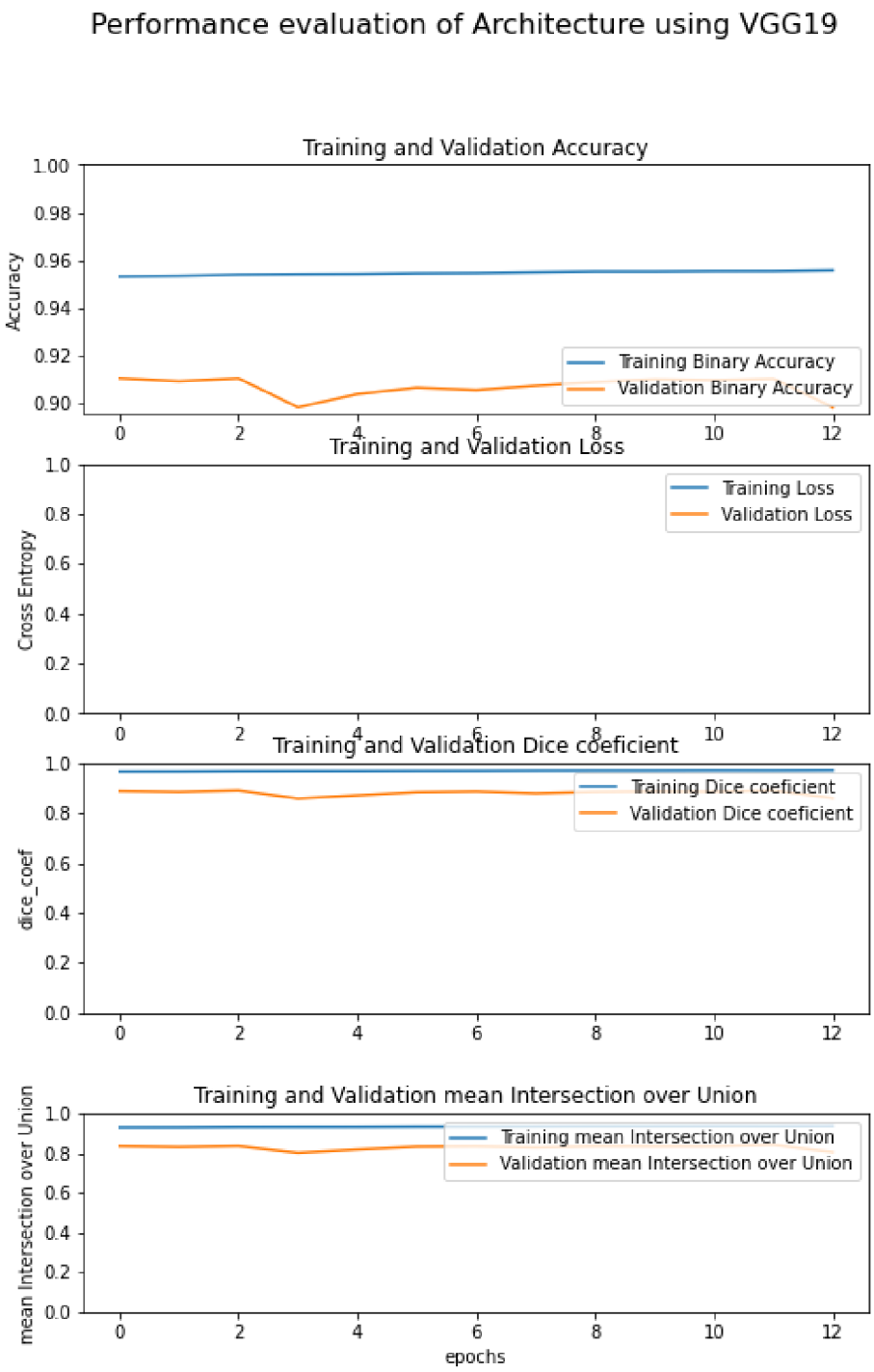

Figure 25. Performance of the custom u-net model. Note the epoch (abscise) graduation with 1 unit = 2 epochs to show the different intersections of the learning and validation curves due to the gradual change in the learning rate up to 0.0001. (Own work)

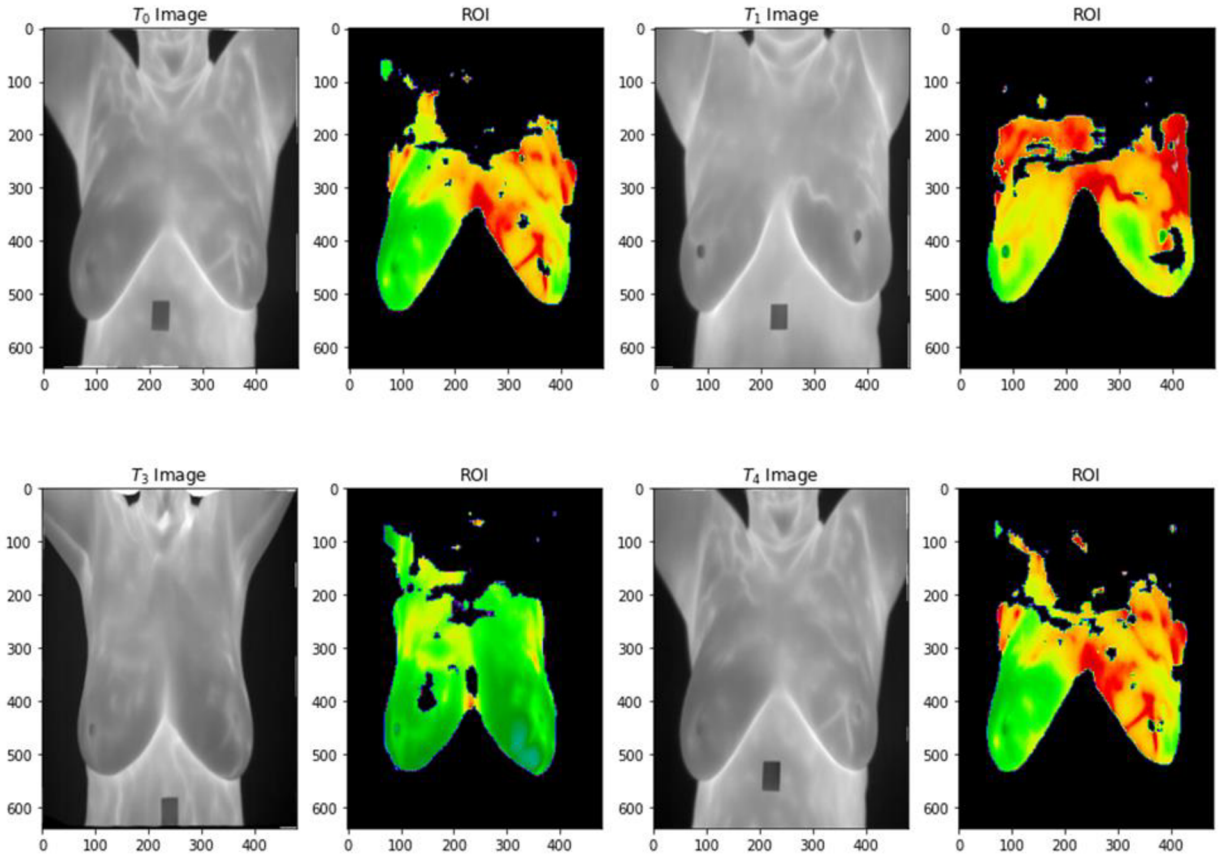

Figure 26. ROI obtained from the processing of Batch of four images submitted as input to the model. Note that the region of high metabolism was revealed and mapped to a specific colour mapping where red represents the highest temperature. (Own work).

Let us assume 1 to g is the grey value scale of an image, p a pixel value and T is the number of pixels.

$$T = \sum_{i=1}^{g} x_i \tag{8}$$

Also, a probability resulting of each pixel is computed as

$$P_p = \frac{x_p}{T} \tag{9}$$

In addition, a division into 2 set S of the grey values is required

$$S_0 = \{1,2,3, \dots v\} \tag{10}$$

$$S_1 = \{v+1, v+2, v+3, \dots g\} \tag{11}$$

Where $v \in \mathbb{N}$

Furthermore, a probability $\mathcal{O}$ of each group can be computed as

$$\mathcal{O}_0 = \sum_{j=1}^{v} \left(\frac{x_i}{T}\right)_j \Rightarrow \mathcal{O}_0 = \sum_{j=1}^{v} \left(P_p\right)_j = \mathcal{O}(v) \quad (12)$$

$$\mathcal{O}_1 = \sum_{j=\mathrm{v}+1}^{g} \left(\frac{x_i}{T}\right)_j \Rightarrow \mathcal{O}_1 = \sum_{j=\mathrm{v}+1}^{g} \left(P_p\right)_j = 1 - \mathcal{O}(v) \quad (13)$$

Besides, the average value A of each set can be found with

$$A_0 = \sum_{i=1}^{v} p\left(\frac{P_p}{\mathcal{O}_0}\right) \Rightarrow A_0 = \frac{A(v)}{\mathcal{O}(v)} \quad (14)$$

$$A_1 = \sum_{j=\mathrm{v}+1}^{g} p\left(\frac{P_p}{\mathcal{O}_1}\right) \Rightarrow A_1 = \frac{A - A(v)}{1 - \mathcal{O}(v)} \quad (15)$$

Going back to the whole image, its average value A is

$$A = \sum_{p=1}^{g} p\left(P_p\right) \quad (16)$$

Considering equation (8) to (15), the good threshold value can be found by adjusting the value v in the equation below:

$$Var(v) = \mathcal{O}_0(A_0 - A)^2 + \mathcal{O}_1(A_1 - A)^2 \quad (17)$$

It can be defined based on the fuzzy map of singular value constructed, looking at a blurred region. A blurred mask is obtained from the threshold image given as input in the previous subsection (see **Figure 27**). The precise evaluation of the area extraction is defined as the quotient of correctly segmented pixels to the image's total number of pixels. The blur of an image is based on two factors: one is the amount of blur in the whole picture, given by the distinct feature (value); become point minimum and maximum operators, respectively.

The second is the quotient of the size of the blurry area for the full image size. On the other hand, the expansion and erosion techniques extend the morphological operators to the domain of whole or real signals considering a Cartesian grid.

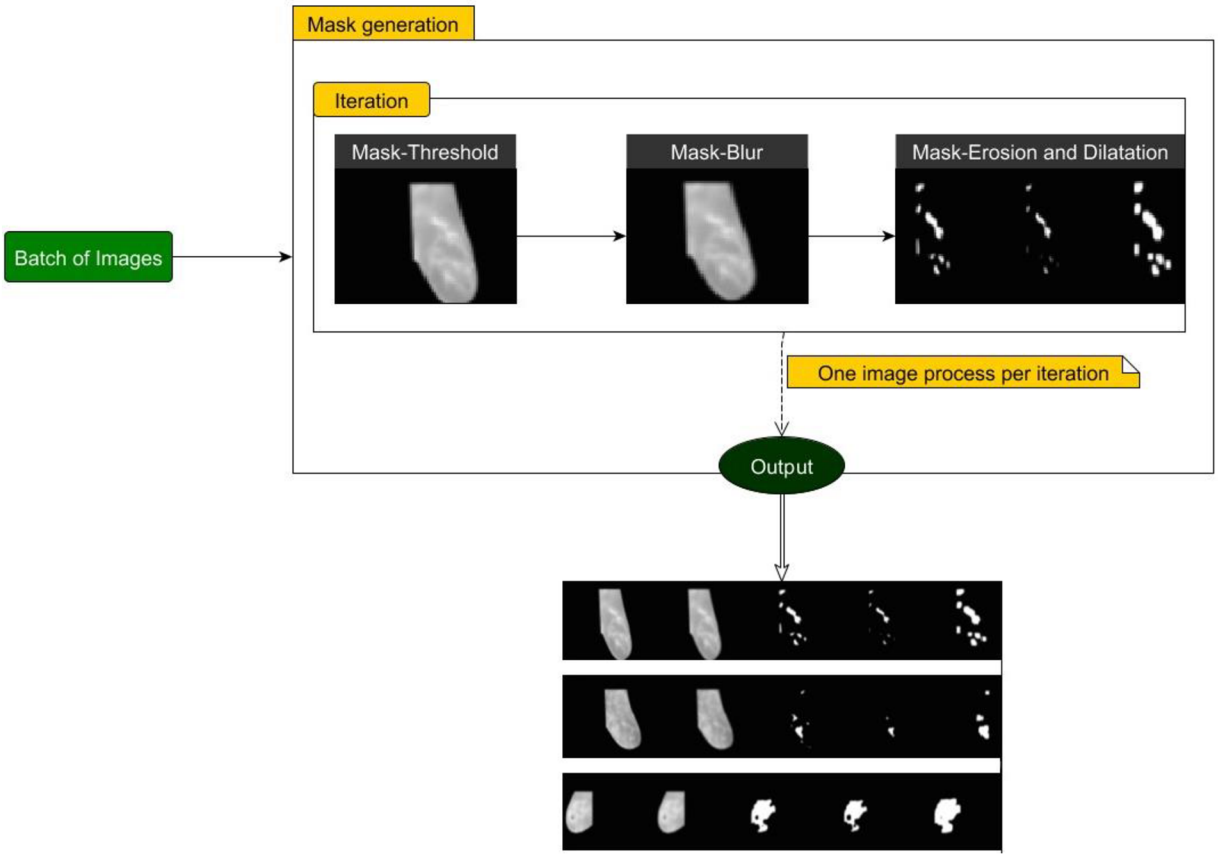

Figure 27. Different stages require to obtain an effective cancerous area (high peak of temperature). It is the whitest zone of the grayscale image. (Own work).

Therefore, considering point-wise maximum denoted by w, the grayscale image's dilatation denoted $f \circ i$ can be computed as:

$$f \circ i = W_{x \in \mathbb{D}_i} f_x \tag{18}$$

At the end of each iteration, a corresponding cancerous area is generated. The resulting analysis can be read from left to Right, where on the middle image (see **Figure 28**), the red areas can be identified as the most subject to breast cancer. The rightmost image draws attention to another small region that should be considered in the final diagnosis to avoid a resurgence of new breast cancer.

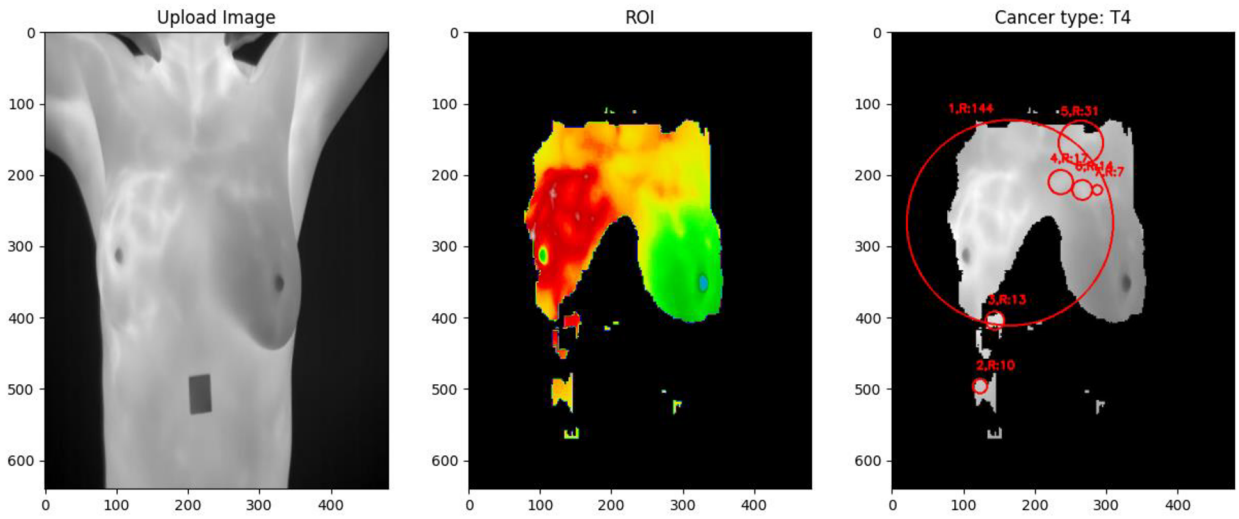

Figure 28. subsequent Mathematical Morphology processes of the Region of Interest (RoI). The input image, the extracted ROI, and the most likely cancer area circled in Red are left to right. (Own work).

As in the article (S. Mambou et al., 2019b), each thermal image went through blurring, erosion, and expansion to reveal the region of interest, in our case, the area with a higher metabolism; hence the highest temperature.

6.4. Case study 2: Deep models applied to MRI Brain Cancer

Considering the need for a dataset with a more representative case of brain cancer, the repository (*Brain MRI Images for Brain Tumor Detection*, 2020) is organized, as shown in the structure below (see **Figure 29**).

6.4.1. Preprocessing Phase.

As mentioned before, one of the essential screening exams for brain tumor diagnosis is MRI. It delivers a considerable amount of pictures with crucial features; however, the processing of those features is sometimes obstructed by hair in the image or by a dark area surrounding the skull.

As mentioned before, one of the essential screening exams for brain tumor diagnosis is MRI. It delivers a considerable amount of pictures with crucial features; however, the processing of those features is sometimes obstructed by hair in the image or by a dark area surrounding the skull.

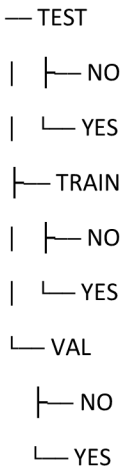

Figure 29. Description of the distribution of brain images in the data set (*Brain MRI Images for Brain Tumor Detection*, 2020). Three main folders appear: The Test folder, which will be used for an active model; the Train folder used during the training phase; and the Val folder, which contains an image.

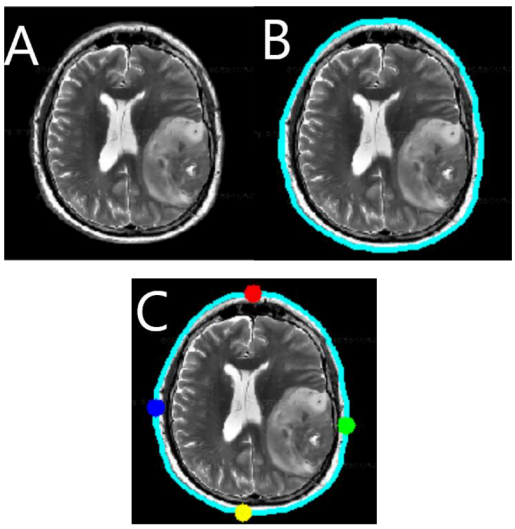

Figure 30. Given an MRI image (A), a preprocessing phase must be applied to extract the largest contour representing the border of the skull (B) and the four symmetrical extreme points that will be used to crop the image (C). (Own work).

To address those issues, a preprocessing phase is required (see **Figure 30**). First, the most significant contour representing the skull's border (B) is extracted, and the four symmetrical extreme points are determined and used to crop the image (C).

Considering the General Data Protection Regulation (GDPR) on data protection and privacy in the European Union, data collection becomes stricter and submits to patient consent. Therefore, it becomes crucial for researchers to find a way to maximize their efficiency using the amount of data available (see **Figure 29**). Again, data augmentation appears to be the solution; a rotation of 15 degrees, in this case, is used (see **Figure 31**).

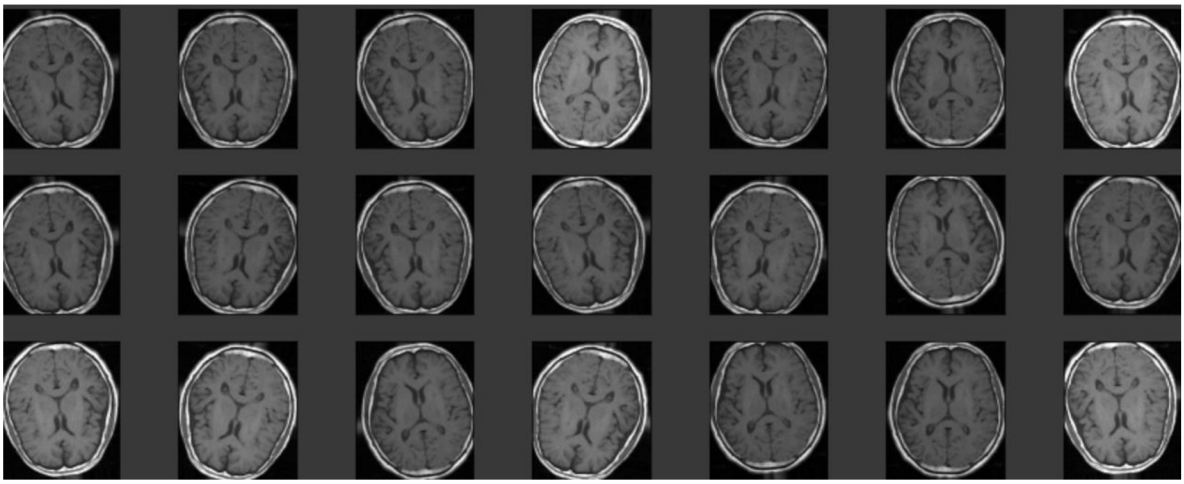

Figure 31. Data augmentation of the brain MRI images. It increases the amount of training and test data for designing and evaluating an effective model. (Own work).

During the preprocessing phase, one of the essential things to do is to implement a data generator that will return a batch of images with the correct size, identical to the input requirements of the custom model. In addition, I mention the importance of checking if for each image the correct mask is associated (see **Figure 32**). The latter can be easily verified by adopting a specific measurement such as "checkboard graduation" to compare the location of the tumor on the two images (original MRI image and segmentation) (see **Figure 33**).

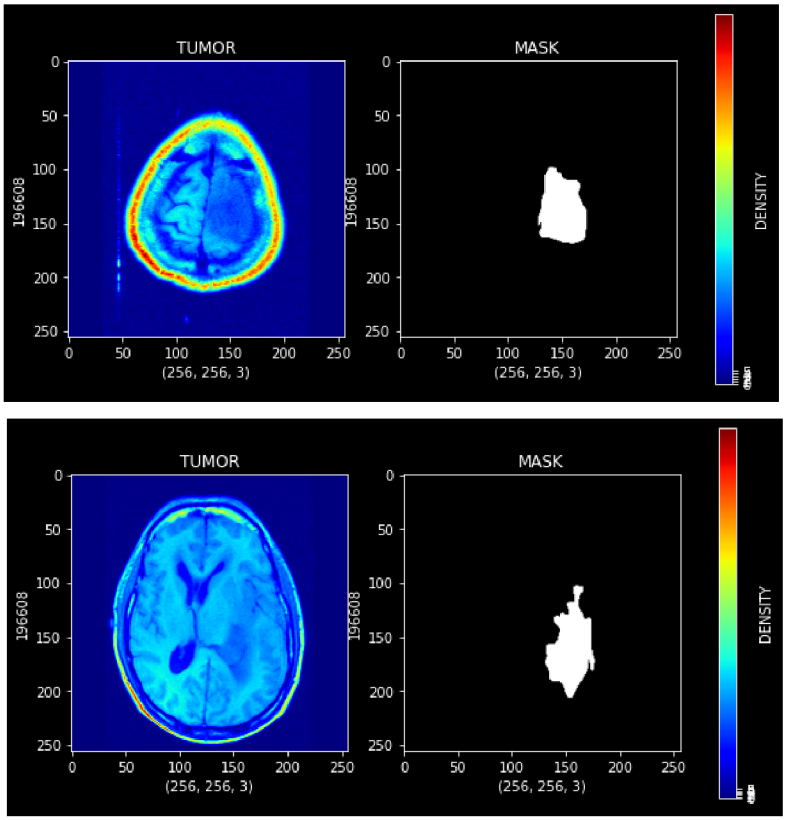

Figure 32. MRI image of two brains with their correspondent ground truth segmentation. *(Own work).*

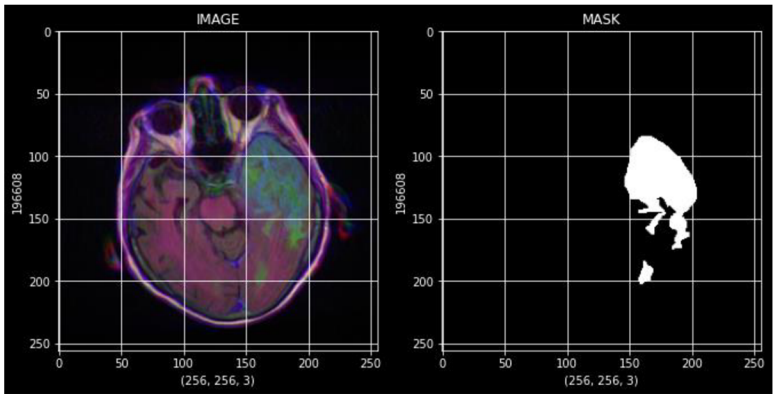

Figure 33. Checkerboard graduation of an image, allowing to compare with an exact measure where the segment is located. (Own work).

Another important point during the preprocessing phase is to understand the data you are working on fully. This can be easily achieved with the visualization process, where you highlight the key component of the dataset. An example can be the dataset containing MRI images of the brains with and without tumors(*Brain MRI Segmentation*, n.d.). For example, relevant colour map application components such as skull border and tumor can be easily seen (see **Figure 34**).

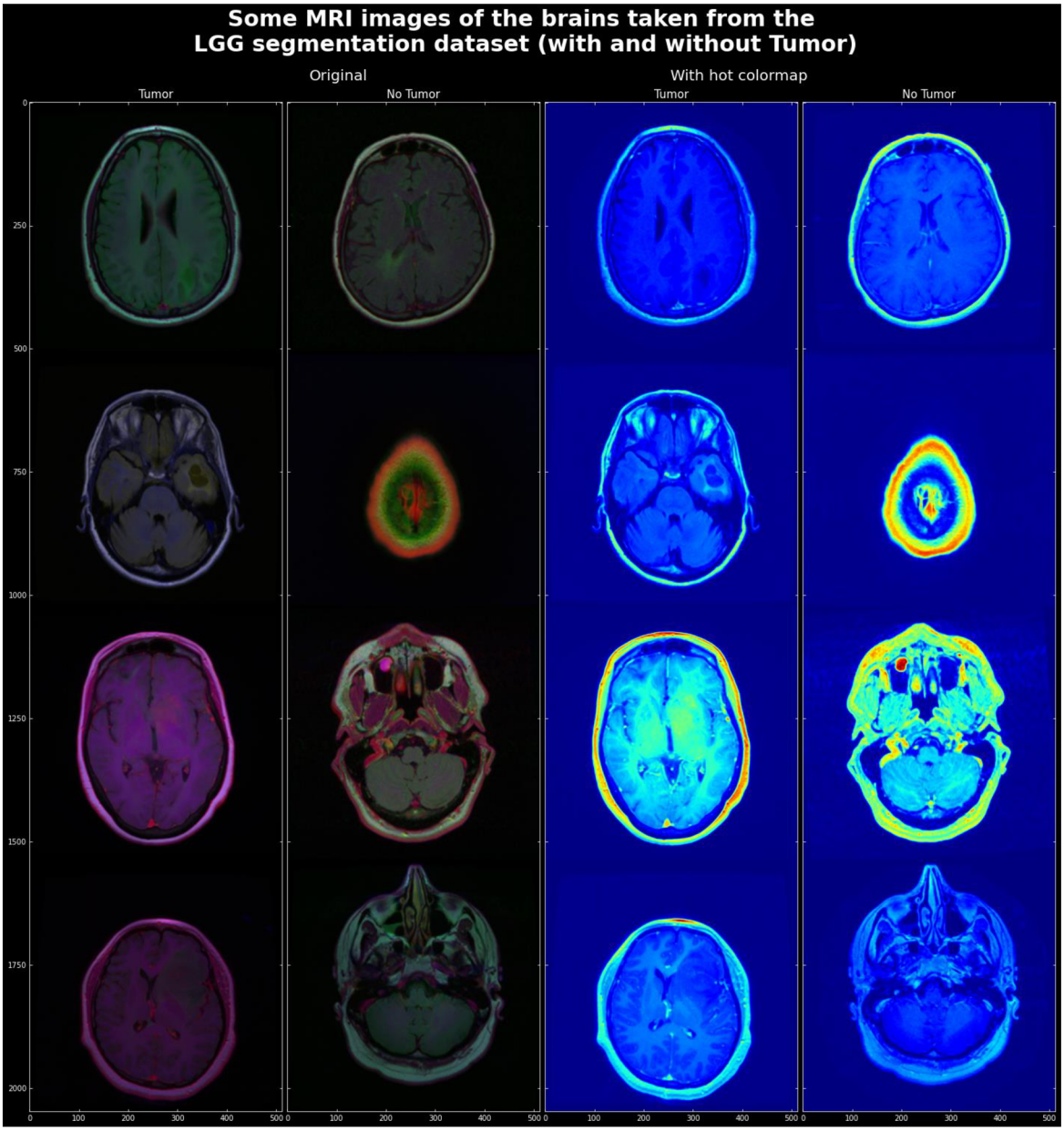

Figure 34. MRI images of the brains with and without tumors(Brain MRI Segmentation, n.d.). A color map is used here to reveal relevant features to human eyes, such as skull border and tumor area. (Own work).

It was necessary to choose the best representation of the region of interest (ROI).

Two main representations were chosen:

- In the first one, the tumor area or ROI is circle by a bold line to drive the doctor's attention.
- The second representation was to superimpose the predicted mask (ROI) to the original image (input image) to see in the brain where the tumor resides (see **Figure *35***)

The latter will be the one used for the rest of the study. Another essential point was to mention that using validation data, the accuracy of the custom model can be quickly evaluated by putting side by side the ground truth mask and the predicted mask (see **Figure *35***).

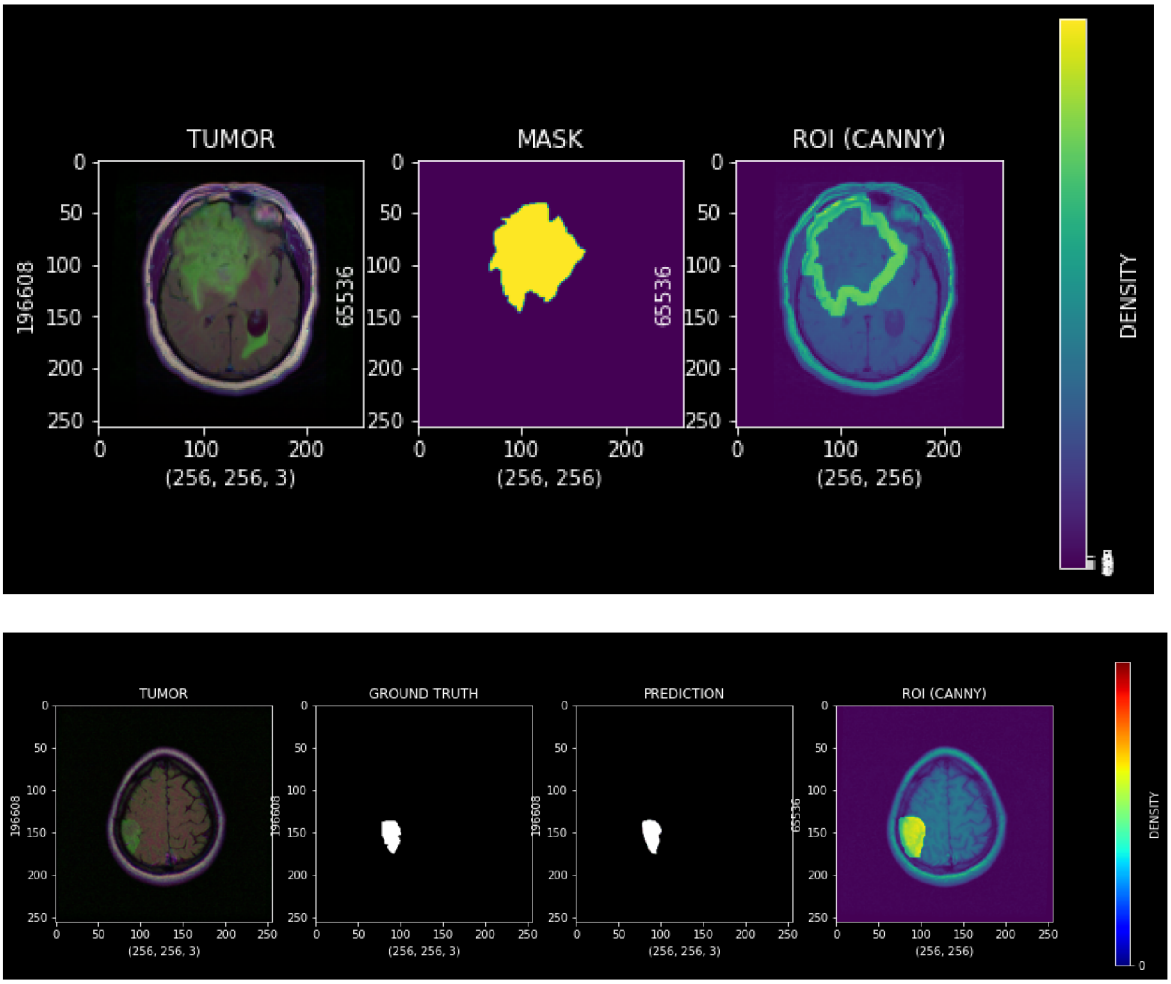

Figure 35. Different representations of the ROI. The ROI is circled by a bold line to drive the doctor's attention. In the second representation, the predicted mask (ROI) and the original image (input image) are superimposed to see where the tumor resides in the brain. (Own work).

It is essential to think and design a hyperparameters tuning algorithm during the preprocessing phase to achieve the best possible result. However, this is feasible only if you understand the architecture and are aware of the possible techniques offered by your development framework, in this case, TensorFlow. It is also essential to go through research papers discussing similar topics to understand their difficulties and how they succeed in overcoming them.

Before introducing the hyperparameters tuning algorithm, let me define what it is meant here by model hyperparameters. A model hyperparameter is a configuration external to the model. Given the data and a problem to be solved, the best value for a model hyperparameter cannot be determined. However, the values used to solve a similar situation, or a rule of thumb can approximate the best hyperparameters in the model. The latter is found mainly through trial and error. I adjust the model hyperparameters to find values that give the most skilful predictions (see Figure 36). Indeed, these parameters directly control the behaviour of the learning algorithm. These have a significant impact on the performance of the model and can make the algorithm shine.

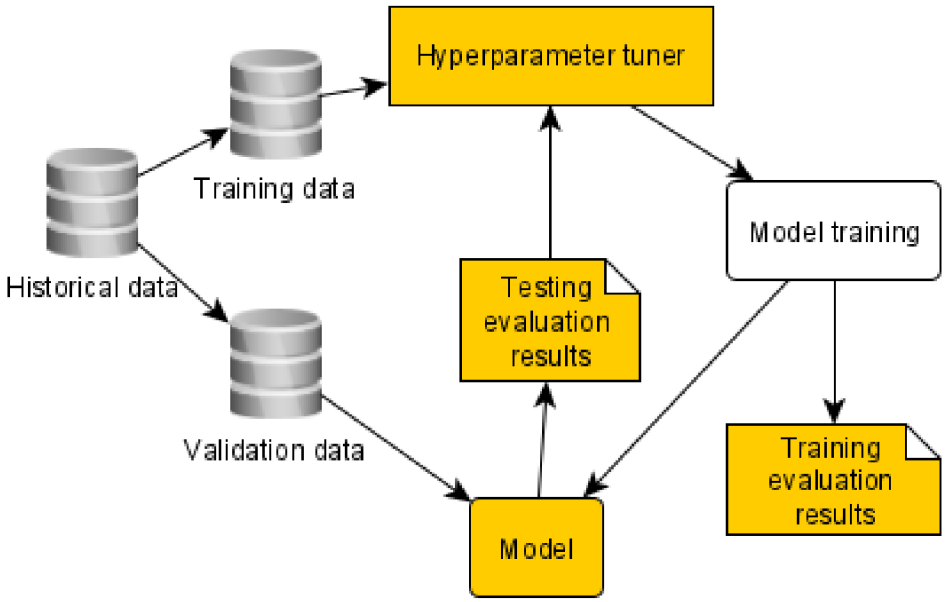

Figure 36. Hyperparameter tuning in the optimization of the training process and accuracy of a given model. (Own work).

6.4.2. An automatic processing of the brain MRI.

Several metrics (Accuracy, dice_coef, mean intersection over union, ...) were described in the previous sub-subsection. Let us look at another relevant element, the loss function used in this study. Binary cross entropy compares each predicted probability to the actual class output, 0 or 1. It then calculates the score that penalizes the possibilities based on distance from the expected value. It means how near or far from the actual value.

Binary cross entropy can be expressed by the formula (19):

$$L_{Pr}(x) = -\frac{1}{N}\sum_{t=1}^{N} v_i \times log(\Pr(v_i)) + (1 - v_i) \times log(1 - \Pr(v_i)) \quad (19)$$

Y is the label (1 for tumor tissue and 0 for other brain tissue) and $\Pr(v)$ is the predicted probability that the point will be part of the tumor area for all N points.

Reading this formula tells you that, for each point of tumor tissue ($v = 1$), it adds the log ($\Pr(v)$) to the loss, that is, the log of the probability that it is a tumor tissue. Conversely, it adds log (1-$\Pr(v)$), i.e., the log of probability that it is another brain tissue, for each brain tissue $v = 0$).

Having said all the above, let us focus on this subsection's main point (to extract the region of interest automatically). As defined in section 5, a custom model is used to segment a given MRI of a brain, the area containing tumor tissue. It is good to mention that the images used here were preprocessed as per the previous sub-section (preprocessing phase).

A VGG19 backbone:

Given a backbone VGG19, the custom model has 22,349,955 parameters, out of which 2,324,611 were subjected to intensive training. After hyperparameters tuning, a mean intersection union reached a value above 91 % on both training and validation data (see Figure 37).
As shown in the training log:

Epoch 00020: val_mean_io_u improved from 0.91291 to 0.91327, saving model to checkpoints_VGG19/vgg_unet_weights.20210628.hdf5

86/86 - 17s - loss: -9.0780e-01 - _dice_coef: 0.9075 - binary_accuracy: 0.9958 - _true_positive_rate: 0.9250 - mean_io_u: 0.8920 - val_loss: -8.7604e-01 - val__dice_coef: 0.8787 - val_binary_accuracy: 0.9940 - val__true_positive_rate: 0.9486 - val_mean_io_u: 0.9133 - lr: 6.4000e-05 Epoch 21/100

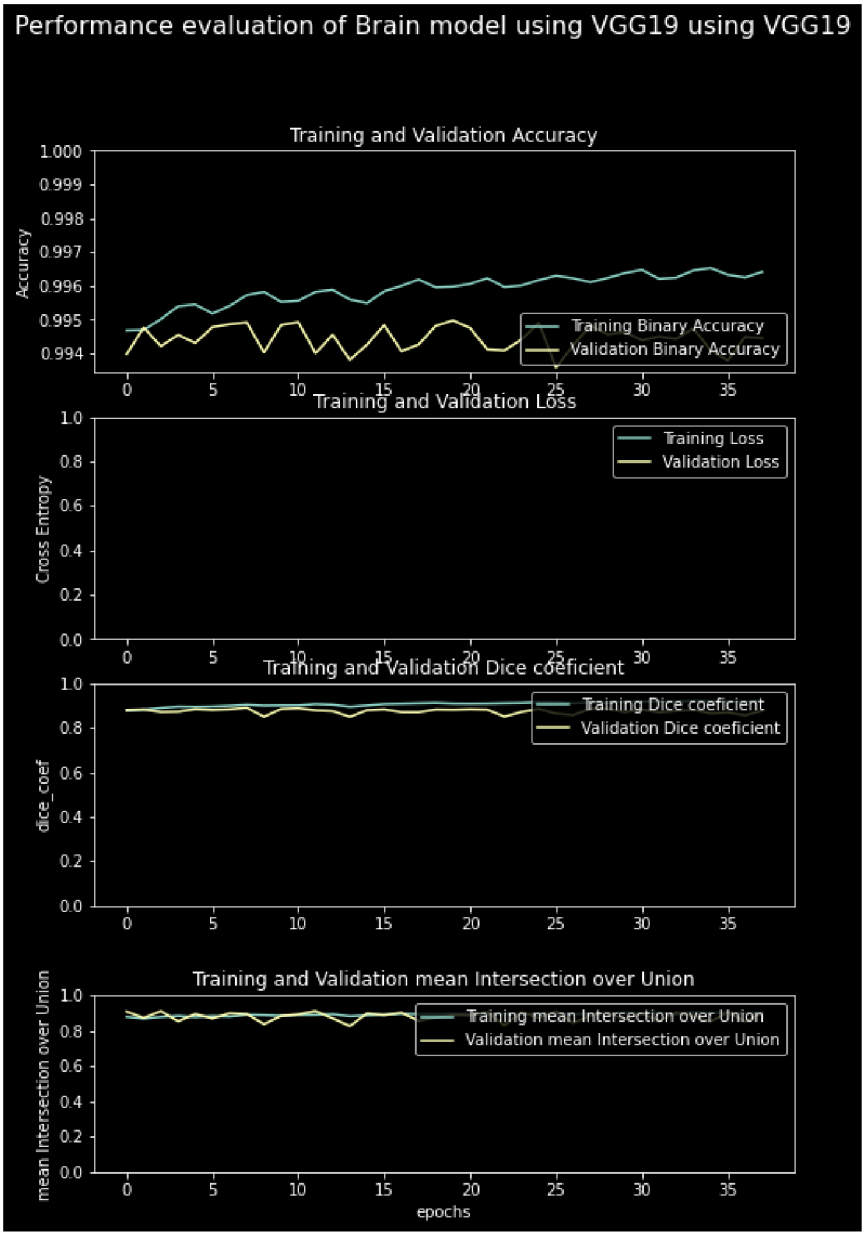

Figure 37. Performance of the custom u-net model using VGG19 on Brain MRI images. Note the epoch (abscise) graduation with 1 unit = 10 epochs to show the different intersections of the learning and validation curves due to the gradual change in the learning rate up to 0.0001. (Own work)

To give the reader a better understanding, a visualization of the result has been given. Here, the model is again fitted by a new image (not known by the system), and the predicted mask (segment)

receives a probabilistic image. The latter is internally converted to a binary image, displayed and superimposed on the original image to clearly show the area where the tumor resides (see **Figure 38**).

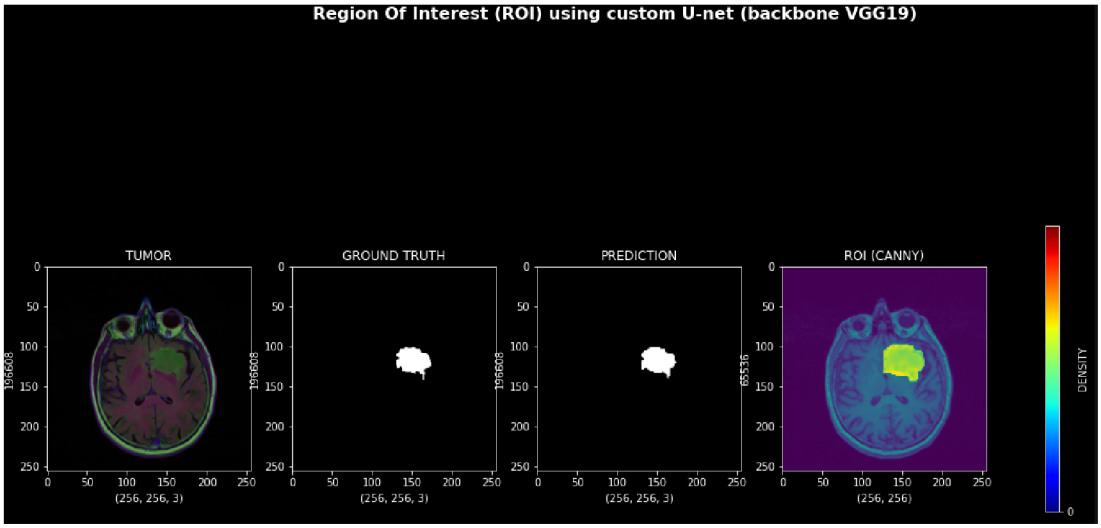

Figure 38. Area of the tumor detected by the custom model (Unet) with backbone VGG19; this was achieved after several iterations. (Own work)

Following the same process, a new backbone was selected, a resnet34 is a 34-layer convolutional neural network that can be utilized as a state-of-the-art image classification model. Also, in this case, the backbone used transfer learning to load the pre-trained model. The latter was trained on the ImageNet dataset, which has 100,000+ images across 200 different classes.

A Resnet34 backbone:

Resnet34 appears as a state-of-the-art model (see **Figure 39**), offering less computation and impressive accuracy and speed. However, the architect appears as the most convolution neural network that means a succession of layers that, when put together, can fit a softmax layer with great features allowing it to perform the classification based on some classes specified before the training.

Following the same evaluation criteria, the same images, tuning algorithm, metrics, loss function, and the same problem to be solved (segmentation of the tumor area). The custom model with backbone restnet34 reached a mean intersection over the union above 82 % for both training and validation data (see **Figure 42**).

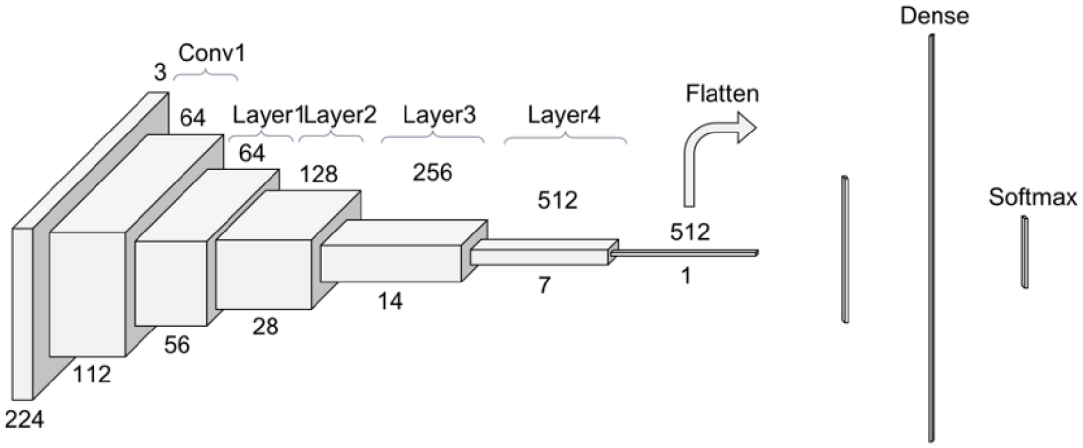

Figure 39. A Restnet34 model. It appears to be a state-of-the-art model, offering less computation and impressive results such as accuracy and speed (Ruiz, 2019).

Epoch 00020: val_mean_io_u improved from 0.80477 to 0.82830, saving model to checkpoint_restnet34/vgg_unet_weights.20210628.hdf5

86/86 - 10s - loss: -9.3160e-01 - _dice_coef: 0.9314 - binary_accuracy: 0.9970 - _true_positive_rate: 0.9489 - mean_io_u: 0.7470 - val_loss: -8.4150e-01 - val__dice_coef: 0.8391 - val_binary_accuracy: 0.9939 - val__true_positive_rate: 0.9040 - val_mean_io_u: 0.8283 - lr: 1.0000e-04

Epoch 21/100

Despite the low mean intersection over the union (meanIoU), a visualization of the predicted mask reveals a prediction not so far from the ground truth, especially when both images (original image and predict tumor area) are superimposed (see **Figure 40**).

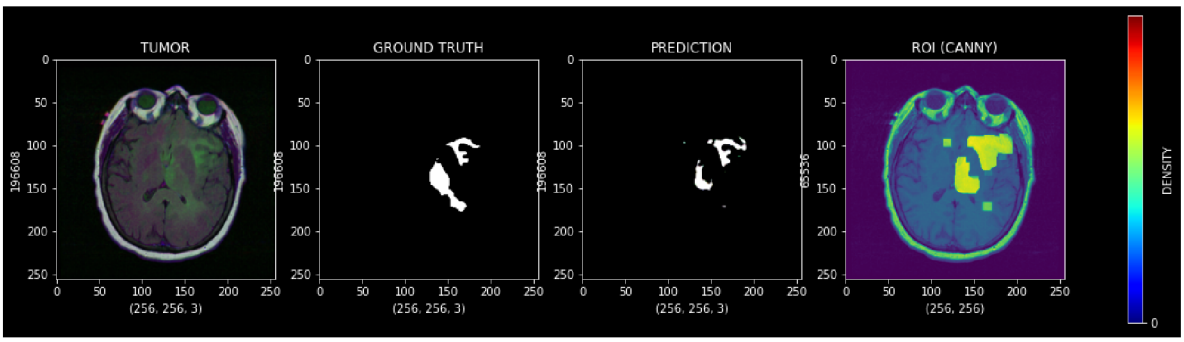

Figure 40. Area of the tumor detected by the custom model (Unet) with backbone Resnet34; this was achieved after several iterations. (Own work)

An InceptionV3 backbone:

Inception v3 proposed in (Szegedy et al., 2015) primarily focuses on consuming less computing power by modifying previous Inception architectures.

Compared to VGGNet, Inception networks have proven to perform well, both in terms of the economic cost incurred (memory and other resources) and the number of parameters generated by the network. However, if changes are made to a launch network, care must be taken to ensure that its primary benefits are not lost. Thus, adopting an Inception network for different use cases turns out to be a problem due to the uncertainty of the efficiency of the new network. In an Inception v3 model, several network optimization techniques have been proposed to relax the constraints and facilitate model adaptation. The techniques include factorized convolutions, regularization, dimension reduction, and parallelized calculations as explained below:

- Factored convolutions: this helps reduce computational efficiency because it reduces the number of parameters involved in a network. It also monitors the efficiency of the network.
- Smaller convolutions: Replacing larger convolutions with smaller convolutions indeed leads to faster training. Let's say a 5 × 5 filter has 25 parameters; two 3 × 3 filters replacing a 5 × 5 convolution only have 18 parameters (3 * 3 + 3 * 3) instead.

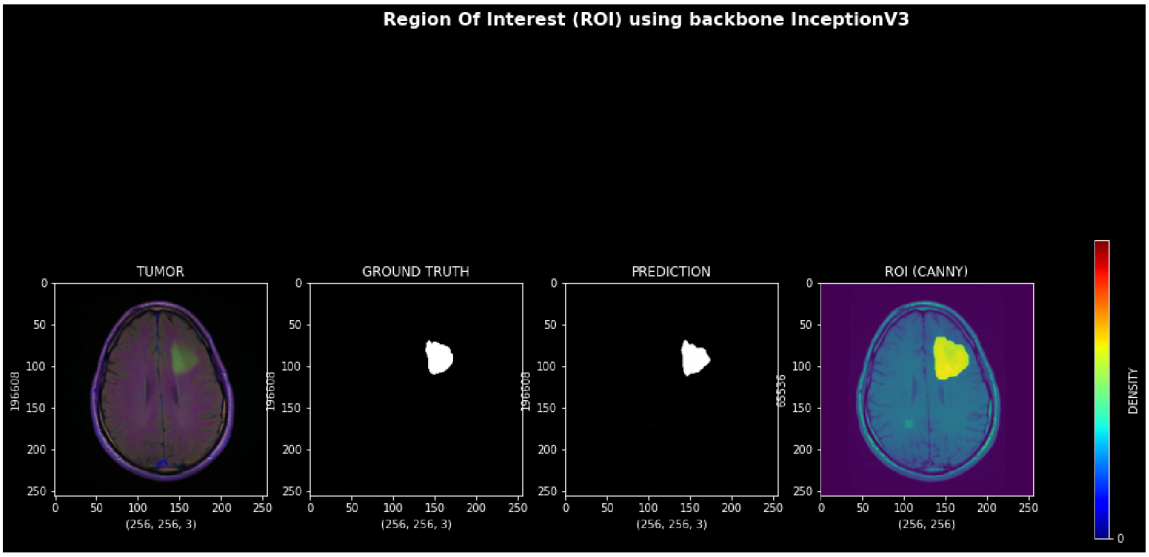

Figure 41. Area of the tumor detected by the custom model (Unet) with backbone InceptionV3; this was achieved after several iterations. (Own work)

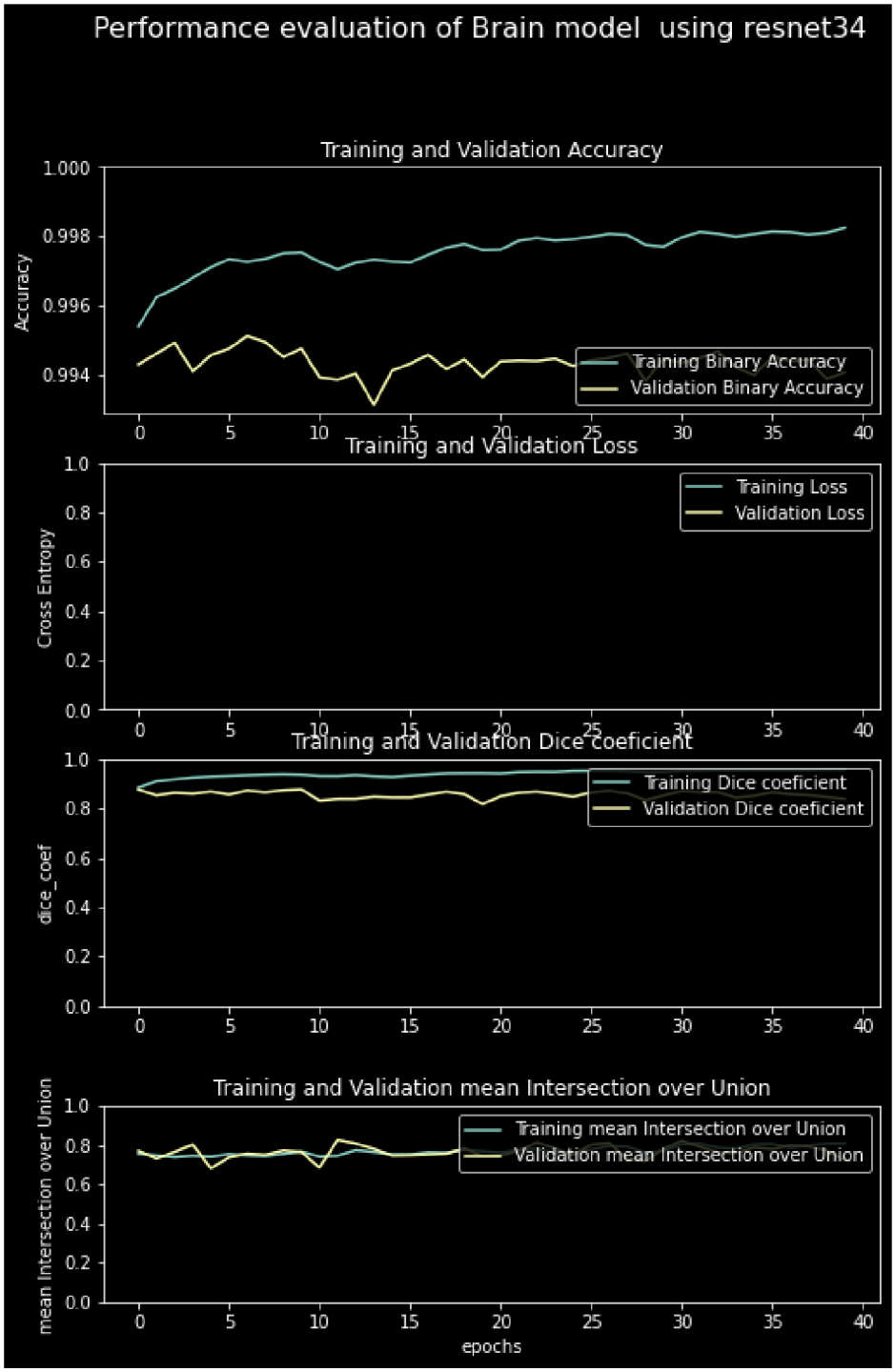

Figure 42. Performance of the custom u-net model using Resnet34 backbone on Brain MRI images. Note the epoch (abscise) graduation with 1 unit = 5 epochs to show the different intersections of the learning and validation curves due to the gradual change in the learning rate up to 0.0001. (Own work)

- Asymmetric convolutions: A 3 × 3 convolution could be replaced by a 1 × 3 convolution followed by a 3 × 1 convolution. If a 2 × 2 convolution replaces a 3 × 3 convolution, the parameters would be slightly higher than the proposed asymmetric convolution.
- Auxiliary Classifier: An auxiliary classifier is a small CNN inserted between layers during training, and the loss suffered is added to the loss of the main network. In GoogLeNet, auxiliary classifiers were used for a deeper network, while in Inception v3, an auxiliary classifier acts as a regularization.
- Reducing the grid's size: Reducing the grid's size is usually done by grouping operations.

  The architecture can be represented as a succession of layers (convolutional layers, Average Pooling layer, Maxpooling layer, …) which, when put together, give a robust network.

A visualization of the predicted mask reveals a prediction not so far from the ground truth, especially when both images (original image and predicted tumor area) are superimposed (see **Error! Reference source not found.**).

Following the same evaluation criteria, the same images, tuning algorithm, metrics, loss function, and the same problem to be solved (segmentation of the tumor area). The custom model with backbone InceptionV3 reached a mean intersection over the union above 70 % for both training and validation data (see

Figure 43).

As shown in the training log:

Epoch 00069: val_mean_io_u improved from 0.68916 to 0.70581, saving model to checkpoint_inceptionv3/vgg_unet_weights.20210628.hdf5

86/86 - 12s - loss: -9.6051e-01 - _dice_coef: 0.9592 - binary_accuracy: 0.9982 - _true_positive_rate: 0.9704 - mean_io_u: 0.6496 - val_loss: -7.7721e-01 - val__dice_coef: 0.7770 - val_binary_accuracy: 0.9918 - val__true_positive_rate: 0.7955 - val_mean_io_u: 0.7058 - lr: 5.1200e-05

Epoch 70/100

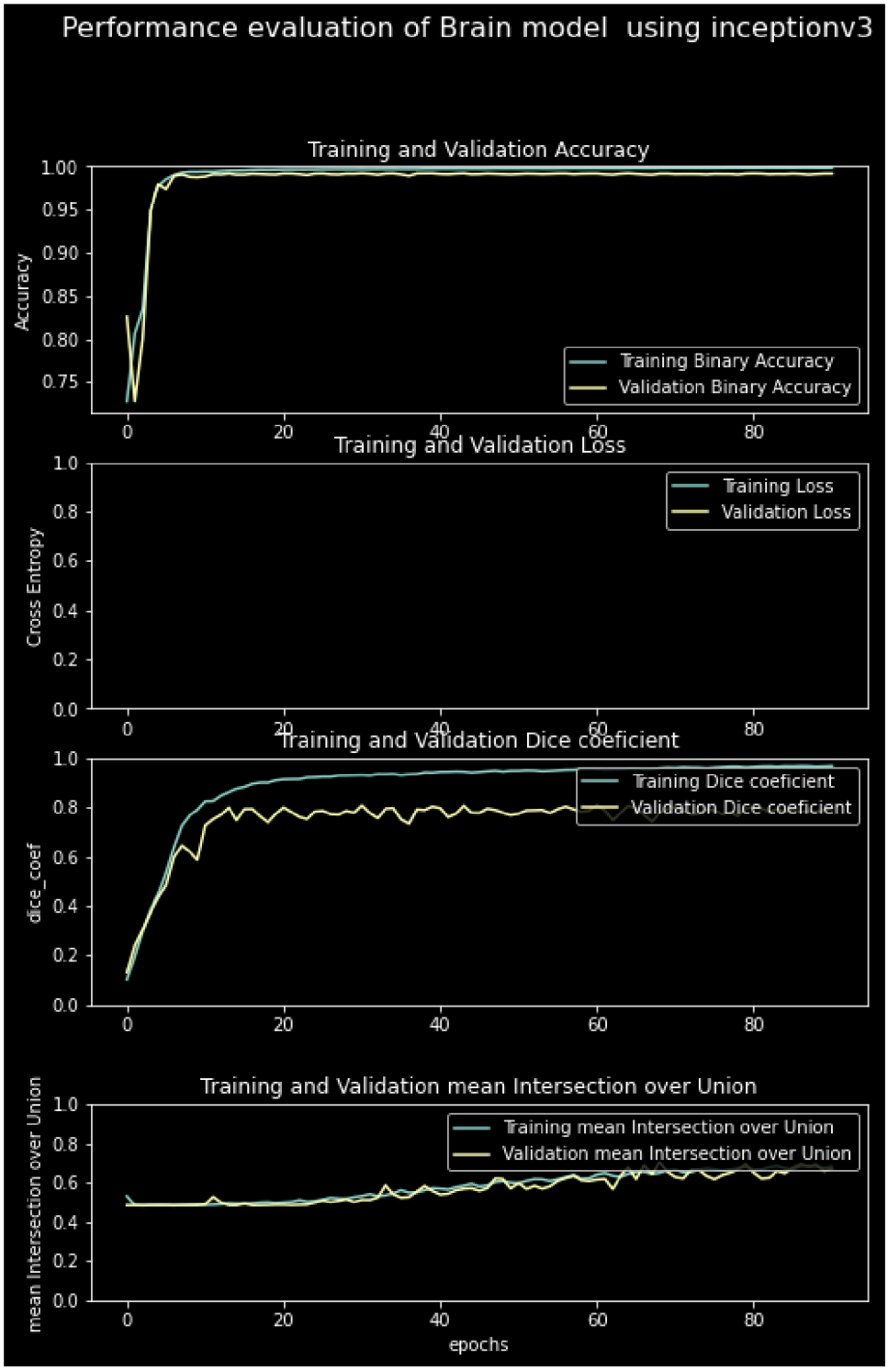

Figure 43. Performance of the custom u-net model using InceptionV3 backbone on Brain MRI images. Note the epoch (abscise) graduation with 1 unit = 20 epochs to show the different intersections of the learning and validation curves due to the gradual change in the learning rate up to 0.0001. *(Own work)*

An Efficientnetb4 backbone:

Proposed in (Tan & Le, 2020), EfficientNet is a new model scaling method that uses a simple but efficient compound coefficient to scale CNNs more structured way. Unlike conventional approaches that arbitrarily scale network dimensions, such as width, depth, and resolution, the authors' method uniformly scales each dimension with a fixed set of scaling coefficients. Using this new scaling method and recent advancements in AutoML, they developed a family of models, called EfficientNets, that outperform peak accuracy with up to 10 times the efficiency (faster and smaller).

To understand the effect of network scaling, they systematically studied the impact of scaling different dimensions of the model. Although scaling individual dimensions improves model performance, they observed that balancing all network dimensions (width, depth, and image resolution) against available resources would best improve the results. Therefore, a grid search method is used in the compound scaling method to find the relationship between the different primary network scaling dimensions under a fixed resource constraint (two times more FLOPS). The obtained relationship helps to determine the appropriate scale coefficient for each of the measurements mentioned above. The authors then apply these coefficients to extend the backbone network to the size of the target model or the desired computational budget.

The architecture can also be represented as a succession of layers (convolutional layers, Average Pooling layer, Maxpooling layer, …). However, the compound scaling method uniformly scales all dimensions in a principled way.

Following the same evaluation criteria, the same images, tuning algorithm, metrics, loss function, and problem to be solved (segmentation of the tumor area); The custom model with backbone EfficientNetb4 reached a mean intersection over the union above 74 % for both training and validation data (see

Figure 45). A visualization of the predicted mask reveals a prediction not so far from the ground truth, especially when both images (original image and predicted tumor area) are superimposed (see

Figure 44).

As shown in the training logs:

Epoch 00072: val_mean_io_u improved from 0.69503 to 0.74039, saving model to checkpoint_efficientnetb4/vgg_unet_weights.20210628.hdf5

86/86 - 20s - loss: -9.5113e-01 - _dice_coef: 0.9511 - binary_accuracy: 0.9978 - _true_positive_rate: 0.9611 - mean_io_u: 0.6900 - val_loss: -8.3932e-01 - val__dice_coef: 0.8384 - val_binary_accuracy: 0.9932 - val__true_positive_rate: 0.9449 - val_mean_io_u: 0.7404 - lr: 5.1200e-05

Epoch 73/100

This result leads us to believe that with further scaling, more data, and a particular focus on the custom model with EfficientNet as the backbone, a better result can be achieved, especially that there is another flavor of the EfficientNet architecture.

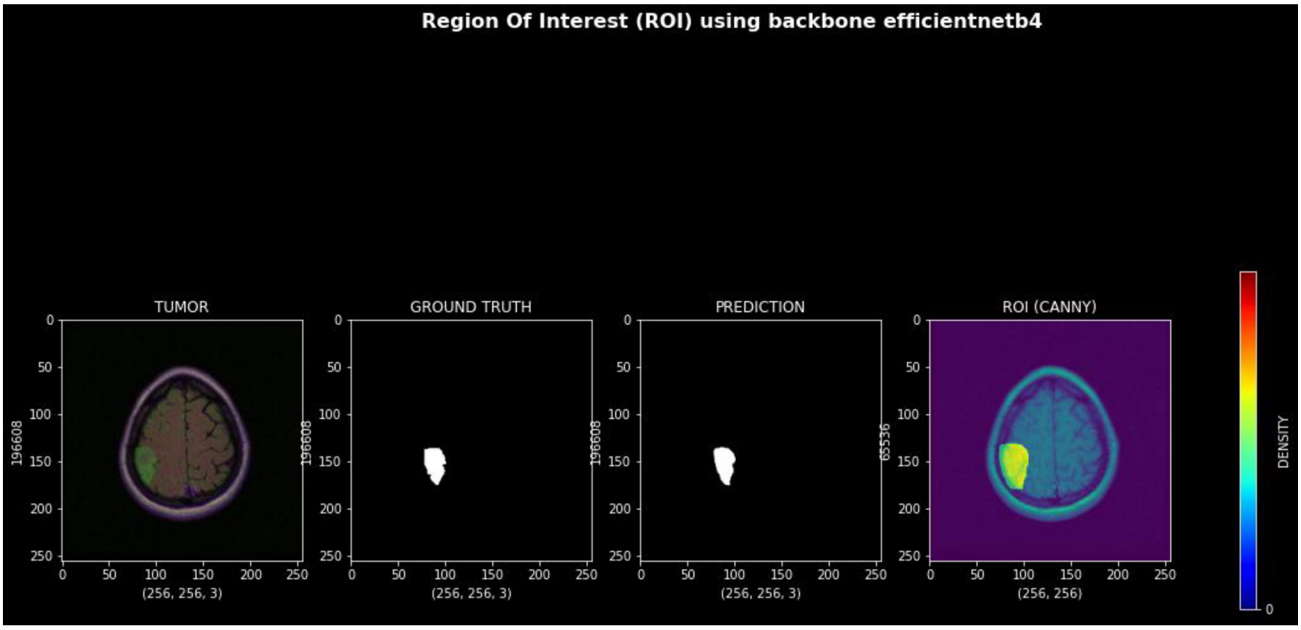

Figure 44. Area of the tumor detected by the custom model (Unet) with backbone Efficientnetb4; this was achieved after several iterations. (Own work)

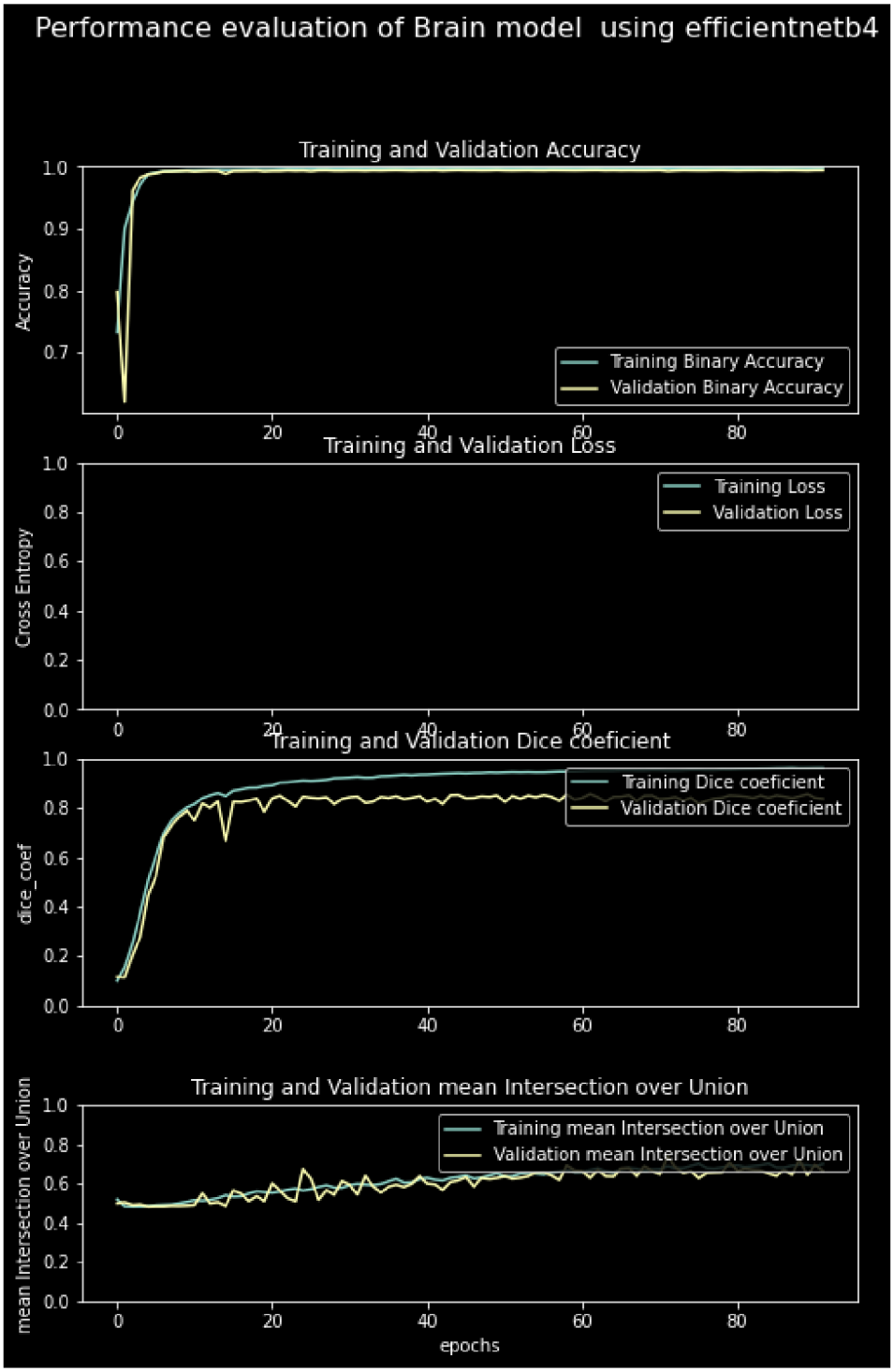

Figure 45. Performance of the custom u-net model using Efficientnetb4 backbone on Brain MRI images. Note the epoch (abscise) graduation with 1 unit = 20 epochs to show the different intersections of the learning and validation curves due to the gradual change in the learning rate up to 0.0001. (Own work).

7. Implementation of proposed Framework

The Internet of Things (IoT) describes physical objects integrated with software, sensors, processing capability, and other technologies, connecting and exchanging data with other devices and systems over the Internet or other communications networks.

Given the need to facilitate computer diagnosis aid, this subsection develops and implements a practical component to respond to a voice request using a set of parts. These last are voice recognition devices coupled to a RaspberryPi containing the BDetector software (the code for detecting breast cancer) (see **Figure 46**). *Note that as part of the second sub-goal mentioned in section 2, I have fully implemented the code in raspberry pi (and AWS) as an independent component that can be used via voice commands (not yet implemented) or a Rest-API (fully implemented). Also, note that the thermal images to be processed are stored in an amazon simple storage service (s3) bucket so that we can achieve a great result with a powerful thermal camera without depending on the manufacturer of a model.*

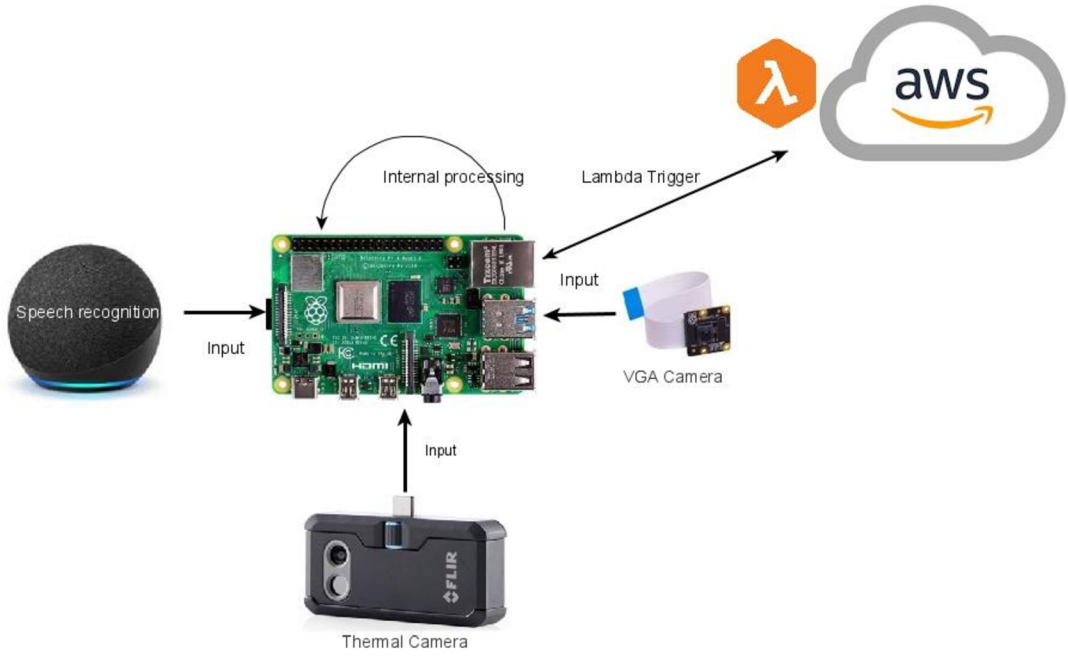

Figure 46. implementation of the proposed framework. Here, several components are put together, such as the voice recognition devices coupled to a RaspberryPi containing the BDetector software (the code for detecting breast cancer). (Own work)

7.1. The proper setup

As specified in the above sections, the design and implementation of this prototype went through a series of experiments where every component was tested. It is important to underline the great collaboration with the Department of Informatics Instituto de Computação, in Brazil via Prof. Aura Conci - IC / UFF - | Universidade Federal Fluminense, who agreed to provide the new thermal data set for the Visual lab project, which I used to improve my algorithm. The visual lab project (*Banco de Imagens Mastológicas*, n.d.) has proven the relevance of using thermal images to detect breast cancer. An interesting facet of this project is that it offers a real basis for future analyzes since it provides for the same patient a mammogram and a thermal image of the breast (The reason why I chose these thermal images as the input to my model).

It is also interesting to note the computational performance requirements of the artificial neural network developed here. According to Amazon and based on our experience, EC2 P3 instances (Table ***3.*** *Suitable EC2 instances* Table 3) have been proven to reduce machine learning training times from days to minutes and increase the number of simulations performed for high-performance computing by three times.

Table 3. Suitable EC2 instances

Instance Size	GPUs - Tesla V100	GPU Memory (GB)
p3.2xlarge	1	16

To ensure the portability of our solution, heavy computing is done in the cloud (Elastic cloud computing instance). Raspberry Pi retrieves the thermal images from the camera, ensures the correct format via a preprocessing phase and queries the BDetect_API (residing on AWS) to obtain the region of interest.

Also, note that the thermal images to be processed are stored in an amazon simple storage service (s3) bucket so that i can achieve a great result with a powerful thermal camera (minimum Thermal sensitivity = 40 mK at 30°C) without depending on the manufacturer of a model.

7.2. A proposed cloud-based Architecture

Cloud computing (CC) can be described as the on-demand availability of computer system resources, especially computing power, and data storage (cloud storage), without direct active management by the user. The term is generally used to describe the data centers available to many users on the Internet. Large clouds, predominant today (such as Amazon Web Services (AWS)), often have functions spread across multiple locations from central servers. If the connection with the user is relatively close, it can be designated an edge server. Some organizations prefer to have their clouds (corporate clouds), but right now, a few more businesses and governments are starting to see the savings they can make by moving to the cloud.

7.2.1. Use case diagram

The use case diagram is the initial form of software/product specifications for new, underdeveloped products. Use cases define the predictable action (what) and do not focus rigorously on the method to achieve it (how). Once established, use cases can be indicated by a visual or/and a textual representation (i.e., use case diagram). One of the main points of use case modelling is that it eases the design of a system from an end-user perspective. Thus, it is an effective technique for communicating the system's behaviour in user terms by specifying all the system's behaviours visible from the outside.

As part of the product resulting from the deployment of the custom U-net model, the end-user is considered the patient with relevant images (MRI of the brain or thermal images of the breast) and who would like to have a quick assessment or other opinions on the known diagnosis. It is also good to mention that doctors can use the system to facilitate their daily work.

Having said that, let us look at the below use case diagram (see **Figure 47**), where the user can perform:

- a login: Here, the users can enter their credentials in a secure layer connection HTTPS. A check credentials case is needed as the login data will be checked against an internal database. However, in the case of a new user, credentials will be saved for future connections.

- Take an appointment: Here, the users can list available doctors and, as per their convenience, select the expert. The appointment will be registered, and both doctor and patient will have the reserved time slot booked in their calendar.
- Automatic diagnosis: The users can upload the medical images via a secure connection set in the log-in case. These images will be checked to ensure they are really what the system expects, as per the comment mentioned before the upload action. Also, the relevant label (MRI of the brain or Thermal image) will be attached to the image as metadata to ease processing by the appropriate machine endpoint. The latter will return a picture with the segmented area, the type of tumor, and the diagnosis.

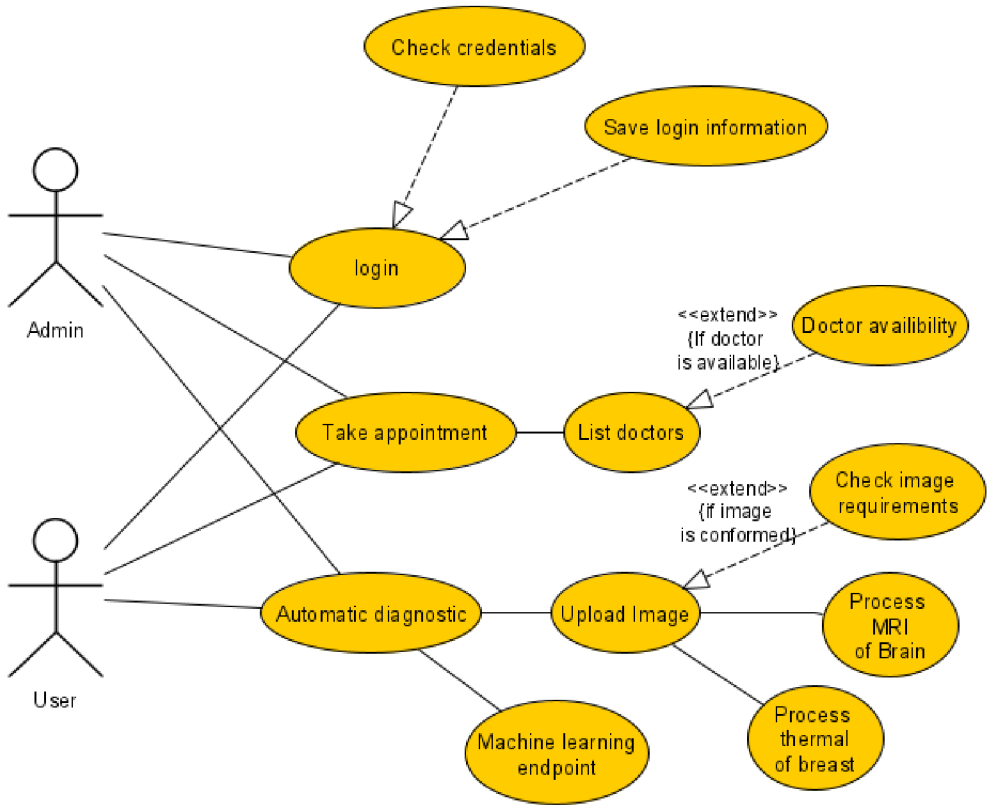

Figure 47. User case diagram of the deployed system (ouidr.com). Here, the user and the admin can perform several actions, but the admin will surpass other users in the design. *(Own work)*

7.2.2. Cloud Architecture

Sharing of resources is one of the main points of Cloud computing; it ensures consistency and economies of scale. The deployment of this project was made possible by the knowledge acquired

on diving in the AWS platform. AWS is a subsidiary of Amazon that provides on-demand cloud computing platforms and APIs to individuals, businesses, and governments on a pay-as-you-go basis. These cloud computing web services offer various basic abstract technical infrastructures and spread computing building blocks and tools. Amount the prevalent services offered by AWS; Amazon Elastic Compute Cloud (EC2) gives impressive benefit; it gives the impression to the end-user of share resources to be working on dedicated resources through the concept of virtual clusters.

Considering the need for a flexible platform, easy to use, and considering the time frame of this project. The choice of AWS platform and the architecture respond to all the above specifications, including the security aspect; note that the model process sensitive medical data that need to be in a secure environment. As shown in the image (see **Figure 48**), the model will reside in an entity called AWS Sagemaker, which is the machine learning (ML) component of AWS. Sagemaker allows the ML engineer to benefit from the concept of "dockerisation" (used of Docker) to develop on-premise and deploy in AWS with the same dependencies (on AWS), which can come from several packages installed during the development phase.

Going back to the diagram (see **Figure 48**), several numbers (1 to 7) are associated with the services. These numbers are present in the diagram to ease the explanation of the workflow of inference of the model. Without further due, let's go step-by-step:

Step 1: the user goes to his/her web browser type ouidr.com.
Step 2: Route53 will resolve the domain name server (DNS) and return the webpage where a login page will be prompted.
Step 3: The credentials entered by the user will be verified by the Aws Cognito service associated with the AWS STS service.
Step 4: A powerful service called CloudFront manages the load from the nearest edge location.
Step 5: Through a serverless design, the request sent to the API gateway will trigger a lambda function that will trigger the Sagemaker endpoint responsible for the machine learning inference (prediction of the model).
Note that all this is done in a fraction of seconds, allowing tremendous scalability if the number of concurrent users increases. Also, as presented in the use case diagram, the deployed system will

include several services (see **Figure 47**) that will ease doctors' work and make it affordable for such diagnoses worldwide.

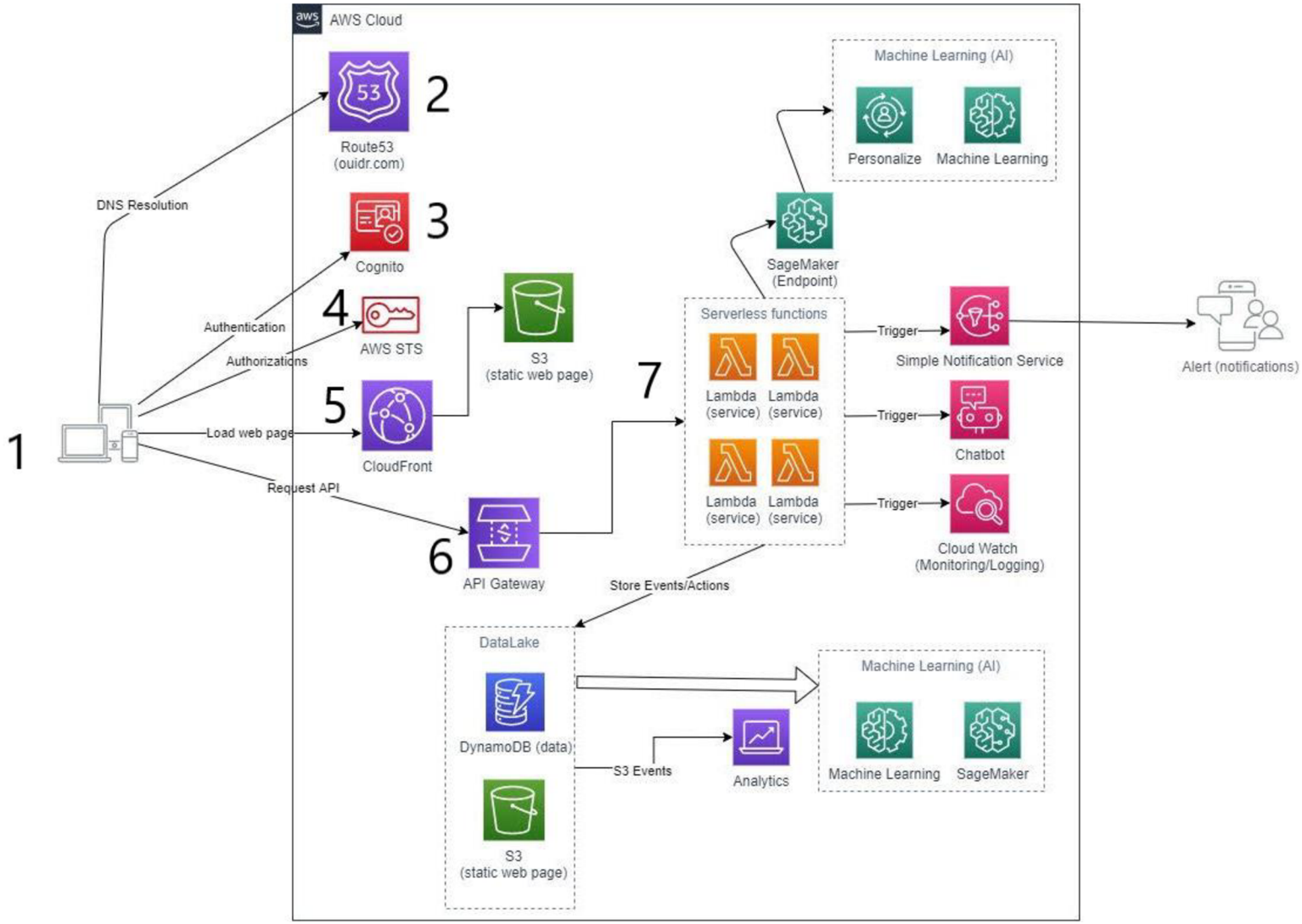

Figure 48. Services involved in the cloud architecture of the entire system, among those services, seven were flag with a number to give a clear picture to the reader of what is used just for the inference of the model described in this thesis. (Own work).

8. Discussion of results

Going through a more in-depth analysis of medical images with new techniques such as machine learning, the relevant findings from the previous section are discussed in the following lines.

8.1. Results of Case Study 1

Through literature (Advances in Breast Cancer Research - National Cancer Institute, 2019), a new process appears, which is 3D mammography, also known as breast tomosynthesis (BT). BT takes images from various angles around the breast and composes them into a 3-D type image. Although this technology is increasingly available in the clinic, it is unknown whether it is better than standard 2D mammography at detecting cancer at an earlier stage.

Taking the analysis further and given our intention to produce the most effective computer aid diagnosis, it was a question for us to minimize human intervention as much as possible. This is why the final concept presented in this article is the automatic extraction of the region of Concern (RC), obtained after designing a robust custom Unet which gave an impressive result to generate the correct mask, which is then used to circumscribe the RC (see **Figure 49**).

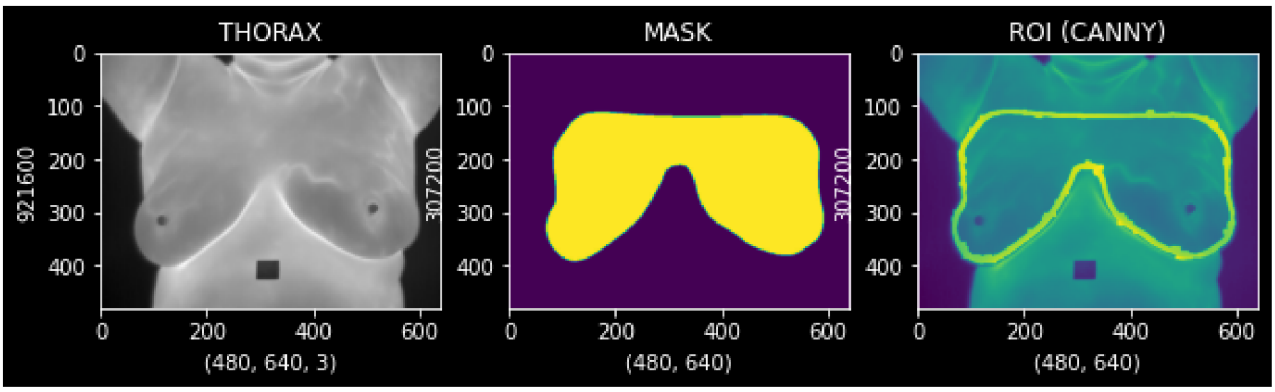

Figure 49. Given a grayscale image of a woman's thorax, a mask (region of concern) is generated and used to outline the area on the input image. This allows the user to see which area is being analyzed clearly. (Own work).

As in all cancer screening, two concerns are rising in breast cancer screening: the potential for diagnosing tumors that will not become life-threatening (overdiagnosis) and the possibility of receiving false-positive test results. As cancer treatment is becoming more individualized,

researchers are looking at ways to personalize breast cancer screening. They are studying screening methods appropriate for each woman's level of risk and limiting the possibility of overdiagnosis.

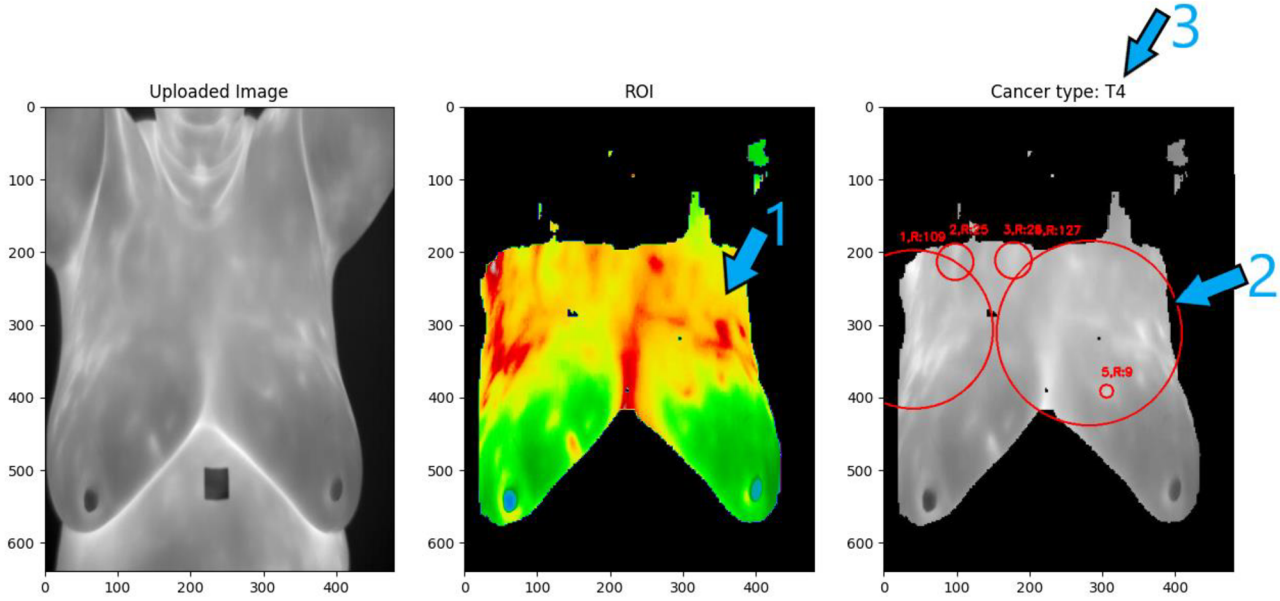

Figure 50. The RoI obtained from the extraction process and the color mapping: 1 represents the significant metabolism area, 2 and 3 show the most affected area and the breast cancer stage. (Own work).

It is one of the reasons why the results shown so far are so valuable. According to the figure above (see **Figure 50**), the system's output will provide a lot of useful information directly to the doctor and the patient. As you can see on the image, from left to right, there are respectively: the input image, upload in the system as per the requirements stated before; the Region of Concern (RC) at not confound with the Region Of Interest (ROI) shown here with number one arrow; the localization of the high metabolism as well the ROIs subject to further classification shown here by number 2 and number 3 as the output of the classification.

A Receiver Operating Characteristic (R.O.C) curve (see **Figure 51**) was used alongside the mean intersection union to choose which backbone will be kept for the inference of our custom Unet.

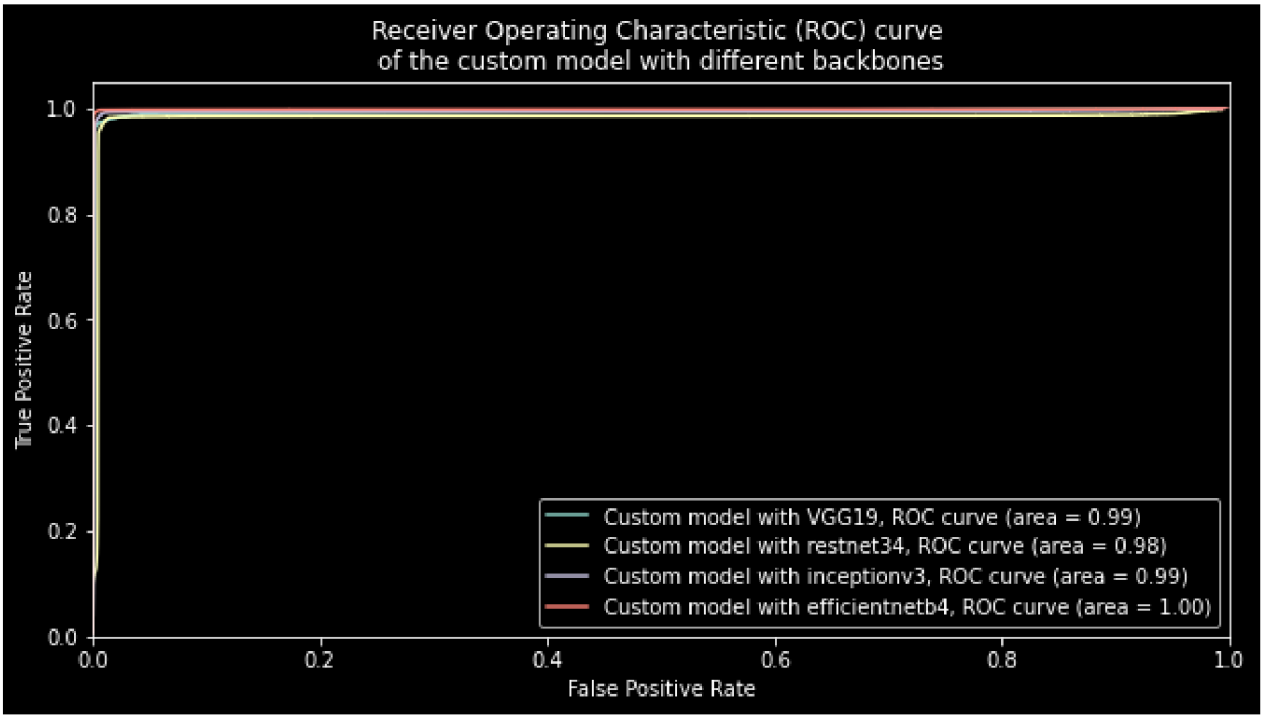

Figure 51. Cutting edge model used as the backbone of the custom Unet and evaluated via a R.O.C. (Own work).

8.2. Results of Case Study 2

Similar to breast cancer diagnosis, brain tumor diagnosis has its challenges. Still, one of the things in common is the need to have an early and accurate diagnosis of the tumor. The same architecture was used in this study, and the model was trained to perform on a 2d lower-grade glioma brain cancer dataset (*Brain MRI Segmentation*, n.d.).

Interestingly, DNN models' earlier layers tend to learn low-level concepts for deep convolutional networks while later layers develop higher-level (and specialized) feature mappings. Thus, i generally need to increase the number of feature maps (channels) as i deepen the network to maintain expressiveness. The latter is not an issue for an image classification task because, for this task, the importance resides on what the image contains (not where it is). Thus, i could lighten the computational load by periodically downsampling the feature maps through pooling or staggered convolutions (i.e., compressing spatial resolution) without worry. However, i would like our model to produce a semantic prediction at full resolution for image segmentation.

A popular approach for image segmentation models is to follow an encoder/decoder structure. Then, i downsample the spatial resolution of the input, developing lower resolution feature mappings that are learned to be very efficient at discriminating between classes oversampling feature representations in a full resolution segmentation map.

Looking closely at the Receive Operation Characteristic (ROC), it becomes clear why the custom model was designed with the VGG19 architecture as the backbone. Note the higher performance of the "Custom model with backbone VGG19" among the other derived models (with different backbones) (see

***Figure* 52**).

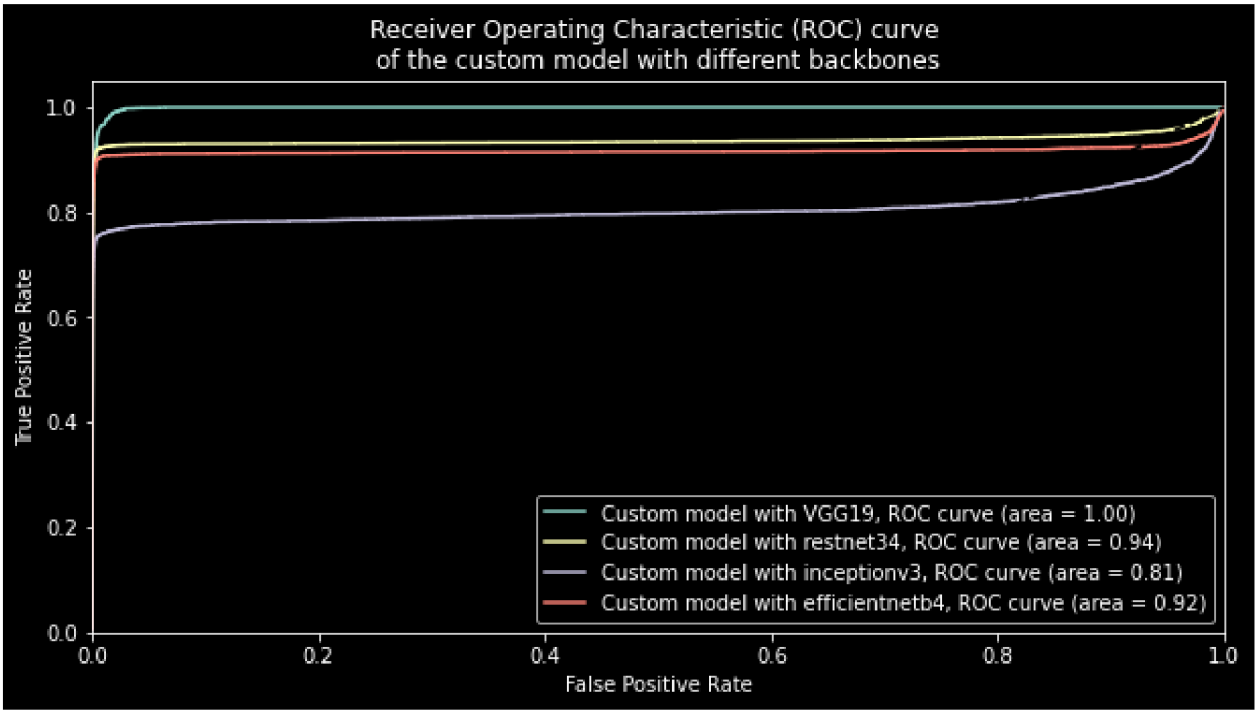

Figure 52. Performance evaluation of the custom model using different backbone architectures for the down sampling phase. After several experiments and a hyperparameter tuning algorithm, the custom model with the VGG19 backbone appears to work incredibly well. (Own work)

The proposed custom model was evaluated using the same input image and several backbones in this sub-section, as shown in the figure below (see

Figure 53). The down sampling backbones from top to bottom are the VGG19, Resnet34, InceptionV3, and EfficientNetb4 models.

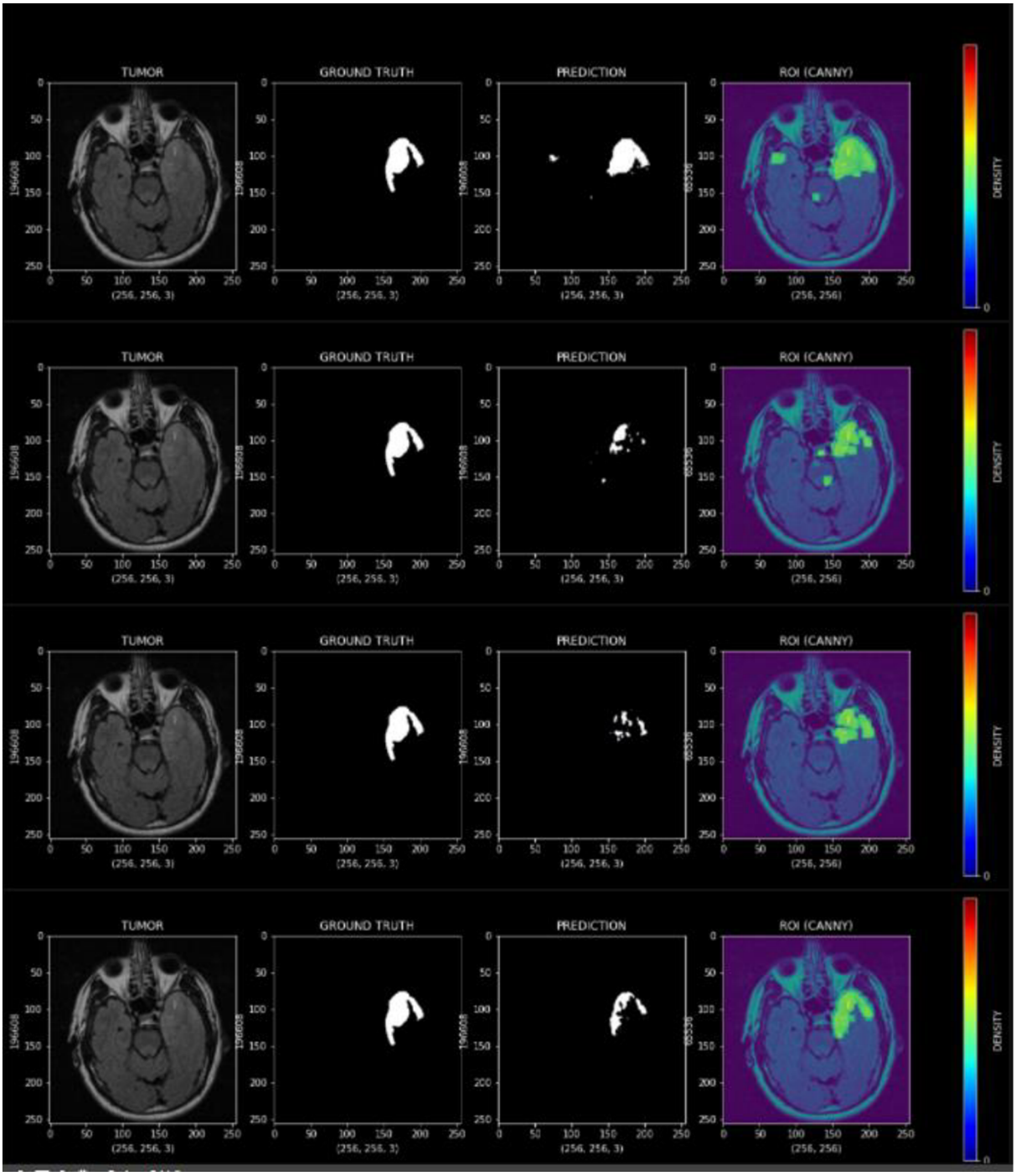

Figure 53. Performance evaluation of the custom u-net model. The latter was evaluated using the same input image and several backbones (VGG19, Resnet34, InceptionV3, and EfficientNetb4 models.). (Own work)

9. Fulfillment of goals dissertation

In this doctoral thesis, I first set out to describe what is meant by abnormalities such as breast cancer and to show the need for better computer-assisted diagnosis (CAD) to detect the tumor at its early stage. Secondly, a framework proposal is presented, implemented, and applied to thermal images of the breast and magnetic resonance imaging of the brain to reveal tumors (anomalies), thus achieving the primary goal and subgoals defined in Section2. These are fulfilled in the following sections of the dissertation and can be briefly given as follow:

- " The main goal is to present a novel framework for detecting anomalies in medical images, more specifically, brain tumor and breast cancer ". This goal is fulfilled in Section 5 and Section 6, respectively, as I propose, a novel framework applied through two case studies in Section 5. I also presented in section 6 the implementations of this framework following a state-of-the-art environment such as the Internet of Things coupled to deployment on the cloud.

- **"The first sub-goal is to design and implement a flexible model capable of being trained to detect and classify brain tumors or breast cancer."** This sub-objective is achieved throughout the doctorate thesis by proposing a novel framework and showing the results of each case study.

- **"The second is to design and implement a working prototype".** This sub-objective is achieved in sections 6 and 7, where the implementation of the prototype is discussed in depth.

Moreover, throughout the doctoral study, other achievements contributing to the main objective of this thesis can be listed as follows:

- The essential part of the literature survey Breast Cancer is prepared as a review paper and published to the High IF Q1 journal, namely Sensor.
- The Research article presenting the key concept of Mathematical morphology applied to breast cancer is prepared and published in Springer.
- The Research article on the use of Machine learning techniques such as Deep Learning to extract and classify breast cancer was submitted and published in springer.

Many other articles were published showing the use of machine learning to extract features and process them more efficiently to have high accuracy results. The work done in these articles (see

Author's Published Works section) was essential to gather the necessary knowledge for the conception of the novel Framework present in this Dissertation.

10. Conclusion

The basic principle of thermographic cancer detection is to capture the skin's thermal effects; infrared imaging makes it possible to evaluate the breasts' skin temperature to assess the associated risk and any thermal anomalies linked to a possible breast tumor. The study presented was mainly divided into two parts: first, sections 4 and 5 gave the background of the research and the research area with a review of the literature on the state of the art of machine learning applied to infrared and MRI medical images. The second part, sections 6 and 7, showed the result obtained with two case studies on breast cancer and brain tumors to support the analysis, implemented the framework, and described the proposed cloud-based architecture.

The presented solution takes advantage of the incredible computing power offered in deep learning. It uses such power to process the extraction, refinement, and display of the relevant characteristics of a specific input medical image. The system was created to detect tumor areas that manifest as high metabolism in the breast. Considering such image (thermal image), the output was staffed by a thorough scan that allows the doctor to process thousands of images and get the tumor type output and tumor location in the breast image (2D thermal image) (see **Figure 54**).

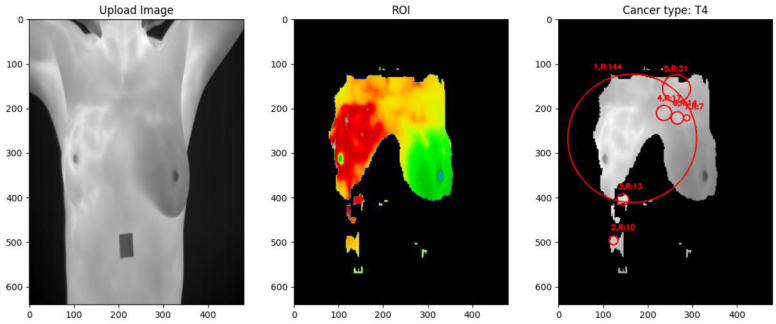

Figure 54. The Region of Concern (RoC) is extracted from the input image, and further analysis is conducted on the image to reveal the region of interest.

This was also the case with brain tumors, where the system was as effective or better on the LGG MRI brain tumor dataset (Brain MRI Segmentation, n.d.). Furthermore, applying the framework in the use cases discussed in section 6 showed the different backbones (VGG19, Resnet34, InceptionV3, and EfficientNetb4 models), and impressive results have been achieved. However, during the doctorate and throughout the literature, a common concern has been raised, namely:

- A small number of thermal datasets: Unlike other modalities such as MRI diagnosis, which has multiple public datasets, thermal breast image datasets are not that common.

- Among the few datasets found, few follow a street protocol. Therefore, a lack of proper labelling required some time to contact the dataset's author to ensure specific values.

I believe that further progress can be made using thermal images coupled with machine learning techniques like a computer-aided diagnosis to aid physicians in their daily consultation and thus help detect breast cancer in its early stages (T0 and T1).

The List of Tables

The List of Figures

References

A dynamic threshold segmentation of infrared image—《Opto-electronic Engineering》2002年06期. (2019, December 21). http://en.cnki.com.cn/Article_en/CJFDTotal-GDGC200206015.htm

Advances in Breast Cancer Research—National Cancer Institute (nciglobal,ncienterprise). (2019, May 2). [CgvArticle]. https://www.cancer.gov/types/breast/research

Agrawal, U., Soria, D., Wagner, C., Garibaldi, J., Ellis, I. O., Bartlett, J. M. S., Cameron, D., Rakha, E. A., & Green, A. R. (2019). Combining clustering and classification ensembles: A novel pipeline to identify breast cancer profiles. *Artificial Intelligence in Medicine*, *97*, 27–37. https://doi.org/10.1016/j.artmed.2019.05.002

Ahmed, M., Naser Mahmood, A., & Hu, J. (2016). A survey of network anomaly detection techniques. *Journal of Network and Computer Applications*, *60*, 19–31. https://doi.org/10.1016/j.jnca.2015.11.016

Al-Olofi, W. A., Rushdi, M. A., Islam, M. A., & Badawi, A. M. (2018). Improved Anomaly Detection in Low-Resolution and Noisy Whole-Slide Images using Transfer Learning. In A. Eldeib, T. Basha, & I. Yassine (Eds.), *2018 9th Cairo International Biomedical Engineering Conference (cibec)* (pp. 114–117). Ieee.

Amri, A., Pulko, S. H., & Wilkinson, A. J. (2016). Potentialities of steady-state and transient thermography in breast tumour depth detection: A numerical study. *Computer Methods and Programs in Biomedicine*, *123*, 68–80. https://doi.org/10.1016/j.cmpb.2015.09.014

ATLAS.ti: The Qualitative Data Analysis & Research Software. (n.d.). ATLAS.ti. Retrieved November 21, 2021, from https://atlasti.com/

Automated Breast Ultrasound Lesions Detection Using Convolutional Neural Networks | IEEE Journals & Magazine | IEEE Xplore. (n.d.). Retrieved July 4, 2021, from https://ieeexplore.ieee.org/document/8003418

Avila-Castro, I. A., Hernández-Martínez, A. R., Estevez, M., Cruz, M., Esparza, R., Pérez, R., & Rodríguez, A. L. (2017). Thorax thermographic simulator for breast pathologies. *Journal of Applied Research and Technology. JART*, *15*(2), 143–151. https://doi.org/10.1016/j.jart.2017.01.008

Bahdanau, D., Cho, K., & Bengio, Y. (2016). Neural Machine Translation by Jointly Learning to Align and Translate. *ArXiv:1409.0473 [Cs, Stat]*. http://arxiv.org/abs/1409.0473

Banco de Imagens mastológicas. (n.d.). Retrieved November 23, 2021, from http://visual.ic.uff.br/dmi/

Bhatele, K. R., & Bhadauria, S. S. (2020). Brain structural disorders detection and classification approaches: A review. *Artificial Intelligence Review*, *53*(5), 3349–3401. https://doi.org/10.1007/s10462-019-09766-9

Boogerd, L. S. F., Handgraaf, H. J. M., Lam, H.-D., Huurman, V. A. L., Farina-Sarasqueta, A., Frangioni, J. V., van de Velde, C. J. H., Braat, A. E., & Vahrmeijer, A. L. (2017). Laparoscopic detection and resection of occult liver tumors of multiple cancer types using real-time near-infrared fluorescence guidance. *Surgical Endoscopy*, *31*(2), 952–961. https://doi.org/10.1007/s00464-016-5007-6

Boquete, L., Ortega, S., Miguel-Jiménez, J. M., Rodríguez-Ascariz, J. M., & Blanco, R. (2012). Automated detection of breast cancer in thermal infrared images, based on independent component analysis. *Journal of Medical Systems*, *36*(1), 103–111. https://doi.org/10.1007/s10916-010-9450-y

Brain MRI Images for Brain Tumor Detection. (2020, February 9). https://kaggle.com/navoneel/brain-mri-images-for-brain-tumor-detection

Brain MRI segmentation. (n.d.). Retrieved June 28, 2021, from https://kaggle.com/mateuszbuda/lgg-mri-segmentation

Brain Tumor—Diagnosis. (2012, June 25). Cancer.Net. https://www.cancer.net/cancer-types/brain-tumor/diagnosis

Breast cancer—Causes, symptoms, diagnosis, treatment, pathology. (2020, February 18). https://www.youtube.com/watch?v=jPtCkcILCGU

Byrne, J. J., Morgan, J. L., Twickler, D. M., McIntire, D. D., & Dashe, J. S. (2020). Utility of follow-up standard sonography for fetal anomaly detection. *American Journal of Obstetrics and Gynecology*, *222*(6), 615.e1-615.e9. https://doi.org/10.1016/j.ajog.2020.01.001

Carrera, D., Manganini, F., Boracchi, G., & Lanzarone, E. (2017). Defect Detection in SEM Images of Nanofibrous Materials. *IEEE Transactions on Industrial Informatics*, *13*(2), 551–561. https://doi.org/10.1109/TII.2016.2641472

Casamitjana, A., Puch, S., Aduriz, A., & Vilaplana, V. (2017). 3D Convolutional Neural Networks for Brain Tumor Segmentation: A Comparison of Multi-resolution Architectures. *ArXiv:1705.08236 [Stat]*. http://arxiv.org/abs/1705.08236

Chandola, V., Banerjee, A., & Kumar, V. (2009). Anomaly detection: A survey. *ACM Computing Surveys*, *41*(3), 15:1-15:58. https://doi.org/10.1145/1541880.1541882

Cheng, J.-Z., Ni, D., Chou, Y.-H., Qin, J., Tiu, C.-M., Chang, Y.-C., Huang, C.-S., Shen, D., & Chen, C.-M. (2016). Computer-Aided Diagnosis with Deep Learning Architecture: Applications to Breast Lesions in US Images and Pulmonary Nodules in CT Scans. *Scientific Reports*, *6*(1), 24454. https://doi.org/10.1038/srep24454

Cireşan, D. C., Giusti, A., Gambardella, L. M., & Schmidhuber, J. (2013). Mitosis Detection in Breast Cancer Histology Images with Deep Neural Networks. In K. Mori, I. Sakuma, Y. Sato, C. Barillot, & N. Navab (Eds.), *Medical Image Computing and Computer-Assisted Intervention – MICCAI 2013* (pp. 411–418). Springer. https://doi.org/10.1007/978-3-642-40763-5_51

Cozzani, V., Tugnoli, A., Bonvicini, S., & Salzano, E. (2013). 9—Threshold-Based Approach. In G. Reniers & V. Cozzani (Eds.), *Domino Effects in the Process Industries* (pp. 189–207). Elsevier. https://doi.org/10.1016/B978-0-444-54323-3.00009-9

Crnkovic, I., Sentilles, S., Vulgarakis, A., & Chaudron, M. R. V. (2011). A Classification Framework for Software Component Models. *IEEE Transactions on Software Engineering*. https://doi.org/10.1109/TSE.2010.83

de Groot, J. E., Broeders, M. J., Grimbergen, C. A., & den Heeten, G. J. (2015). Pain-preventing strategies in mammography: An observational study of simultaneously recorded pain and breast mechanics throughout the entire breast compression cycle. *BMC Women's Health*, *15*. https://doi.org/10.1186/s12905-015-0185-2

Dolz, J., Desrosiers, C., Wang, L., Yuan, J., Shen, D., & Ben Ayed, I. (2020). Deep CNN ensembles and suggestive annotations for infant brain MRI segmentation. *Computerized Medical Imaging and Graphics*, *79*, 101660. https://doi.org/10.1016/j.compmedimag.2019.101660

ESMO. (n.d.). *2020 Cancer Incidence and Mortality in EU-27 Countries*. Retrieved September 7, 2020, from https://www.esmo.org/oncology-news/2020-cancer-incidence-and-mortality-in-eu-27-countries

Female patients' perception of pain caused by mammography in the Western Region of Saudi Arabia. (n.d.). Retrieved April 15, 2020, from https://www.ncbi.nlm.nih.gov/pmc/articles/PMC5556287/

Foundation, C.-12. (n.d.). *Central Nervous System*. Retrieved October 4, 2020, from https://www.ck12.org/c/biology/central-nervous-system/lesson/Central-Nervous-System-BIO/

GitHub—Sevakon/unet-keras: U-Net: Convolutional Network for Biomedical Image Segmentation using Keras. (n.d.). Retrieved July 26, 2020, from https://github.com/sevakon/unet-keras

Guo, A., Zhang, K. W., Reynolds, K., & Foraker, R. E. (2020). Coronary heart disease and mortality following a breast cancer diagnosis. *Bmc Medical Informatics and Decision Making*, *20*(1), 88. https://doi.org/10.1186/s12911-020-1127-y

Head, J. F., & Elliott, R. L. (2002). Infrared imaging: Making progress in fulfilling its medical promise. *IEEE Engineering in Medicine and Biology Magazine: The Quarterly Magazine of the Engineering in Medicine & Biology Society*, *21*(6), 80–85. https://doi.org/10.1109/memb.2002.1175142

Head, J. F., Wang, F., & Elliott, R. L. (1993). Breast thermography is a noninvasive prognostic procedure that predicts tumor growth rate in breast cancer patients. *Annals of the New York Academy of Sciences*, *698*, 153–158. https://doi.org/10.1111/j.1749-6632.1993.tb17203.x

Huang, Q., Yang, F., Liu, L., & Li, X. (2015). Automatic segmentation of breast lesions for interaction in ultrasonic computer-aided diagnosis. *Information Sciences*, *314*, 293–310. https://doi.org/10.1016/j.ins.2014.08.021

Introduction to Statistical Learning. (n.d.). Retrieved June 14, 2020, from http://faculty.marshall.usc.edu/gareth-james/ISL/

Isard, H. J., Sweitzer, C. J., & Edelstein, G. R. (1988). Breast thermography. A prognostic indicator for breast cancer survival. *Cancer*, *62*(3), 484–488. https://doi.org/10.1002/1097-0142(19880801)62:3<484::aid-cncr2820620307>3.0.co;2-w

Isensee, F., Kickingereder, P., Wick, W., Bendszus, M., & Maier-Hein, K. H. (2019). No New-Net. *ArXiv:1809.10483 [Cs]*. http://arxiv.org/abs/1809.10483

Jevnisek, R. J., & Avidan, S. (2017). Co-occurrence Filter. *ArXiv:1703.04111 [Cs]*. http://arxiv.org/abs/1703.04111

Jia, W., Shukla, R. M., & Sengupta, S. (2019). Anomaly Detection using Supervised Learning and Multiple Statistical Methods. *2019 18th IEEE International Conference On Machine Learning And Applications (ICMLA)*, 1291–1297. https://doi.org/10.1109/ICMLA.2019.00211

Jiang, Z., Ding, C., Liu, M., & Tao, D. (2020). Two-Stage Cascaded U-Net: 1st Place Solution to BraTS Challenge 2019 Segmentation Task. In A. Crimi & S. Bakas (Eds.), *Brainlesion: Glioma, Multiple*

Sclerosis, Stroke and Traumatic Brain Injuries (pp. 231–241). Springer International Publishing. https://doi.org/10.1007/978-3-030-46640-4_22

Kamnitsas, K., Bai, W., Ferrante, E., McDonagh, S., Sinclair, M., Pawlowski, N., Rajchl, M., Lee, M., Kainz, B., Rueckert, D., & Glocker, B. (2017). Ensembles of Multiple Models and Architectures for Robust Brain Tumour Segmentation. *ArXiv:1711.01468 [Cs]*. http://arxiv.org/abs/1711.01468

Kamnitsas, K., Ledig, C., Newcombe, V. F. J., Simpson, J. P., Kane, A. D., Menon, D. K., Rueckert, D., & Glocker, B. (2017). Efficient multi-scale 3D CNN with fully connected CRF for accurate brain lesion segmentation. *Medical Image Analysis*, *36*, 61–78. https://doi.org/10.1016/j.media.2016.10.004

Kandlikar, S. G., Perez-Raya, I., Raghupathi, P. A., Gonzalez-Hernandez, J.-L., Dabydeen, D., Medeiros, L., & Phatak, P. (2017). Infrared imaging technology for breast cancer detection – Current status, protocols and new directions. *International Journal of Heat and Mass Transfer*, *108*, 2303–2320. https://doi.org/10.1016/j.ijheatmasstransfer.2017.01.086

Kim, T.-Y., Son, J., & Kim, K.-G. (2011). The Recent Progress in Quantitative Medical Image Analysis for Computer Aided Diagnosis Systems. *Healthcare Informatics Research*, *17*(3), 143–149. https://doi.org/10.4258/hir.2011.17.3.143

Kontos, M., Wilson, R., & Fentiman, I. (2011). Digital infrared thermal imaging (DITI) of breast lesions: Sensitivity and specificity of detection of primary breast cancers. *Clinical Radiology*, *66*(6), 536–539. https://doi.org/10.1016/j.crad.2011.01.009

Krishna, S., & George, B. (2021). An affordable solution for the recognition of abnormality in breast thermogram. *Multimedia Tools and Applications*. https://doi.org/10.1007/s11042-021-11082-w

Krizhevsky, A., Sutskever, I., & Hinton, G. E. (2012). ImageNet Classification with Deep Convolutional Neural Networks. *Advances in Neural Information Processing Systems*, *25*. https://papers.nips.cc/paper/2012/hash/c399862d3b9d6b76c8436e924a68c45b-Abstract.html

Lecun, Y., Bottou, L., Bengio, Y., & Haffner, P. (1998). Gradient-based learning applied to document recognition. *Proceedings of the IEEE*, *86*(11), 2278–2324. https://doi.org/10.1109/5.726791

Lin, W.-C., Ke, S.-W., & Tsai, C.-F. (2015). CANN: An intrusion detection system based on combining cluster centers and nearest neighbors. *Knowl. Based Syst.* https://doi.org/10.1016/j.knosys.2015.01.009

Long, J., Shelhamer, E., & Darrell, T. (2015). Fully convolutional networks for semantic segmentation. *2015 IEEE Conference on Computer Vision and Pattern Recognition (CVPR)*, 3431–3440. https://doi.org/10.1109/CVPR.2015.7298965

Lozano, A., & Hassanipour, F. (2019). Infrared imaging for breast cancer detection: An objective review of foundational studies and its proper role in breast cancer screening. *Infrared Physics & Technology*, *97*, 244–257. https://doi.org/10.1016/j.infrared.2018.12.017

Ma, G., & Soleimani, M. (2020). Spectral Capacitively Coupled Electrical Resistivity Tomography for Breast Cancer Detection. *IEEE Access*, *8*, 50900–50910. https://doi.org/10.1109/ACCESS.2020.2980112

Ma, X., Tao, Z., Wang, Y., Yu, H., & Wang, Y. (2015). Long short-term memory neural network for traffic speed prediction using remote microwave sensor data. *Transportation Research Part C: Emerging Technologies*, *54*(0). https://trid.trb.org/view/1350260

Malhotra, P., Vig, L., Shroff, G., & Agarwal, P. (2015). Long Short Term Memory Networks for Anomaly Detection in Time Series. *Computational Intelligence*, 6.

Mambou, S. J., Maresova, P., Krejcar, O., Selamat, A., & Kuca, K. (2018). Breast Cancer Detection Using Infrared Thermal Imaging and a Deep Learning Model. *Sensors (Basel, Switzerland)*, *18*(9), Article 9. https://doi.org/10.3390/s18092799

Mambou, S., Krejcar, O., Kuca, K., & Selamat, A. (2018). Novel Human Action Recognition in RGB-D Videos Based on Powerful View Invariant Features Technique. In A. Sieminski, A. Kozierkiewicz,

M. Nunez, & Q. T. Ha (Eds.), *Modern Approaches for Intelligent Information and Database Systems* (pp. 343–353). Springer International Publishing. https://doi.org/10.1007/978-3-319-76081-0_29

Mambou, S., Krejcar, O., Maresova, P., Selamat, A., & Kuca, K. (2019a). Novel Four Stages Classification of Breast Cancer Using Infrared Thermal Imaging and a Deep Learning Model. In I. Rojas, O. Valenzuela, F. Rojas, & F. Ortuño (Eds.), *Bioinformatics and Biomedical Engineering* (pp. 63–74). Springer International Publishing.

Mambou, S., Krejcar, O., Maresova, P., Selamat, A., & Kuca, K. (2019b). Novel Four Stages Classification of Breast Cancer Using Infrared Thermal Imaging and a Deep Learning Model. In I. Rojas, O. Valenzuela, F. Rojas, & F. Ortuño (Eds.), *Bioinformatics and Biomedical Engineering* (pp. 63–74). Springer International Publishing.

Mambou, S., Krejcar, O., Selamat, A., Dobrovolny, M., Maresova, P., & Kuca, K. (2020). Novel Thermal Image Classification Based on Techniques Derived from Mathematical Morphology: Case of Breast Cancer. In I. Rojas, O. Valenzuela, F. Rojas, L. J. Herrera, & F. Ortuño (Eds.), *Bioinformatics and Biomedical Engineering* (pp. 683–694). Springer International Publishing. https://doi.org/10.1007/978-3-030-45385-5_61

Meiser, B., Kaur, R., Morrow, A., Peate, M., Wong, W. K. T., McPike, E., Cops, E., Nichols, C., Austin, R., Fine, M., Thrupp, L., Ward, R., Macrae, F., Hiller, J. E., Trainer, A. H., Mitchell, G., Susman, R., Pachter, N., Goodwin, A., … for the ICCon Audit Study Collaborative Group. (2021). Impact of national guidelines on use of BRCA1/2 germline testing, risk management advice given to women with pathogenic BRCA1/2 variants and uptake of advice. *Hereditary Cancer in Clinical Practice*, *19*(1), 24. https://doi.org/10.1186/s13053-021-00180-3

Moon, W. K., Lo, C.-M., Chen, R.-T., Shen, Y.-W., Chang, J. M., Huang, C.-S., Chen, J.-H., Hsu, W.-W., & Chang, R.-F. (2014). Tumor detection in automated breast ultrasound images using quantitative tissue clustering. *Medical Physics*, *41*(4), 042901. https://doi.org/10.1118/1.4869264

Morales-Cervantes, A., Kolosovas-Machuca, E. S., Guevara, E., Maruris Reducindo, M., Bello Hernández, A. B., Ramos García, M., & González, F. J. (2018). An automated method for the evaluation of breast cancer using infrared thermography. *EXCLI Journal*, *17*, 989–998. https://doi.org/10.17179/excli2018-1735

Myronenko, A. (2018). 3D MRI brain tumor segmentation using autoencoder regularization. *ArXiv:1810.11654 [Cs, q-Bio]*. http://arxiv.org/abs/1810.11654

Namikawa, T., Sato, T., & Hanazaki, K. (2015). Recent advances in near-infrared fluorescence-guided imaging surgery using indocyanine green. *Surgery Today*, *45*(12), 1467–1474. https://doi.org/10.1007/s00595-015-1158-7

Pandeeswari, N., & Kumar, G. (2016). Anomaly Detection System in Cloud Environment Using Fuzzy Clustering Based ANN. *Mobile Networks and Applications*, *21*(3), 494–505. https://doi.org/10.1007/s11036-015-0644-x

Pavlík, T., Májek, O., Büchler, T., Vyzula, R., Petera, J., Ryska, M., Ryška, A., Cibula, D., Babjuk, M., Abrahámová, J., Vorlíček, J., Mužík, J., & Dušek, L. (2014). Trends in stage-specific population-based survival of cancer patients in the Czech Republic in the period 2000–2008. *Cancer Epidemiology*, *38*(1), 28–34. https://doi.org/10.1016/j.canep.2013.11.002

Pleijhuis, R. G., Langhout, G. C., Helfrich, W., Themelis, G., Sarantopoulos, A., Crane, L. M. A., Harlaar, N. J., de Jong, J. S., Ntziachristos, V., & van Dam, G. M. (2011). Near-infrared fluorescence (NIRF) imaging in breast-conserving surgery: Assessing intraoperative techniques in tissue-simulating breast phantoms. *European Journal of Surgical Oncology (EJSO)*, *37*(1), 32–39. https://doi.org/10.1016/j.ejso.2010.10.006

Population Changes in the Czech Republic. (n.d.). Population Changes in the Czech Republic. Retrieved April 15, 2020, from https://www.czso.cz/csu/czso/4001-04-in_2004-metodicke_vysvetlivky

Quellec, G., Lamard, M., Cozic, M., Coatrieux, G., & Cazuguel, G. (2016). Multiple-Instance Learning for Anomaly Detection in Digital Mammography. *IEEE Transactions on Medical Imaging*, *35*(7), 1604–1614. https://doi.org/10.1109/TMI.2016.2521442

RAD — Outlier Detection on Big Data—Netflix TechBlog. (n.d.). Retrieved June 13, 2020, from https://netflixtechblog.com/rad-outlier-detection-on-big-data-d6b0494371cc

Rampun, A., Scotney, B. W., Morrow, P. J., Wang, H., & Winder, J. (2018). Breast Density Classification Using Local Quinary Patterns with Various Neighbourhood Topologies. *Journal of Imaging*, *4*(1), 14. https://doi.org/10.3390/jimaging4010014

Rasheed, W., & Tang, T. B. (2020). Anomaly Detection of Moderate Traumatic Brain Injury Using Auto-Regularized Multi-Instance One-Class SVM. *IEEE Transactions on Neural Systems and Rehabilitation Engineering*, *28*(1), 83–93. https://doi.org/10.1109/TNSRE.2019.2948798

Ronneberger, O., Fischer, P., & Brox, T. (2015). U-Net: Convolutional Networks for Biomedical Image Segmentation. *ArXiv:1505.04597 [Cs]*. http://arxiv.org/abs/1505.04597

Ruiz, P. (2019, April 23). *Understanding and visualizing ResNets*. Medium. https://towardsdatascience.com/understanding-and-visualizing-resnets-442284831be8

Salman, T., Bhamare, D., Erbad, A., Jain, R., & Samaka, M. (2017). Machine Learning for Anomaly Detection and Categorization in Multi-Cloud Environments. *2017 IEEE 4th International Conference on Cyber Security and Cloud Computing (CSCloud)*, 97–103. https://doi.org/10.1109/CSCloud.2017.15

Schlemper, J., Oktay, O., Schaap, M., Heinrich, M., Kainz, B., Glocker, B., & Rueckert, D. (2019). Attention Gated Networks: Learning to Leverage Salient Regions in Medical Images. *ArXiv:1808.08114 [Cs]*. http://arxiv.org/abs/1808.08114

Schwenzfeier, N., & Gruhn, V. (2018). Towards a practical process model for anomaly detection systems. *Proceedings of the 1st International Workshop on Software Engineering for Cognitive Services - SE4COG '18*, 41–44. https://doi.org/10.1145/3195555.3195568

Sedik, A., Emara, H. M., Hamad, A., Shahin, E. M., A. El-Hag, N., Khalil, A., Ibrahim, F., Elsherbeny, Z. M., Elreefy, M., Zahran, O., El-Khobby, H. A., El Banby, G. M., Elwakeil, M., El-Shafai, W., Khalaf, A. A. M., Rihan, M., Al-Nuaimy, W., Taha, T. E., Attia, M. A., … Abd El-Samie, F. E. (2019). Efficient anomaly detection from medical signals and images. *International Journal of Speech Technology*, *22*(3), 739–767. https://doi.org/10.1007/s10772-019-09610-z

Seeböck, P., Orlando, J. I., Schlegl, T., Waldstein, S. M., Bogunović, H., Klimscha, S., Langs, G., & Schmidt-Erfurth, U. (2020). Exploiting Epistemic Uncertainty of Anatomy Segmentation for Anomaly Detection in Retinal OCT. *IEEE Transactions on Medical Imaging*, *39*(1), 87–98. https://doi.org/10.1109/TMI.2019.2919951

Shan, J., Cheng, H. D., & Wang, Y. (2012). A novel segmentation method for breast ultrasound images based on neutrosophic l-means clustering. *Medical Physics*, *39*(9), 5669–5682. https://doi.org/10.1118/1.4747271

Siddiqui, S. Y., Haider, A., Ghazal, T. M., Khan, M. A., Naseer, I., Abbas, S., Rahman, M., Khan, J. A., Ahmad, M., Hasan, M. K., A, A. Mohammed., & Ateeq, K. (2021). IoMT Cloud-Based Intelligent Prediction of Breast Cancer Stages Empowered With Deep Learning. *IEEE Access*, *9*, 146478–146491. https://doi.org/10.1109/ACCESS.2021.3123472

Silva, L., Saade, D., Sequeiros Olivera, G., Silva, A., Paiva, A., Bravo, R., & Conci, A. (2014). A New Database for Breast Research with Infrared Image. *Journal of Medical Imaging and Health Informatics*, *4*, 92–100. https://doi.org/10.1166/jmihi.2014.1226

Song, W., Dong, W., & Kang, L. (2020). Group anomaly detection based on Bayesian framework with genetic algorithm. *Information Sciences*, *533*, 138–149. https://doi.org/10.1016/j.ins.2020.03.110

Szegedy, C., Vanhoucke, V., Ioffe, S., Shlens, J., & Wojna, Z. (2015). Rethinking the Inception Architecture for Computer Vision. *ArXiv:1512.00567 [Cs]*. http://arxiv.org/abs/1512.00567

Tan, M., & Le, Q. V. (2020). EfficientNet: Rethinking Model Scaling for Convolutional Neural Networks. *ArXiv:1905.11946 [Cs, Stat]*. http://arxiv.org/abs/1905.11946

The Most Common Brain Tumor: 5 Things You Should Know. (n.d.). Retrieved October 4, 2020, from https://www.hopkinsmedicine.org/health/wellness-and-prevention/the-most-common-brain-tumor-5-things-you-should-know

Tong, L., Mitchel, J., Chatlin, K., & Wang, M. D. (2020). Deep learning based feature-level integration of multi-omics data for breast cancer patients survival analysis. *BMC Medical Informatics and Decision Making*, *20*(1), 225. https://doi.org/10.1186/s12911-020-01225-8

Touvron, H., Cord, M., Douze, M., Massa, F., Sablayrolles, A., & Jégou, H. (2021). Training data-efficient image transformers & distillation through attention. *ArXiv:2012.12877 [Cs]*. http://arxiv.org/abs/2012.12877

Van Hulse, J., Khoshgoftaar, T. M., Napolitano, A., & Wald, R. (2012). Threshold-based feature selection techniques for high-dimensional bioinformatics data. *Network Modeling Analysis in Health Informatics and Bioinformatics*, *1*(1), 47–61. https://doi.org/10.1007/s13721-012-0006-6

Vaswani, A., Shazeer, N., Parmar, N., Uszkoreit, J., Jones, L., Gomez, A. N., Kaiser, L., & Polosukhin, I. (2017). Attention Is All You Need. *ArXiv:1706.03762 [Cs]*. http://arxiv.org/abs/1706.03762

Verdoja, F., & Grangetto, M. (2020). Graph Laplacian for image anomaly detection. *Machine Vision and Applications*, *31*(1–2), 11. https://doi.org/10.1007/s00138-020-01059-4

Visual Lab—Laboratorio de Computação visual. (n.d.). Retrieved October 12, 2021, from http://visual.ic.uff.br/

Wang, G., Li, W., Ourselin, S., & Vercauteren, T. (2018). Automatic Brain Tumor Segmentation using Cascaded Anisotropic Convolutional Neural Networks. *ArXiv:1709.00382 [Cs]*, *10670*, 178–190. https://doi.org/10.1007/978-3-319-75238-9_16

Wang, H., Li, Y., Khan, S. A., & Luo, Y. (2020). Prediction of breast cancer distant recurrence using natural language processing and knowledge-guided convolutional neural network. *Artificial Intelligence in Medicine*, *110*, 101977. https://doi.org/10.1016/j.artmed.2020.101977

Wang, X., Girshick, R., Gupta, A., & He, K. (2018). Non-local Neural Networks. *ArXiv:1711.07971 [Cs]*. http://arxiv.org/abs/1711.07971

Whelehan, P., Evans, A., Wells, M., & Macgillivray, S. (2013). The effect of mammography pain on repeat participation in breast cancer screening: A systematic review. *Breast (Edinburgh, Scotland)*, *22*(4), 389–394. https://doi.org/10.1016/j.breast.2013.03.003

Wu, L.-W., & Yu, R.-F. (2010). A threshold-based method for selfish nodes detection in MANET. *2010 International Computer Symposium (ICS2010)*, 875–882. https://doi.org/10.1109/COMPSYM.2010.5685389

Wyatt, K. D., Jenkins, S. M., Plevak, M. F., Venegas Pont, M. R., & Pruthi, S. (2019). A personalized, web-based breast cancer decision making application: A pre-post survey. *BMC Medical Informatics and Decision Making*, *19*(1), 196. https://doi.org/10.1186/s12911-019-0924-7

Xian, M., Zhang, Y., & Cheng, H. D. (2015). Fully automatic segmentation of breast ultrasound images based on breast characteristics in space and frequency domains. *Pattern Recognition*, *48*(2), 485–497. https://doi.org/10.1016/j.patcog.2014.07.026

Zhang, J., & Hu, J. (2008). Image Segmentation Based on 2D Otsu Method with Histogram Analysis. *2008 International Conference on Computer Science and Software Engineering*, *6*, 105–108. https://doi.org/10.1109/CSSE.2008.206

Zhang, J., Jiang, H., Huang, L., Yao, Y.-D., & Li, S. (2019). Visibility Attribute Extraction and Anomaly Detection for Chinese Diagnostic Report Based on Cascade Networks. *IEEE Access*, *7*, 116402–116412. https://doi.org/10.1109/ACCESS.2019.2932842

Zhang, Z., Liu, Q., & Wang, Y. (2018). Road Extraction by Deep Residual U-Net. *IEEE Geoscience and Remote Sensing Letters*, *15*(5), 749–753. https://doi.org/10.1109/LGRS.2018.2802944

Zhao, Y.-X., Zhang, Y.-M., & Liu, C.-L. (2020). Bag of Tricks for 3D MRI Brain Tumor Segmentation. In A. Crimi & S. Bakas (Eds.), *Brainlesion: Glioma, Multiple Sclerosis, Stroke and Traumatic Brain Injuries* (pp. 210–220). Springer International Publishing. https://doi.org/10.1007/978-3-030-46640-4_20

Zhou, J., & Tung, A. K. H. (n.d.). *SMiLer: A Semi-Lazy Time Series Prediction System for Sensors*. 16.

Zhou, Z., Siddiquee, M. M. R., Tajbakhsh, N., & Liang, J. (2018). UNet++: A Nested U-Net Architecture for Medical Image Segmentation. *ArXiv:1807.10165 [Cs, Eess, Stat]*. http://arxiv.org/abs/1807.10165

Zimek, A., & Schubert, E. (2017). Outlier Detection. In L. Liu & M. T. Özsu (Eds.), *Encyclopedia of Database Systems* (pp. 1–5). Springer. https://doi.org/10.1007/978-1-4899-7993-3_80719-1

Participation at projects

IT4Neuro(degeneration), 2019 - 2022. Main proposer: doc. Ing. Miroslav Lísa, Ph.D. (FS UHK), reg. no.: CZ.02.1.01/0.0/0.0/18_069/0010054.

- Member of working group – FIM UHK at 30% FTE.

Grant Agency of Excellence project - Smart Solutions for Ubiquitous Computing Environments, Faculty of Informatics and Management University of Hradec Kralove, 2018-2021.

- Member of the research team as a junior researcher.

Internal student research project SPEV - Smart Solutions for Ubiquitous Computing Environments, Faculty of Informatics and Management University of Hradec Kralove, 2018-2021.

- Member of the research team as a junior researcher.

CA Broadcom Inc: “Parallel and distributed computing project” on Z architecture for high-performance computing.

- Member of the Research and Development team

Author's Published Works

Journal Publications

1. Mambou, S., Krejcar, O., Kuca, K., Selamat, A.: Novel Cross-View Human Action Model Recognition Based on the Powerful View-Invariant Features Technique. Future Internet. 10, 89 (2018). **ESCI https://doi.org/10.3390/fi10090089.**

2. Mambou, S., Krejcar, O., Maresova, P., Selamat, A., Kuca, K.: Novel Hand Gesture Alert System. Applied Sciences. 9, 3419 (2019). **IF = 2,679, Q3, Q2, Q3, Q2. https://doi.org/10.3390/app9163419.**

3. Mambou, S.J., Maresova, P., Krejcar, O., Selamat, A., Kuca, K.: Breast Cancer Detection Using Infrared Thermal Imaging and a Deep Learning Model. Sensors (Basel). 18, (2018**). IF = 3,576, Q1, Q2, Q1. https://doi.org/10.3390/s18092799.**

Conference Publications

1. Mambou, S., Krejcar, O.: Novel Scene Recognition Using TrainDetector. In: Vera-Rodriguez, R., Fierrez, J., and Morales, A. (eds.) Progress in Pattern Recognition, Image Analysis, Computer Vision, and Applications. pp. 504–512. Springer International Publishing, Cham (2019). https://doi.org/10.1007/978-3-030-13469-3_59.

2. Mambou, S., Krejcar, O., Maresova, P., Selamat, A., Kuca, K.: Novel Four Stages Classification of Breast Cancer Using Infrared Thermal Imaging and a Deep Learning Model. In: Rojas, I., Valenzuela, O., Rojas, F., and Ortuño, F. (eds.) Bioinformatics and Biomedical Engineering. pp. 63–74. Springer International Publishing (2019).

3. Mambou, S., Krejcar, O., Selamat, A.: Approximate Outputs of Accelerated Turing Machines Closest to Their Halting Point. In: Nguyen, N.T., Gaol, F.L., Hong, T.-P., and Trawiński, B. (eds.) Intelligent Information and Database Systems. pp. 702–713. Springer International Publishing (2019).

4. Mambou, S., Maresova, P., Krejcar, O., Selamat, A., Kuca, K.: Breast Cancer Detection Using Modern Visual IT Techniques. In: Sieminski, A., Kozierkiewicz, A., Nunez, M., and Ha, Q.T.

(eds.) Modern Approaches for Intelligent Information and Database Systems. pp. 397–407. Springer International Publishing, Cham (2018). https://doi.org/10.1007/978-3-319-76081-0_34.

5. Mambou, S., Krejcar, O., Kuca, K., Selamat, A.: Novel Human Action Recognition in RGB-D Videos Based on Powerful View Invariant Features Technique. In: Sieminski, A., Kozierkiewicz, A., Nunez, M., and Ha, Q.T. (eds.) Modern Approaches for Intelligent Information and Database Systems. pp. 343–353. Springer International Publishing, Cham (2018). https://doi.org/10.1007/978-3-319-76081-0_29.

6. Mambou, S., Krejcar, O., Maresova, P., Selamat, A., Kuca, K.: The Need for Mobile Apps for Maternal and Child Health Care in Center and East Europe. In: Awan, I., Younas, M., Ünal, P., and Aleksy, M. (eds.) Mobile Web and Intelligent Information Systems. pp. 95–108. Springer International Publishing, Cham (2019). https://doi.org/10.1007/978-3-030-27192-3_8.

7. Mambou, S., Krejcar, O., Kuca, K., Selamat, A.: Novel Human Action Recognition in RGB-D Videos Based on Powerful View Invariant Features Technique. In: Sieminski, A., Kozierkiewicz, A., Nunez, M., and Ha, Q.T. (eds.) Modern Approaches for Intelligent Information and Database Systems. pp. 343–353. Springer International Publishing, Cham (2018). https://doi.org/10.1007/978-3-319-76081-0_29.

8. Mambou, S., Krejcar, O., Selamat, A., Dobrovolny, M., Maresova, P., Kuca, K.: Novel Thermal Image Classification Based on Techniques Derived from Mathematical Morphology: Case of Breast Cancer. In: Rojas, I., Valenzuela, O., Rojas, F., Herrera, L.J., and Ortuño, F. (eds.) Bioinformatics and Biomedical Engineering. pp. 683–694. Springer International Publishing, Cham (2020). https://doi.org/10.1007/978-3-030-45385-5_61.

9. Dobrovolny, M., Mls, K., Krejcar, O., Mambou, S., Selamat, A.: Medical Image Data Upscaling with Generative Adversarial Networks. In: Rojas, I., Valenzuela, O., Rojas, F., Herrera, L.J., and Ortuño, F. (eds.) Bioinformatics and Biomedical Engineering. pp. 739–749. Springer International Publishing, Cham (2020). https://doi.org/10.1007/978-3-030-45385-5_66.